A STUDY OF NUCLEAR DISINTEGRATIONS PRODUCED BY COSMIC RADIATION.

Thesis

submitted by

Margaret D. Wilson

B.Sc. (Edinburgh)

for the Degree of

Doctor of Philosophy

University of Edinburgh

May 1958.

Table of Contents.

Chapter I. INTRODUCTION 1

Chapter II. TREATMENT OF THE NUCLEAR EMULSION PLATES 4

1. Exposure of the nuclear emulsion plates 4

2. Processing of the emulsions 5

Chapter III. EXPERIMENTAL PROCEDURE 10

1. Examination of the plates 11

2. Classification of cosmic ray stars 14

3. Measurement of the tracks 20

3.1. Range 20

3.2. Angle 23

Chapter IV. PARTICLE IDENTIFICATION 25

1. Grain density 27

2. Residual range 30

3. Delta-rays 31

4. Multiple Coulomb scattering 34

4.1. Experimental procedure.
A. The coordinate method 35

4.2. Experimental procedure.
B. The constant sagitta method 48

Chapter V. THE GAP COUNT METHOD AND GRAIN DENSITY MEASUREMENTS 51

1. Estimation of grain density from gap density measurements 55

2. Variation of gap density with grain density and gap size 61

3. Change in gap size with inclination of the track 67

4. Comparison of the results from grain and gap counting 69

5. Errors involved in gap and grain measurements 73

5.1. Errors due to uneven processing of the emulsions 73

5.2. Errors in measurement 75

5.3. Statistical fluctuations in gap and grain measurements 77

6. Applications of the gap count method 84

6.1. The mass of slow particles 85

6.2. Joining tracks.
A. The residual range method 90

B. The χ^2 test 94

6.3. Wet tracks 96

7. Conclusions 103

Chapter VI. PROTON ENERGY LOSS AND GRAIN DENSITY 105

1. Energy loss as a function of velocity, kinetic energy and residual range 105

2. Grain density as a function of velocity, kinetic energy and residual range 113

3. Some remarks on the constants in Demers' function 121

Chapter VII. EXPERIMENTAL RESULTS 127

1. Cosmic ray stars 128

1.1. Properties of stars 128

1.2. Size distributions of stars 135

2. Neutral star-producing radiation 151

2.1. Absorption of the radiation in air and in ice 152

2.2. Variation of the mean absorption length with geomagnetic latitude 156

2.3. Absorption cross-section of the neutral star-producing radiation in air and in ice 160

2.4. The flux of neutral star-producing particles in the lower atmosphere 166

3. Conclusions 176

Chapter VIII. CONCLUSIONS 179

ACKNOWLEDGMENTS 185

REFERENCES 186.

APPENDIX Inside back cover.

Chapter I.

INTRODUCTION.

In the last decade of the nineteenth century, extensive studies of the conductivity of air by C.T.R. Wilson, Geitel, Elster and others led to the suggestion that the surface of the earth was continually bombarded by some form of radiation of unknown origin. Later experiments, notably by Gockel, Hess and Kohlhorster, revealed that this penetrating radiation came from some extra-terrestrial source, but many more years were to pass before its constituent parts were identified. From the time of its discovery to the present day, the so-called "cosmic radiation" has been the subject of countless experiments, and from these studies have come many fundamental discoveries of new particles and new processes.

Briefly, the principal properties of the cosmic radiation may be summarised as follows. High energy charged corpuscular radiation enters the earth's atmosphere where it may interact with the atoms of the air, giving rise to a secondary radiation which consists of a penetrating or hard component made up largely of mesons, protons and neutrons, and a soft component of electrons and photons. This secondary radiation has been the concern of most of the experiments, and in what follows the term "cosmic radiation" will refer only to this secondary component. The intensity and energy of the particles comprising this radiation vary with geomagnetic

latitude, with altitude and with the depth below the top of an absorbing medium, and these variations reflect the behaviour of the charged primary radiation in the magnetic field of the earth.

During the early years of cosmic ray research, experiments were carried out using ionisation chambers, and subsequently with Wilson cloud chambers. In 1934, however, Blau and Wambacher discovered that sensitised photographic emulsions are capable of recording the passage of individual cosmic ray particles, and the "stars" which result from the disintegration of the emulsion nuclei by this radiation, and since then many workers have used this method of investigating the properties of the radiation. Observations on the stars produced in an emulsion can yield valuable information concerning the nature of the radiation and its interactions with atomic nuclei. They may also be used in geophysical problems, as a means of determining the intensity of the star-producing radiation and its variations with altitude, geomagnetic latitude and depth in an absorbing medium such as the atmosphere or ice.

The present investigation was made possible by the exposure of two sets of nuclear emulsion plates at mountain altitudes in Arctic Norway, and the subsequent examination of these plates was carried out with a view to determining the flux of cosmic ray neutrons in the

atmosphere at high geomagnetic latitude, from observations on the nuclear disintegrations produced by these particles in the photographic emulsions. As some of the plates were exposed under ice, and others at sea level, it was also possible to measure the rate of absorption of neutrons in ice and in the atmosphere, and the properties of the stars produced at different levels.

In the course of the examination of the plates, it became obvious that a quick, reliable method was required for the determination of the nature and energy of the particles released in the disintegrations, and for this purpose a particular study was made of the variation with energy, of the ionisation produced by charged particles during their passage through the emulsion. The ionisation produced along the track of a particle may be determined from the grain density of the track, and a method of measuring grain density, similar to that † of Evans (unpublished). [redacted], is described and compared with other methods. Finally, the variation of the grain density with the kinetic energy and residual range of particles in Ilford G5 emulsions is determined.

† Evans, G.R. (unpublished) Private communication and also quoted by Tennent, R.M., Ph.D. Thesis, University of London, 1953.

Chapter II.

TREATMENT OF THE NUCLEAR EMULSION PLATES.

II.1. Exposure of the nuclear emulsion plates.

The first series of nuclear emulsion plates was exposed to the cosmic radiation on the Syd Jekkevarra at an altitude of 5600 feet and geomagnetic latitude 66.2°N, by the 1953 Edinburgh University Expedition to Arctic Norway. Four boxes of plates, each packed in a light-tight metal container, were buried for 50 days in the ice cap, at depths between 0 and 4.5 metres below the surface, while a fifth box remained at the expedition's base camp at sea level so that the intensity of the radiation received in the mountain plates during the outward and homeward journeys could be measured. All the plates were inserted vertically into the tins which were maintained in a vertical position with one particular side always facing north. Unfortunately, during the 50 day mountain exposure, ablation of about 2 metres of firn occurred and this caused random orientation of the top tin. Development of the plates was subsequently carried out in Edinburgh, after a total exposure time, from the date of manufacture to the date of development, of 100 days, of which 50 days were spent on the mountain top.

In 1955, a Durham University Expedition to the

Svartisen ice cap carried a second series of emulsions which were exposed at an altitude of 3000 feet and geomagnetic latitude 65°N. Three boxes of emulsions, packed and orientated as before, were taken to the mountain top, and buried at depths of 0, 1.4 metres and 2.8 metres below the ice for 38 days, while a fourth box remained at sea level, and all were returned to Edinburgh for development 112 days after manufacture.

Ilford G5 emulsions 400 μ thick were used for both expeditions, but in the 1955 expedition 3" x 3" unbacked emulsions replaced the 2" x 2" emulsions mounted on glass plates, which were used in the earlier series, so that cosmic ray tracks could be more easily traced from one emulsion to the next. Before development, the unbacked emulsions were mounted separately on glass plates, a 0.1% solution of gelatin being used as adhesive.

II.2. Processing of the emulsions.

The processing of all the plates was carried out by the temperature development method first described by Dilworth, Occhialini and Payne, using the solutions specified in Table I. The developer solution was cooled to 4°C and the plates immersed in the ice-cold developer for 4 hours to allow the solution to diffuse through the emulsions to the bottom without any chemical reaction taking place. At the end of this time, the plates were

Table I.

PROCESSING SOLUTIONS.

Developer (prepared immediately before use)		
Crystalline sodium sulphite ($Na_2SO_3.7H_2O$)	36	gm.
Potassium bromide	0.85	gm.
Amidol	4.5	gm.
Distilled water to	1000	ml.
Stop bath solution		
Sodium metabisulphite	5	gm.
Distilled water to	100	ml.
Fixing solution		
Crystalline sodium thiosulphate ($Na_2S_2O_3.5H_2O$)	40	gm.
Distilled water	100	ml.
2½% glycerine solution		
Glycerine	3.4	gm.
Distilled water	100	ml.

removed from the cold developer and the excess moisture on the surface mopped off with filter paper before they were transferred to a warmed space at a temperature of 22.2°C. Development was allowed to proceed for 30 minutes as it was found that this produced a plate in which the minimum ionisation tracks were fully developed, and yet the number of background grains was relatively small. After development, the plates were immersed in a stop bath which was at the temperature of active development, [redacted], and they remained there for 30 minutes while the stop bath solution was allowed to return slowly to room temperature. On many of the plates a thin layer of silver formed during the processing, causing a surface stain, and this was gently rubbed off with a moistened finger immediately after the plates were removed from the stop bath. The plates were then transferred to the fixing bath, which was at room temperature, and left there in a horizontal position for 1½ times the length of time required for complete clearing, usually about 72 hours.

During the last 12 hours of clearing, the fixing bath solution was diluted in small stages by adding small quantities of water to it at frequent intervals. At the end of this time, when the strength of the solution had been reduced to about one half of its original value, a thin stream of water was allowed to flow continuously

through the fixing bath. After the washing of the plates had proceeded for some time, the washing water was tested for residual hypo by comparing the decolourisation of a drop of potassium permanganate solution produced by a sample of water from the washing bath with that produced by an equal volume of tap water. When the colour persisted for the same length of time in both samples, no hypo remained in the plates and washing was complete.

The plates were dried in a horizontal position and then placed in a glycerine solution for a few hours, in an attempt to replace the glycerine leached out of the emulsion during processing, before they were finally dried. This replacement of the glycerine in the emulsion was a precautionary measure to make the emulsions tougher, and less likely to peel off the glass plates in the dry atmosphere of the laboratory.

Some of the emulsions, particularly those of the first expedition, were found to be still quite opaque after the processing was completed, and events in them were difficult to observe in the microscope. This opacity was caused principally by the formation of a deposit of colloidal silver in the gelatin, and was removed after the initial washing and drying of the plates, but before their immersion in glycerine, by the method of clearing described by Dilworth, Occhialini and Samuel

(1948). The plates were immersed for 45 minutes, in a solution containing 1 part of concentrated hydrochloric acid in 1200 parts of water, and were then thoroughly rinsed before being transferred to a fixing bath for 3 or 4 hours. Finally, after they had been washed until no trace of hypo could be detected in the washing water, the plates were dried and treated with glycerine as before.

It was found that during the washing process some of the emulsions tended to rise off the glass plates, forming irregular blisters, which caused considerable distortion especially when they burst. This phenomenon was particularly noticeable in plates which were only a short distance below the surface of the water in the washing tank, and seldom occurred in plates which were several inches below the water surface. One possible explanation of this localised distortion may be obtained by considering the behaviour of an emulsion during washing, and the effect on it of non-uniformity in the properties of the adhesive used for mounting.

When the fixing bath solution is diluted with water the concentration and solution pressure of the liquid outside the plates will be less than that of the solution inside the emulsion, and there will be a tendency for the pressures on either side of the interface, the emulsion surface, to equalise. Consequently, water

will flow into the emulsion, and since this acts as an inefficient semi-permeable membrane, the hypo will diffuse out of it more slowly than the water flows in. Thus during the washing process the emulsion will swell as its water content increases, and at points where the adhesive is weak it will tend to rise off the plate unless the pressure of the water above is sufficient to keep the swollen emulsion pressed flat upon the plate. If localised blistering and distortion are to be avoided, it is important that the plates should be washed in a considerable depth of water in order that the effect of variations in the properties of the adhesive may be overcome.

Chapter III.

EXPERIMENTAL PROCEDURE.

An interaction between the incoming cosmic radiation and one of the nuclei of a photographic emulsion may result in the disintegration of the nucleus, and the simultaneous ejection of several ionising particles from it. Events of this type, commonly termed "cosmic ray stars", were thus characterised by the tracks formed by these ionising particles during their passage through the emulsion. For the purposes of the present work, a star was defined as having two or more tracks originating from one point, and at least one of these tracks was required to have a range greater than 60 μ or less than 10 μ. This limitation on track length was imposed in order to exclude those stars which were produced by radioactive disintegrations.

The process of formation of cosmic ray stars has been the subject of many experimental and theoretical investigations. Stars formed by high energy particles have been found to consist of tracks of two types:

(1) lightly ionised tracks formed by fast "knock-on" or "prompt" protons which have escaped from the nucleus as a result of collisions within it,

(2) heavily ionised tracks formed by low energy particles (protons, deuterons, α-particles etc.), which have been ejected during the de-excitation of the

residual nucleus, and are usually termed "evaporation particles".

Low energy primary particles are capable of producing stars with evaporation tracks only, while at very high energies there is a possibility of a third process occurring, namely that of meson formation, but relatively few events of this type were observed owing to the low altitude exposure of the plates.

The velocity of the particles produced in a nuclear disintegration may be conveniently determined by the amount of ionisation which they produce, and in succeeding chapters the following notation will be used:

	Grain density, n.
Thin tracks	$n < 18$ grains/50μ
Grey tracks	$18 < n < 60$ grains/50μ
Black tracks	$n > 60$ grains/50μ.

On the whole, these three groups represent mesons, prompt particles and evaporation particles respectively, although the third group will contain a considerable number of prompt particles as well as all the evaporation particles.

III.1. Examination of the plates.

Systematic searching of the plates for cosmic ray stars and other events was carried out principally on a Cooke, Troughton and Simms binocular microscope, although

a Prior binocular microscope was also used for some of the plates. Air objectives, with magnifications of the order of x 20, and x 6 eyepieces were employed for scanning, but oil immersion objectives and eyepieces of a higher magnification were required for the more detailed work of star analysis, such as range determinations and angular separation measurements on the tracks emerging from the stars.

Of the first series of plates, all those exposed at sea level and on top of the ice were searched, together with two from each box exposed under the ice, but only two plates from each of the second expedition boxes were used. An area of between 2 sq. cm. and 5 sq. cm. in the centre of each plate was systematically searched from top to bottom of the emulsion, and all the cosmic ray stars which lay within these areas were recorded. Owing to the difficulty of distinguishing and identifying the fast tracks of stars which lay near the top and bottom surfaces of the emulsion, any star whose origin was nearer than 20 μ to either surface was omitted from the total number of stars. This distance of 20 μ was chosen because in a minimum ionisation track there are only 13 grains in each 50 μ interval, and these tracks would be easily overlooked or not recognised as tracks if only a small part of them lay within the emulsion. Removal of the surface stain on the emulsion during

processing was assumed to have reduced the total thickness of it by 10 μ, and the limitation imposed on the depth of emulsion included in the searching further reduced the overall depth searched from 400 μ to 350 μ. The area and volume systematically searched in each box of plates are shown for both expeditions in Table II.

Table II.

Position during exposure	First expedition		Second expedition	
	Area sq. mm.	Volume cu. mm.	Area sq. mm.	Volume cu. mm.
Sea level	2018	706	406	142
Mountain top	2017	706	860	301
Under ice 1	817	286	408	143
Under ice 2	832	292	403	141
Under ice 3	858	301		
Total	6542	2291	2077	727

Range, grain density, angular distribution and scattering measurements were made on many of the tracks emerging from the cosmic ray stars, in order to determine the nature of the primary and secondary particles, and the total energy released in the disintegrations. Where it was necessary, the tracks were traced through to the adjacent emulsion, but this procedure was

complicated by the fact that the emulsions of the first expedition were separated from each other by glass plates. However, it was easily carried out in the second set of plates which had been separated only by layers of thin paper, during exposure.

III.2. Classification of cosmic ray stars.

All the events arising from the interactions of cosmic rays, which conformed to the requirements laid down for stars, were classified according to the number of ionising secondary particles of range greater than 5μ, produced in the disintegration, regardless of the nature of these particles. Thus, a star consisting of two lightly ionising tracks, and five evaporation tracks was included in the number of seven prong stars. Short tracks of total range less than 5μ, were not counted as prongs, but were recorded separately under the heading "nuclear recoils", and short electron tracks arising from the beta decay of the residual nucleus were similarly excluded from the total number of prongs. Single prong stars produced in nuclei other than hydrogen were omitted because they did not fulfil the requirements of a "star", but their intensity was later computed by a theoretical method.

The stars were also divided into three groups according to the nature of the star-producing particle

which could be a neutral particle, a fast charged particle or a slow negative π-meson. Primaries of the second kind were accepted only if they lay on the axis of symmetry of the emitted fast particles, and provided they had enough energy to produce the star. Where no fast ionising secondaries were present, the energy of the primary had to be at least as great as that calculated by LeCouteur (1950) for evaporation stars, and the conditions of momentum balance had to be satisfied.

In the course of the work on the classification of stars, it was found that unless some other method were devised for determining the distribution of the secondary particles of each star in space, it was necessary to make detailed angular measurements on nearly every star in order to decide which, if any, of its lightly ionised tracks represented the primary particle. The method which was used was the construction of a three-dimensional model of the star, the tracks being represented by small pieces of coloured wire mounted in plasticine, as shown in the photograph of a six prong cosmic ray star, in figure 1. By this means it was possible to obtain very quickly a reasonably accurate picture of each star, and moreover the number of measurements which had to be made was considerably reduced, since only the inclinations of the tracks to the horizontal were required, together with an estimation of the angle in the

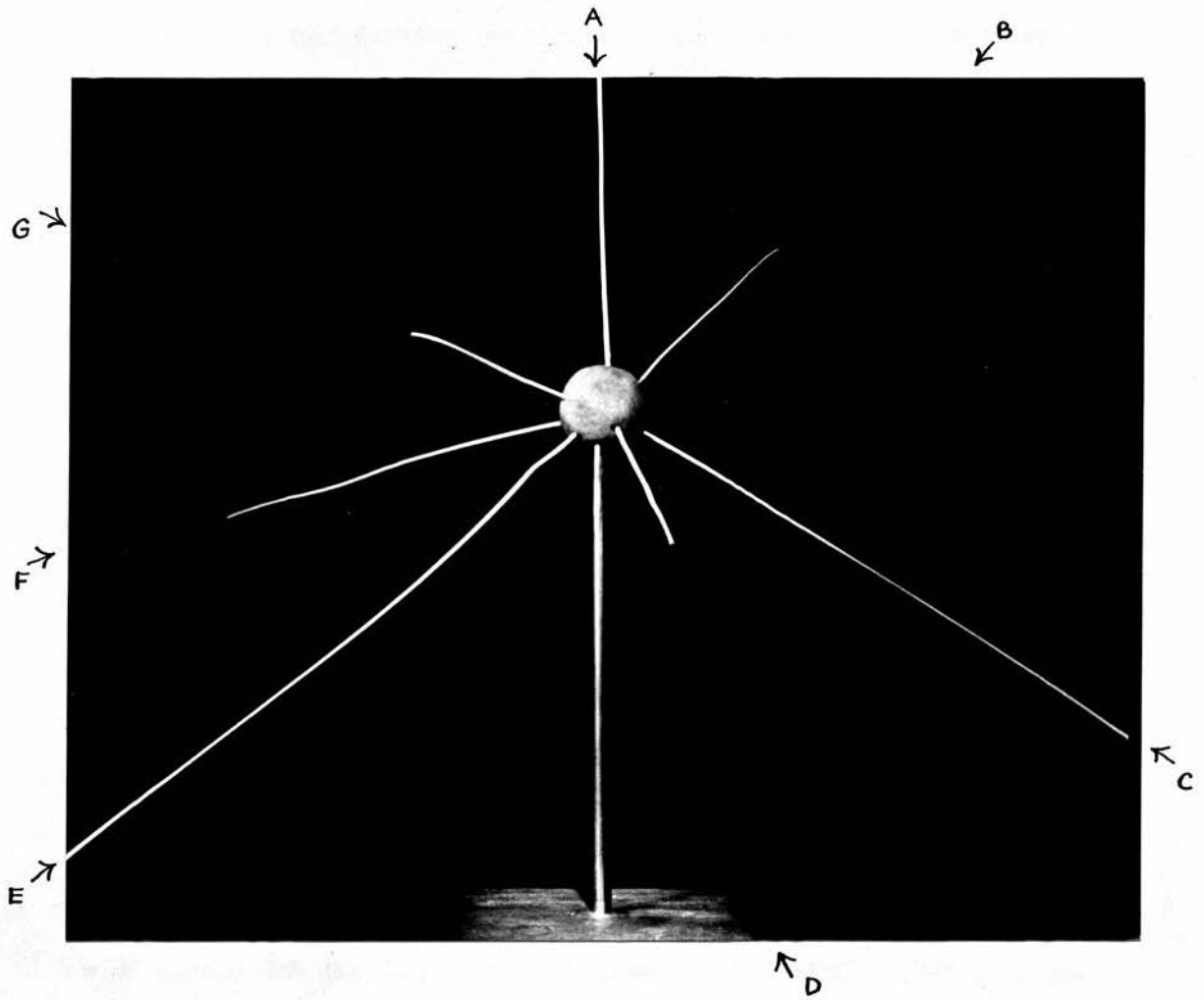

FIGURE 1 Three dimensional model of a six prong star produced by a charged particle

Track A : primary particle
Tracks C and E : grey tracks (prompt particles)
Tracks B, D, F and G : black tracks (evaporation particles)

plane of the emulsion between adjacent tracks. This method was, however, not infallible, and the reconstruction of the stars in space did not always yield further information, particularly when the direction of motion of the fast particles could not be determined, either because their tracks were too short, or because their velocities were too great to show any appreciable change in grain density along the tracks.

Many of the single proton tracks recorded during the systematic searching, and some of the tracks associated with stars, were observed to suffer a single large deflection, sometimes as great as 90°, probably as a result of an elastic collision with one of the emulsion nuclei. The criteria used to distinguish these deflections from two prong stars varied with the velocity of the particles; if the particle had a relatively high velocity, the grain densities of the two parts of the track on either side of the deflection should be equal, allowing for statistical fluctuations, as the energy loss would be small, and the change in grain density imperceptible. However, if the particle were near the end of its range, where the rate of loss of energy changes rapidly, the grain densities should correspond to those of a standard proton over the same range. In measurements of this kind it was important that changes in the inclination of the track be taken into consideration.

After the emission of the high energy and evaporation particles in a nuclear disintegration, the nucleus which remains may have a certain amount of momentum which will enable it to produce a track in the emulsion. Because of its charge, a residual nucleus is capable of ionising the silver bromide grains, but since it is massive its track can seldom exceed 5 μ in length and cannot be used to determine the charge and mass of the nuclear fragment. In an examination of the range distribution of the short tracks from nuclear disintegrations, Hodgson (1954) found that there was a sharp peak at very small ranges, which could be ascribed to nuclear recoils, superimposed on the broader distribution of low energy α-particles which extended to greater ranges. None of the very short tracks comprising the sharp peak had a range of more than 4 μ, which was in agreement with approximate calculations of the range of nuclear recoils.

All tracks with an overall range of less than 5 μ were assumed to be the tracks of recoiling nuclei, and were not included in the total prong numbers of the stars. There were, however, exceptions to this rule because in some stars more than one such low energy particle was emitted. Events of this kind are almost certainly due to the disintegration of a light nucleus as the potential barrier of a heavy nucleus is too great

to allow the emission of very low energy particles, and fission of the nucleus remaining after disintegration is most unlikely to occur at such low excitation energies. Stars of this kind were therefore classified according to the total number of visible prongs, regardless of their range.

This method of classifying stars according to the number of prongs greater than 5 μ in length, except where two or more short prongs are present, has the advantage that the assignment of star size does not depend on whether the very short tracks are visible or not. Since the recoil tracks are of very short range, they may be easily confused with long delta rays near the beginning of other tracks associated with a star. Confusion may also occur in the case of short, heavy tracks which begin in the emulsion, and suffer a single deflection as a result of a collision shortly before coming to rest. It is seldom possible to determine the direction of travel of the particles producing these tracks, and consequently a deflection may not be distinguishable from a nuclear recoil. Further, the residual nucleus may not have enough energy to produce any observable ionisation, with the result that there will not be a visible recoil track in the emulsion. Added to this is the fact that very short tracks are frequently obscured by the rather large areas of developed grains at the origins of stars and

it must therefore be concluded that the visibility of recoil tracks depends on the type and degree of development of the emulsion.

The apparent absence of a recoil track is relatively unimportant in a multi-pronged star since it does not affect the prong number, but it does cause serious errors in the estimation of the number of one prong neutron-induced stars. A single proton track in the emulsion can arise in either of two ways: it may be the result of an inelastic collision between a neutron and one of the nuclei of the emulsion, other than hydrogen, or it may be a proton recoil produced when a neutron suffers an elastic collision with a hydrogen nucleus. However, unless a nuclear recoil is produced along with the proton in the inelastic collision, it is not possible to distinguish between these two types of event, with the result that many one prong stars were erroneously classed as proton recoil tracks, and consequently the total number of cosmic ray stars was considerably reduced.

Short electron tracks originating in the stars were occasionally observed, having been produced in the decay of the nuclei which remained after disintegration. When all the fast particles and the evaporation particles have been ejected from a bombarded nucleus, the remaining nucleus may be unstable to beta-decay, and will

therefore require the emission of a low energy electron before it can achieve a stable state. These tracks, like the nuclear recoil tracks, were considered to be a property of the residual nucleus, and not of the disintegration proper, and as such were not included in the total number of prongs of the star to which they belonged.

III.3. Measurement of the tracks.

III.3.1. Range.

Three dimensional range measurements of the tracks emerging from cosmic ray stars and other events were carried out using oil immersion objectives, and x 10 or x 15 eyepieces, and the overall length of each track as it was formed in the unprocessed emulsion was obtained from measurements of its horizontal and vertical projections.

As neither the length nor the breadth of the emulsions changed in size as a result of processing (Powell, 1946), the horizontal projections measured in the processed emulsion were equal to those of the tracks as they were originally formed. Calibrated eyepiece graticules, in which one scale division was equal approximately to 1μ, were used for these measurements, and it was found that these scales could be read to 0.2μ.

For very long tracks, it was sometimes found

convenient to measure the horizontal projections by means of the stage micrometers of the Cooke, Troughton and Simms microscope, which could be read to 0.2 μ in both the x- and y-directions. Where a particle was seen to have changed direction in the course of its passage through the emulsion, the track was divided into straight line segments, and the overall lengths of all the segments were measured and summed to give the total track length. In accordance with current practice, the measurements were made between the centres of the grains which defined the segments or tracks. However, this procedure was not always possible, because the exact point of origin of a track emerging from a star could not be accurately located, and depth differences across small segments of steep or heavy tracks were often difficult to measure.

Vertical measurements were made by means of the graduated fine-focusing adjustment of the microscope, which was always racked upwards to minimise mechanical lag, and although the number of microns represented by one scale division varied widely from one microscope to another, it was possible to read the scale to 0.2 μ on the Cooke microscope, and to 0.5 μ on the Prior microscope. However, the total error in a depth measurement depended also on the shrinkage factor of the emulsion, and on the limitations imposed on the accuracy by the

finite depth of focus of the microscope, and by the imperfections in its focusing mechanism.

Before measuring the vertical projections of the tracks, it was necessary to determine the relationship between the true vertical projection in the unprocessed emulsion, and the reading of the fine adjustment scale. Originally the emulsions were 400 μ thick, but during processing the top surfaces were rubbed to remove surface stain, and this was assumed to have reduced the thickness to 390 μ. The method of calibrating the fine adjustment scale was then to find the average distance, in scale divisions, between developed grains on the top and bottom surfaces of the emulsion, and since this reading represented 390 μ of unprocessed emulsion, the change in depth for a scale reading difference of one division could be readily determined. This constant, which depends on the shrinkage factor of the emulsion and on the refractive index between the emulsion and the immersion oil, was assumed to hold for all tracks in a given area of plate, regardless of their inclination and position relative to the emulsion surface.

Owing to the variation in the humidity of the atmosphere in the laboratory throughout the day, the emulsion thickness varied with time, making it necessary to calibrate the fine adjustment scale very frequently. A day to day change of up to 8% in the depth of the

emulsion was not uncommon, and it was in fact found convenient to determine the conversion constant as each set of readings was taken. In this way, allowance was made for variations in thickness due to changes in humidity and also for non-uniformity of the processed emulsion.

III.3.2. Angle.

Measurements of the angle between two tracks were made by determining the x-, y- and z-coordinates (x- and y-directions in the plane of the emulsion), of three points, one on each track and the third at the junction of the two tracks. The angle was then calculated using the well-known cosine law:

$$\cos\theta = \frac{(x_1-x_2)(x_1-x_3)+(y_1-y_2)(y_1-y_3)+(z_1-z_2)(z_1-z_3)}{\sqrt{\left[(x_1-x_2)^2+(y_1-y_2)^2+(z_1-z_2)^2\right]}\sqrt{\left[(x_1-x_3)^2+(y_1-y_3)^2+(z_1-z_3)^2\right]}}$$

In this way, the angle could be determined to within approximately 5°.

Angle measurements of this kind were sufficiently accurate to allow the identification of elastic collisions between protons in the incident radiation and hydrogen nuclei in the emulsion. After an elastic collision between a moving particle of mass m_1 and a stationary particle of mass m_2, the directions of motion of the two particles are defined by the equation

$$\frac{m_1}{m_2} = \frac{\sin(\theta_1 + 2\theta_2)}{\sin\theta_1}$$

where θ_1 and θ_2 are the angles which the paths of m_1 and m_2 make respectively with the original direction of motion of m_1. Where the two masses are equal, as in the case of a proton and a hydrogen nucleus, the angle between their paths after collison, ($\theta_1 + \theta_2$), is 90°. Elastic collisions of this kind may thus be distinguished from inelastic events in which a proton produces a two prong star, because the probability that the two star prongs will be at right angles to each other is very small.

Chapter IV.

PARTICLE IDENTIFICATION.

In any study of the nuclear disintegrations produced in a photographic emulsion, the main problem is the identification of the particles responsible for the disintegrations and of the secondary particles which they produce. The parameters required for the complete specification of a particle are the ratio of its charge Ze (where Z is the atomic number and e the electronic charge) to its mass m, and β, the ratio of the velocity v of the particle, to c, the velocity of light. When the charge of a particle is known, the problem of identification becomes a matter of determining m and β alone, and for this purpose at least two equations containing these parameters are required.

The most important factors in the identification of a particle are the following properties of its track:

(1) grain density, which is a function of Z and v,

(2) residual range, which depends only on the kinetic energy of the particle, and on the rate of energy loss and is therefore a function of m, Z, and v,

(3) delta-rays, whose density is a function of Z and v,

(4) multiple scattering, which is a function of $\frac{p\beta}{Z}$, where p is the momentum of the particle.

When the results from either (1) or (3) are combined

with the information obtained from either scattering or range measurements, the nature of the particle may be established, but grain density and delta-ray measurements taken together are not sufficient.

In the identification of particles which are brought to rest in an emulsion, the residual range is commonly used in conjunction with one of the other track parameters. However, in the case of particles which escape from the emulsion, the residual range cannot be determined, and the values of m and β must be obtained by combining the results from grain density and multiple scattering measurements. Where there are other known particles available for comparison, it is sometimes possible to determine the nature of a particle from measurements of the variation of grain density, scattering parameter or delta-ray density over a known range of the track. In the present work, this second method was found to be the most practicable and reliable as it involved only one type of measurement apart from a determination of distance along the track. Grain density was the parameter used as it could be more accurately determined than either the scattering parameter or the delta-ray density. The variations of grain density with velocity, residual range and kinetic energy have been calculated and will be described in Chapter VI.

The applications of grain density, range, delta-ray

and multiple scattering measurements to the tracks of particles travelling through an emulsion will now be considered.

IV.1. Grain density.

When a charged particle passes through matter, it loses energy chiefly as a result of three different processes:

(a) inelastic collisions with the atoms, in which energy is transferred directly to the atoms resulting in ionisation or excitation.

(b) inelastic collisions with the nuclei of the atoms which result in their disintegration and the production of stars.

(c) the emission of radiation (Bremsstrahlung).

Of these, (b) and (c) are nuclear processes, while (a) involves only the orbital electrons of the atoms. A heavy particle, as for example a proton or a π-meson, can lose its energy either gradually by (a) or catastrophically by (b), but a μ-meson which seldom produces stars will lose energy by ionisation and excitation only. The contribution of the process (c) to the total energy loss of these particles is extremely small and can be neglected unless the velocity of the particles is very great. Electrons, on the other hand, are involved in the processes (a) and (c), and at very high

velocities (c) is responsible for the major part of the energy loss.

The amount of energy lost in ionisation by particles passing through matter was first calculated by Bohr (1913) using the classical theory, and since then more precise investigations have been carried out on a quantum mechanical basis, by many authors. An expression for the energy lost per centimetre of its path by a particle travelling through a stopping medium is given by the following formula (Livingston and Bethe, 1937):

$$-\frac{dE}{dx} = \frac{4\pi e^4 z^2 NZ}{mc^2\beta^2}\left[\log_e \frac{2mc^2\beta^2}{I(1-\beta^2)} - \beta^2\right] \qquad (1)$$

where ez= the charge of the incident particle

β = its velocity relative to that of light, c

m = the electronic mass

N = the number of atoms per cm.^{3} of the stopping medium

Z = the atomic number of the stopping medium

I = the average excitation potential of the atoms.

While this equation is subject to certain conditions, and requires the addition of a correction term for slow particles in a medium of high atomic number, it is valid for all energies of interest in this work. When $\beta = 0.94$, the expression has a minimum value, and when $\beta > 0.94$ the rate of loss of energy increases slowly with velocity. At very high velocities ($\beta > 0.98$)

the equation (1) must be modified on account of polarisation effects. For slow particles, the equation may be written

$$-\frac{dE}{dx} = A\frac{z^2}{\beta^n} \qquad (v \ll c)$$

where A is a constant and n has a value between approximately 1.4 and 2, depending on v. Thus, the energy loss increases rapidly as the velocity decreases.

A charged particle travelling through a photographic emulsion, which consists of silver halide grains in gelatin, produces ionisation of the atoms of the emulsion. As a result of this ionisation, the silver halide grains will become developable provided a certain minimum number of ions has been formed within each one. If a smaller number of ions is formed, the grains will not be visible in the developed plate, and thus the ability of an emulsion to record the passage of particles of a given velocity depends upon the average number of ions which must be produced in the grains in order to render them developable.

It follows therefore that the number of developed grains per unit length of a particle track depends upon the ionisation which the particle produces, and this in turn is a function only of the energy lost by the particle in its passage through the emulsion. Thus, the

grain density n (usually expressed in units of grains/ 50 μ) may be expressed as a function of the velocity and charge of the particle, and is independent of the mass.

$$n = f_1(z, v)$$

At very high velocities, where the rate of loss of energy is small, the ionising power of a particle will be such that it allows only a few grains per unit length of the track to become developable. Conversely, at low velocities sufficient energy will be released to produce ionisation of all the available grains. For all singly charged particles travelling with the same velocity, the grain densities along their tracks will be equal.

The experimental methods of determining the grain density along a track will be considered in detail in the next chapter, and in Chapter VI the relationship between grain density and energy loss will be derived.

IV.2. Residual range.

The residual range R(E) of a particle of kinetic energy E may be defined as the distance which the particle will travel before its kinetic energy becomes so small that it can no longer produce ionisation. Since this distance depends only on the kinetic energy and charge of the particle and on the stopping power of the material through which it is travelling, it follows that for a given medium the range is a function only of kinetic

energy and charge of the particle; thus

$$R(E) = mf_2(v,z)$$

If two particles of equal charge, and masses m_1 and m_2, are travelling with the same velocity, it may be shown that

$$\frac{R_1}{R_2} = \frac{m_1}{m_2}$$

and at these points their tracks will have equal grain densities.

Methods of measuring the range of tracks in the developed emulsion have already been described.

IV.3. Delta-rays.

In the equation (1) the energy lost per centimetre of its path by a particle travelling through a medium includes the rare large transfers of energy which do not contribute to the ionisation of the grains along the path of the particle, as the energy is received by the orbital electrons of the atoms which are then capable of producing ionisation on their own account. The short tracks of these electrons, known as delta-rays, appear as small protuberances on either side of the main track, and their density in any portion of its track gives a measure of the velocity of the particle at that point of its residual range, provided its charge is known.

An expression for d, the total number of delta-rays

per unit length of track, which have energies between ω_1 and ω_2, may be obtained from the Thomson formula:

$$d(\omega_1, \omega_2) = \frac{2\pi N e^4 z^2}{m v^2}\left(\frac{1}{\omega_1} - \frac{1}{\omega_2}\right) \qquad (2)$$

where N = number of electrons per cm.^{3} of emulsion

m = mass of the electron

ze = charge of the incident particle

v = velocity of the incident particle.

If $\omega_2 = 2mv^2$, the maximum energy which a heavy particle, travelling at non-relativistic velocity, can transfer to an electron, the equation (2) becomes

$$d(\omega_1, \omega_2) = \frac{2\pi N e^4 z^2}{m v^2}\left(\frac{1}{\omega_1} - \frac{1}{2mv^2}\right) \qquad (3)$$

From this equation it follows that the delta-ray density is a function of both velocity and charge, and varies as z^2. This equation applies only to non-relativistic particles; for particles travelling at relativistic velocities the form of ω_2 given above must be replaced by

$$\omega_2 = \frac{2\mu\beta^2}{1-\beta^2} \qquad (\mu = mc^2)$$

It may be seen from equation (3) that when the velocity of the particle

$$v < \sqrt{\frac{\omega_1}{2m}}$$

no delta-rays of energy greater than ω_1 can be produced, and that above this critical cut-off the density of delta-rays will rise to a maximum when the velocity of

the particle

$$v = \sqrt{\frac{\omega_1}{m}}$$

Far beyond this maximum, the density will vary inversely with the square of the particle velocity. The value of ω_1, the minimum delta-ray energy, is chosen according to the range of the shortest delta-rays recognisable, and depends upon the mass of the particle. In general, $5 \text{ keV} < \omega_1 < 20 \text{ keV}$.

Experimentally, the number of delta-rays with ranges greater than a certain minimum (determined by ω_1) is obtained in successive intervals along the track of an unidentified particle, and from these values, the density of delta-rays for different values of the residual range is calculated. By comparing these distributions with those of particles of known mass and charge, the identity of the particle may be established.

Demers and Lechno-Wasiutynska have calculated the linear delta-ray densities for particles of different mass and charge, up to a residual range of 100 metres in emulsion, using a form of the equation (3) which includes the relativistic correction. Using the curves drawn by these authors, it is in principle possible to identify slow particles by their delta-ray distributions, and to determine the residual range of particles of known mass.

In practice, this procedure is limited because of the difficulty of distinguishing the shorter delta-rays

from other parts of the main track. Many are hidden from view by the track itself, and others may be confused either with background grains or with track grains displaced from the line of the track. Despite these experimental difficulties, however, the method was successfully used for the identification of some low energy π^- mesons, protons and α-particles.

IV.4. Multiple Coulomb scattering.

When a charged particle traverses a medium it suffers frequent small angle deflections due to elastic collisions with the nuclei of the atoms composing the medium. At high energies, the effect of scattering on a particle is small, but as the velocity decreases the effect becomes greater and may be observed towards the end of the track of any particle in a photographic emulsion. The mean projected deflection, $\bar{\alpha}(t)$, experienced by a particle in traversing a path length t in a scattering medium, gives a measure of the quantity $\frac{p\beta}{z}$ where p is the momentum of the particle.

i.e. $$\frac{p\beta}{z} = \frac{K_s t^{\frac{1}{2}}}{\bar{\alpha}(t)}$$

where K_s is known as a scattering constant. From a knowledge of the scattering parameter $\bar{\alpha}(t)$, at a given residual range, it is possible to establish the identity of unknown particles.

This method of identifying cosmic ray particles brought to rest in an emulsion, by investigating the multiple Coulomb scattering along their tracks, was first employed by Bose and Chouduri (1941), and has since been extensively developed by many workers. In principle, the method is similar to that applied to tracks in Wilson cloud chambers operated in a magnetic field, and the analysis of emulsion tracks by this method is based on theoretical studies of the behaviour of fast charged particles in a scattering medium by Williams (1939, 1940), Molière (1948) and others.

IV.4.1. Experimental Procedure: A. The coordinate method.

Several methods of determining the scattering parameter $\bar{\alpha}(t)$ in emulsions have been suggested by different authors, but in the present work only one of these, the "coordinate" or "sagitta" method was used. As described by Fowler (1950), the procedure is to align the track parallel to one direction of motion of the microscope stage, usually the x-direction, and with the eyepiece scale perpendicular to the track, lateral track coordinates y_1, y_2, y_3 etc., are read at successive displacements t along the x-direction, over the required portion of the track. The first differences of successive coordinate readings, $S_1 = y_1 - y_2$, $S_2 = y_2 - y_3$ etc., give a measure of the inclinations of adjacent chords in

the track, and from the second differences, $S_1 - S_2$, $S_2 - S_3$ etc., the deviations D_1, D_2 etc., between successive chords are obtained. The arithmetic mean of these deviations,

$$\bar{D} = \frac{\sum_n |D|}{n}$$

determined without regard to sign, from the n individual values of second difference in the track, can then be used to evaluate the scattering parameter and the quantity $\frac{p\beta}{z}$ using the relations:

$$\bar{\alpha}(t) = \frac{\bar{D}}{t} \times \frac{180}{\pi} \text{ degrees} \quad (4)$$

and

$$\bar{\alpha}(t) = \frac{K_s z t^{1/2}}{p\beta} \times 10^{-1} \text{ degrees} \quad (5)$$

where K_s is the "scattering constant" for the emulsion, $p\beta$ is in units of MeV/c and all lengths are measured in microns. K_s is in units of MeV degree/$(100\,\mu)^{\frac{1}{2}}$.

A Prior binocular microscope fitted with a rotating stage and a micrometer adjustment on the x-motion of the stage was used for all multiple scattering measurements. The advantage of the rotating stage was that the tracks could be quickly and easily aligned in the required direction, and maintained accurately in position while the measurements were made. Values of y were determined at intervals along the track, the distance between successive readings being 25μ, or more when the tracks were formed by very fast particles. From these observations, the mean deviations $\bar{D}(t)$ were calculated for

overlapping cells of different lengths.

It was found that the most convenient method of analysing the data was to set out the readings as shown in the scheme below (Table IIIa), where as an example overlapping cells of 100 μ are obtained from readings taken every 25 μ along the track of a cosmic ray particle. In the first four columns, the values of y are entered in order, and from these the first differences for 100 μ cells, $S_n = (y_n - y_{n+4})$, and the second differences $D_n = (S_n - S_{n+4})$ are obtained; the two sets of differences are entered in their respective columns as illustrated. The mean value of the deviation, $\bar{D}(100\mu)$ is then calculated from the sum of all the second differences D_n, which can be conveniently found and checked by adding the columns both vertically and horizontally. As each D_n is determined from three readings of y, it follows that in each vertical row of the third set of columns only every third value is statistically independent, although each one is independent of the others in the same horizontal row, at least so far as readings errors are concerned. The numerical values shown in the second part of the table (IIIb) have been taken from the measurements made on a track of one of the cosmic ray stars. Figures in the first four columns are the readings on the eyepiece scale in units of 0.1 scale divisions (1 scale division = 0.834 μ).

Table III.

(a)

y_1	y_2	y_3	y_4								
				S_1	S_2	S_3	S_4				
y_5	y_6	y_7	y_8					D_1	D_2	D_3	D_4
				S_5	S_6	S_7	S_8				
y_9	y_{10}	y_{11}	y_{12}					D_5	D_6	D_7	D_8
				S_9	S_{10}	S_{11}	S_{12}				
y_{13}	y_{14}	y_{15}	y_{16}					D_9	D_{10}	D_{11}	D_{12}
				S_{13}	S_{14}	S_{15}	S_{16}				
y_{17}	y_{18}	y_{19}	y_{20}					D_{13}	D_{14}	D_{15}	D_{16}
				S_{17}	S_{18}	S_{19}	S_{20}				
y_{21}	y_{22}	y_{23}	y_{24}								

(b)

22	21	20	18								
				4	5	5	2				
18	16	15	16					0	5	5	0
				4	0	0	2				
14	16	15	14					1	1	2	3
				3	1	2	$\bar{1}$				
11	15	13	15					7	1	4	2
				$\bar{4}$	0	$\bar{2}$	$\bar{1}$				
15	15	15	16					4	1	1	3
				0	$\bar{1}$	$\bar{1}$	$\bar{4}$				
15	16	16	20					0	3	3	9
				0	2	2	5				
15	14	14	15								

A similar analysis of the data was made to determine the values of D, and hence of $\bar{\alpha}$, for different values of t, ranging from 50μ to 400μ, or more depending on the nature of the track under observation. The relation between the scattering parameters for varying cell lengths is:

$$\frac{\bar{\alpha}(t_1)}{\bar{\alpha}(t_2)} = \left(\frac{t_1}{t_2}\right)^{1/2} \qquad (6)$$

In general, the quantity $\frac{p\beta}{z}$ was evaluated using $\bar{\alpha}(100\mu)$ which can be obtained by means of equation (6) from any of the $\bar{\alpha}(t)$; for cell lengths of 100μ, equation (5) is reduced to

$$\frac{p\beta}{z} = \frac{K_s}{\bar{\alpha}(100\mu)} \qquad (7)$$

with $p\beta$ in MeV/c as before.

The problem of determining the value of this scattering constant K_s, which is applicable to emulsions, has been the subject of many experimental and theoretical studies. Williams (1940) expressed the mean projected deflection, $\bar{\phi}$, experienced by a particle of charge ze, traversing a path length t in a scattering medium of atomic number Z, containing N atoms per unit volume, as

$$\bar{\phi} = \frac{2e^2(NZ^2)^{1/2}\, t^{1/2}\, z}{p\upsilon} \left[\log_e\left(\frac{\phi^2_{max}}{\phi^2_{min}}\right)\right]^{1/2} \qquad (8)$$

where the angle ϕ_{max} is the greatest single scattering angle which can contribute to the observed deflection, and ϕ_{min} is an effective minimum angle. An expression

† For a given value of $p\beta$ the cell size must be chosen so that

(i) the signal-to-noise ratio has at least the minimum acceptable value (~2)

(ii) a sufficient number of independent readings of D is obtained in the limited region of track over which $p\beta$ is constant.

Thus, long cells are required for the tracks of fast particles, and short cells for the tracks of slow particles. However, since the scattering constant increases with cell size, and decreases with increasing velocity, the values of K_s appropriate to these two sets of tracks will not differ appreciably.

for ϕ_{min} was derived by Moliere (1947, 1948) by making an exact quantum mechanical calculation of the cross section for single scattering.

From the equation (8) it follows that the scattering constant has a value of $2e^2(NZ^2)^{1/2} \times L$ where L is the logarithmic factor in the above equation. L depends chiefly on the properties of the scattering medium, and also upon the velocity of the particle and the cell length chosen. Thus K_s, the scattering constant, is in fact not a constant, and it may be shown that it increases with cell size, and decreases with increasing velocity.

see below †

In the present work, the value of K_s used for the tracks of particles no matter what their velocity was that determined experimentally by Gottstein et al., namely

$$K_s = 26.0 \text{ MeV degree}/(100\mu)^{\frac{1}{2}}.$$

These authors suggest that for the tracks of particles other than electrons, this value of the scattering constant may be used over the whole range of measurement, except perhaps in the extreme relativistic region where $\beta^2 \rightarrow 1$, and that its use over this region cannot introduce a systematic error greater than $\pm$ 8%.

see opposite †

Corrections to the mean values of the second differences used in the determination of the scattering parameter included a "cut-off" for large deflections and

† These variations of K_s have been confirmed experimentally by Gottstein et al. (Ref. 27 and 60-63) using protons, π-mesons, and positrons in photographic emulsions.

an estimation of the "noise-level scattering". The first correction, which requires the elimination of all values of D greater than a certain minimum value, arises from the fact that there is a finite probability that a particle which is traversing a scattering medium will suffer a single large deflection as the result of a collision with one of the atoms of the medium. Deflections of this kind must be distinguished from the true multiple Coulomb scattering of the particle. Goldschmidt-Clermont et al. (1948) have shown that this cut-off is best applied at a scattering angle equal to $4\bar{\alpha}_{co}$, where $\bar{\alpha}_{co}$ is the arithmetic mean of all values of α less than the cut-off. In relation to the present work, this indicates a cut-off at a deviation of $4\bar{D}_{co}$.

The method of determining $\bar{D}_{co}$ was first to calculate the mean of all the second differences, say $\bar{D}_1$, and to exclude from a second evaluation of the mean all those differences which were greater than $4\bar{D}_1$. Second differences greater than $4\bar{D}_2$ were next excluded, and the procedure of calculating mean values was continued until all the second differences remaining were smaller than 4 times the final mean. This value was then $\bar{D}_{co}$. In order to avoid confusion with suffixes, it will be assumed in all that follows that $\bar{D}$ refers to the mean second difference with cut-off.

The values of $\bar{D}$ are found to decrease with

decreasing cell size only to a certain point; for the smallest cells $\bar{D}$ becomes very nearly constant and independent of t. This is due to what is commonly termed "noise-level scattering" which consists of those apparent charges in track direction not caused by true particle scattering. There are three main components determining the magnitude of the noise-level scattering, each of which has, in general, an approximately Gaussian distribution:

$\bar{d}_1$ due to the random distribution of the centres of the developed grains about the true path of the particle,

$\bar{d}_2$ introduced by reading errors, and errors in the alignment of the track,

$\bar{d}_3$ due to random irregularities in the stage motion, and the noise-level $\bar{D}_n$ is defined as the root mean square value of the sum of these three statistically independent errors

$$\bar{D}_n = \left(\bar{d}_1^2 + \bar{d}_2^2 + \bar{d}_3^2 \right)^{1/2}$$

Various methods of eliminating these errors have been suggested, and in the present work the following method was applied. It can be seen from equations (4) and (5) (page 36) that the mean deviation $\bar{D}$ can be expressed by the relation

$$\bar{D} = \frac{K_s z t^{3/2}}{p\beta} \times 10^{-1} \times \frac{\pi}{180} \qquad (9)$$

For a given track, provided the change in energy over the measured region is small, the quantity

$\frac{K_s z}{\rho\beta} \times 10^{-1} \times \frac{\pi}{180}$ is approximately constant, and the equation (9) may be expressed in the form:

$$\bar{D} = Ct^{3/2}$$

from which it follows that

$$(\bar{D})^2 = C^2 t^3 \qquad (10)$$

This implies that the graph of $(\bar{D})^2$ as a function of t^3 is a straight line passing through the origin, but this will be the case only if the contribution of the noise-level scattering is zero. Where this contribution is not zero, the equation (10) must be replaced by

$$(\bar{D})^2 = C^2 t^3 + (\bar{D}_n)^2 \qquad (11)$$

where $\bar{D}_n$ represents the resultant noise-level. Thus, in order to determine $(\bar{D}_n)^2$, the mean second differences, with cut-off, were calculated for different cell lengths, and the values of $(\bar{D})^2$ plotted against t^3. The value of $(\bar{D}_n)^2$ was then found from the position of the intercept on the y or $(\bar{D})^2$ axis, of the best straight line through all the experimental points except those representing the very small cells which were not always consistent with the other results.

For 25μ and 50μ cells, reading errors assume great importance, and in some cases they may be out of all proportion to the quantity being measured. On the other hand, the use of long cells limits the number of independent observations available for calculating $\bar{D}$, and it is therefore necessary to choose cell lengths

which will allow a large enough number of observations without introducing large reading errors.

When the contribution of the noise-level scattering was known, the mean deviations and the mean scattering parameter, $\bar{\alpha}_{100}$, were determined, and substitution in the equation (4) then gave a measure of the quantity $\frac{p\beta}{z}$. Alternatively $\frac{p\beta}{z}$ could be calculated directly from the slope of the graph of $(\bar{D})^2$ as a function of t^3, given the value of the scattering constant.

An illustration of the application of this method is given by the following results, which were obtained from the track of the ionising primary of one of the cosmic ray stars observed during the systematic searching of the plates. Over the entire range in the emulsion, nearly 14 mm., the grain density of the track was 25 grains/50μ, and from this it was concluded that the particle was singly charged, as the minimum grain density which can be produced by a doubly charged particle is approximately 50 grains/50μ. Of all the singly charged particles, those which most frequently produce stars are protons and negative π- mesons, deuterons and K-mesons, and it was in order to establish the identity of this primary that multiple scattering measurements were made on its track.

Readings of the lateral track coordinates were made every 50μ along the entire track, and from these observations the mean deviations, with cut-off, were

calculated for overlapping cells of lengths between 100 μ and 400 μ, using the method described on page 37. The values of these mean deviations are given in Table IV where the uncertainties quoted are the standard deviations calculated from the independent values of the second differences, that is those in every third row of the scheme as described previously. Also shown in this table are the numbers of cells used in the calculations of the mean deviations with cut-off.

Table IV.

$t\ \mu$	Number of overlapping cells of $t\ \mu$	$\bar{D}$
100	271	0.218 ± 0.018
150	270	0.27 ± 0.022
200	271	0.331 ± 0.027
250	269	0.418 ± 0.033
300	267	0.495 ± 0.045
350	264	0.631 ± 0.054
400	263	0.76 ± 0.062

In Table V, the values of t^3 and $(\bar{D})^2$ are given, and from these the graph of $(\bar{D})^2$ as a function of t^3 was plotted, as shown in figure 2. For convenience the values of the cell length t in Table V are given in units of 50 μ.

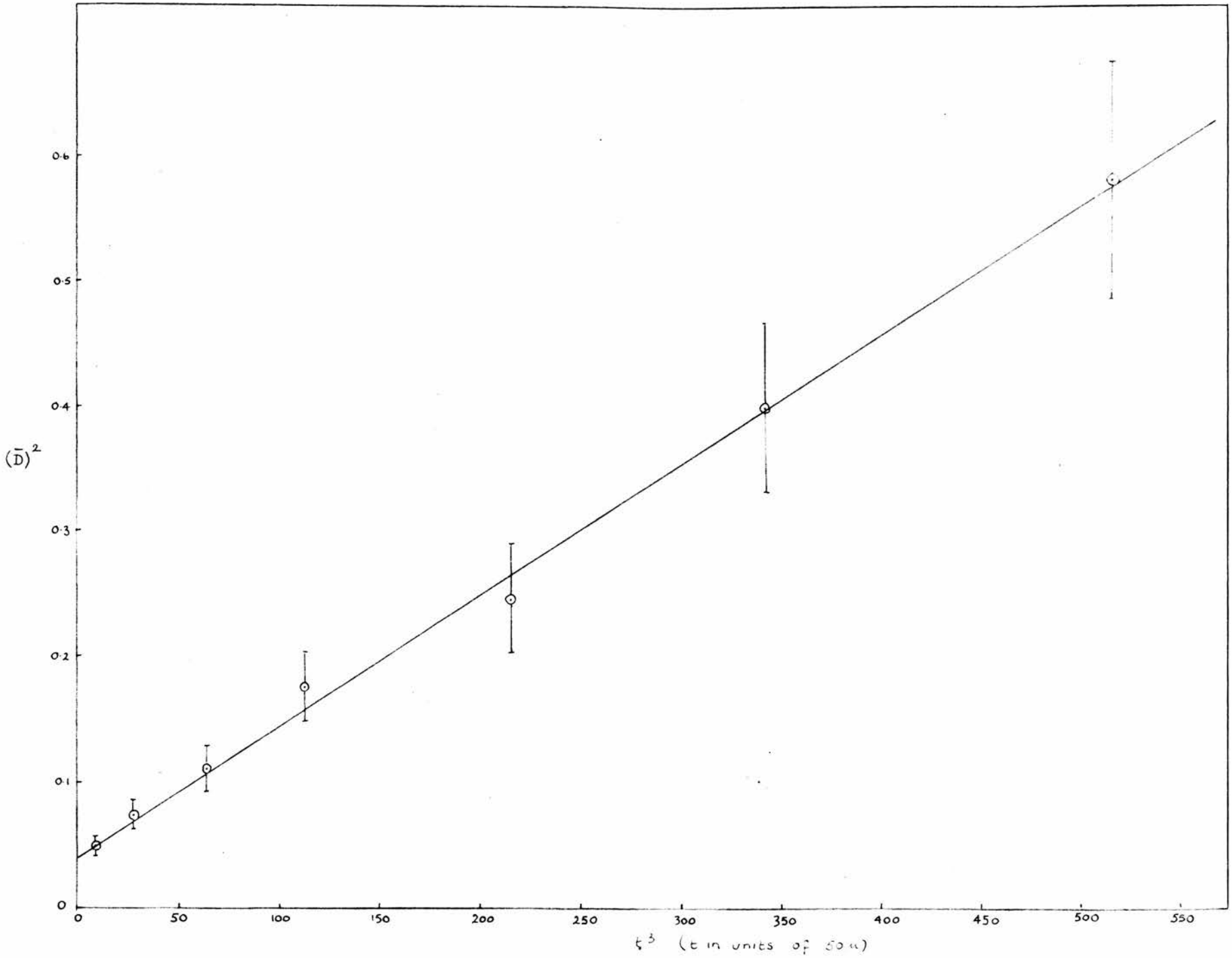

FIGURE 2 Graph of $(\bar{D})^2$ v. t^3 for the track of a fast particle in an Ilford G5 emulsion, where $\bar{D}$ is the mean deviation and t the cell length measured in units of 50 μ.

Table V.

t^3	$(\bar{D})^2$
8	0.048 ± 0.008
27	0.073 ± 0.012
64	0.110 ± 0.018
125	0.175 ± 0.028
216	0.245 ± 0.045
343	0.398 ± 0.068
512	0.58 ± 0.09

The constants in the equation (11)

i.e. $$(\bar{D})^2 = C^2 t^3 + (\bar{D}_n)^2$$

together with their uncertainties, were calculated from the straight line graph by the method of least squares, with the following results:

$C^2 = (1.043 \pm 0.015) \times 10^{-3}$ (t in units of 50μ)

$(\bar{D}_n)^2 = 0.040 \pm 0.004$

where $C = \frac{K_s z}{p\beta} \times 10^{-1} \times \frac{\pi}{180}$ as before, and $\bar{D}_n$ represents the noise-level.

Using these results, it was then possible to determine the value of the quantity $\frac{p\beta}{z}$ for the ionising primary, and further to calculate its momentum, velocity and kinetic energy. Given the value of the scattering constant, K_s = 26.0 MeV degree/$(100\mu)^{\frac{1}{2}}$, the charge z = 1, and C^2 the slope of the graph as above, it

Table VIa

Particle	β	E MeV.	n grains / 50μ
Deuteron	0·48	264	45
K-meson	0·79	306	20

was found that

$$p\beta = 497 \pm 4 \text{ MeV/c}$$

the uncertainty being calculated from the error in c^2. This uncertainty, however, does not include the systematic errors due to factors such as the curvature of the track, irregularities in the stage motion other than those allowed for in $\bar{d}_3$ (see page 41), and the adoption of a constant value of K_s regardless of the cell size and particle velocity. A more realistic estimation of the total error involved would be of the order of ± 10%.

From this value of $p\beta$, the corresponding kinetic energies and β values for a proton, a deuteron, and K and π - mesons were calculated, as shown in Tables VI, VIa. The grain densities appropriate to these β values were obtained from the graph of grain density (n) as a function of β which appears in figure 20 and will be described in Chapter VI.

Table VI.

Particle	β	E MeV	n grains/50
Proton	0.64	286	28
π - meson	0.96	382	13

It is clear from these results that the only possible primary particle is a proton.

Measurements of the scattering parameters of the

tracks of high energy particles which produce little ionisation, proved unsatisfactory for several reasons. In the first place, systematic curvature of the track, introduced by distortion of the emulsion and mechanical imperfections in the stage motions of the microscope, causes apparent deviations in the tracks, which are often considerably greater than the deviations due to multiple scattering. [redacted]

The background grains in the emulsion can also have a serious effect on the scattering measurements on a thin track, where it is not always possible to distinguish them from the grains which belong to the track. In the course of the measurements, many of the readings had to be made in the gaps between the grains, and in these cases the value of "y" was assumed to be the mean of the readings for the grains on either side. If one of these grains was in fact a background grain lying near the track, not only would the value of y be incorrect, but the first and second differences and the mean deviation would also be affected. The magnitude of the errors introduced by background grains will vary according to the conditions, as it depends on the ability of the observer to distinguish the track grains, on the

degree of ionisation of the track, and on the density of the background.

A further disadvantage of the small angle scattering method as a means of measuring the energy of fast particles arose from the necessity of using cells which were long enough to give an acceptable signal-to-noise ratio. This condition limited the choice of tracks for scattering measurements to those whose range in the emulsion was great enough to give a useful number of observations. Steep tracks, and those which showed evidence of distortion, also proved unsuitable for this type of measurement.

In general, the method of estimating energy by means of the scattering parameter was confined to those particles whose tracks had a grain density of more than 20 grains/50μ, and which showed little or no change in velocity over the portion of track under observation. It was of use particularly in finding the energies of several particles assumed to be protons which were used for calibration purposes (see Chapter VI), and as a means of verifying results obtained by other methods.

IV.4.2. Experimental Procedure: B. The constant sagitta method.

Multiple Coulomb scattering measurements were also used in combination with range measurements in the estimation of the mass of singly charged particles. For this purpose, the constant sagitta method described by

* [These measurements were made using a series of cell lengths (calculated by Dilworth et al.) which are half those suitable for a π-meson. The mean value of the second differences D, for cell lengths of 2, 3, 4 etc. times the fundamental cell were calculated, and the noise-level was found as in the coordinate method. The mean value of D which was approximately 4 times the noise-level was then used to determine the mass of the particle. For π-mesons and protons, the values of $\bar{D}$ used, were those corresponding to cell lengths of 2 and 4 times the fundamental cell.]

Dilworth et al. (1954) was used, in which the cell length is varied continuously along the track so that the second differences are kept constant over the whole residual range, and measurements are always made at the optimum cell length. This method is applicable only to particles which come to rest in the emulsion, or whose residual range at a given point is known, and is of use only as a means of estimating the mass of these particles (i.e. the stopped particles).

As in the previous method, the tracks were aligned parallel to the x-motion of the stage, and readings were taken of the positions, y, of the grains at the ends of successive cells. From these results, the mean value of the second difference $\bar{D}$ was determined, for the appropriate cell length, with the usual correction for noise and the cut-off for large angles. The mass M of the particle was then determined by comparing this value with the mean second difference obtained from the track of a known particle.

Following the technique of Dilworth et al., the measured $\bar{D}$ were reduced to a standard D_s by applying a correction factor λ^{-1} which is a function of the range and of the mass of the particle, and takes account of variations in the scattering constant with range and cell length, and of the range-energy relation at low energies. Values of λ^{-1} are given by Dilworth et al. For protons, these authors found (taking $K_s = 24$ MeV degree/$(100\mu)^{1/2}$ and using cell lengths equal to 4 times the fundamental cell):

In traversing a path length $t\mu$ in a scattering medium, a particle experiences a projected deflection $\alpha(t)$ given by

$$\alpha(t) = \frac{K_s z t^{1/2}}{p\beta} \times 10^{-1} \text{ degrees.}$$

Now, in the non-relativistic region, $p\beta \simeq 2E$ where E is the energy of the particle in MeV, and, provided the residual range R (in μ) is not too small, E may be written approximately

$$E = 0{\cdot}251\, z^{1{\cdot}16} M^{0{\cdot}42} R^{0{\cdot}58}$$ where ze is the charge of the particle, and M its mass in units of proton mass.

Thus $$\alpha(t) = 0{\cdot}199\, K_s t^{1/2} z^{-0{\cdot}16} M^{-0{\cdot}42} R^{-0{\cdot}58}$$

and D, the second difference of the sagitta is

$$D = \alpha(t) \times t \times \frac{\pi}{180} = 0{\cdot}00348\, K_s t^{3/2} z^{-0{\cdot}16} M^{-0{\cdot}42} R^{-0{\cdot}58}.$$

In the tracks of slow particles, where short cells are used, the noise-level in the measurement of y is practically independent of t. Thus, the signal-to-noise ratio is independent of t provided D is kept constant, i.e. provided t is chosen so that

$$t^{3/2} \propto K_s^{-1} z^{0{\cdot}16} M^{0{\cdot}42} R^{0{\cdot}58},$$

and measurements may be made at optimum cell length over the whole track.

The masses M_1 and M_2 of two particles are then in the ratio

$$\frac{M_1}{M_2} = \left(\frac{\bar{D}_2}{\bar{D}_1}\right)^{2{\cdot}38}$$

where $\bar{D}_1$ and $\bar{D}_2$ are the mean values of the second differences for the two tracks (with the appropriate corrections for noise-level and cut-off).

$$D_{sp} = 0.565$$

and so the mass of an unidentified particle may be calculated from the relation which is derived as shown opposite :

$$\frac{M}{M_p} = \left(\frac{D_{sp}}{D_s}\right)^{2.38} = \left(\frac{0.565}{\lambda^{-1} D}\right)^{2.38}$$

The errors involved in a mass determination of this type arise from sources similar to those discussed earlier, with the exception of the errors which are peculiar to thin tracks. Percentage errors in the mass vary with the length of track used, from 30-40 per cent. when measurements are made only on 1 mm., to about 10 per cent. when more than 1 cm. of track is used. This scattering-range method is therefore not accurate enough to give good resolution unless the track length is greater than say 1 cm., but it can be used to give an approximate mass value and as a means of verifying other measurements.

Chapter V.

THE GAP COUNT METHOD AND GRAIN DENSITY MEASUREMENTS.

It has been stated in the previous chapter that the number of developed grains which mark the path of a charged particle through a nuclear emulsion is a measure of the ionisation produced by the particle. Since the ionisation is a function of the charge and velocity of the particle, so also is the grain density.

At the present time there are a number of different experimental methods employed for the measurement of grain density, and these may be summarised as follows.

(a) Direct grain counting. In this method, the numbers of grains in successive intervals of the track are counted, and the mean density of the grains is estimated directly from these results. When almost all of the individual grains are clearly resolved, as is the case in tracks of low grain density (up to 20 grains/ 50μ), this procedure yields values of the grain density

[redacted] which are consistent from one observer to another. Even in the thinnest tracks, however, there is a tendency for the developed grains to form clusters, and the accuracy of the results will depend upon how well these clusters can be resolved.

The numbers of grains in these clusters may be

determined either by counting the number of bright "diffraction centres" which may be seen, or by dividing the length of the cluster by the accepted grain diameter. Neither of these methods is very satisfactory, since they do not allow for overlapping of the grains, and the estimated number of grains in a cluster may vary significantly from one observer to another. To overcome these difficulties, a technique which is applicable to tracks which have a large number of clogged segments, namely "blob counting", was developed.

† (b) Blob counting. In this method, the grain density is calculated from the total number of "blobs" or clusters in a given length of track. Each cluster is counted as a single blob regardless of its size, and this procedure not only leads to greater speed in counting, but it also tends to reduce the personal errors involved. Blob counting of thin and grey tracks presents little difficulty because, on the whole, the blobs are clearly defined, and separated from each other by appreciable gaps. Black tracks, on the other hand, contain large numbers of grains in each segment of track, and have very few gaps greater than 0.5 μ in size. Many of the gaps are in fact so small that they are almost completely masked by the diffraction patterns of the grains, and the accuracy with which the blob counts can be made therefore depends to a great extent upon the optical

† Voyvodic (1954). (Ref. 64).

conditions. Blob density determinations on a heavy track will vary from one microscope to another, and from one observer to another.

The blob density may also be determined from the number of spaces between the blobs, as the number of gaps or spaces per unit length of a track is equal to the number of blobs per unit length. Alternatively, the gap density may be used to calculate the grain density without reference to the blobs, and since both the size and frequency of the gaps are taken into account, this method can be adapted for use on both thin and heavy tracks.

(c) Gap counting. The grain density of a track may be obtained from the gaps in it either by determining the total (overall) gap length in unit length of the track, or by finding the mean gap length, or thirdly by counting the number of gaps of length greater than some minimum value. In the present investigation the third method was used, and in some cases more than one minimum gap length was chosen.

Measurements were made of the distances between the inside edges of the grains, or groups of grains, which defined the gaps, and the criterion used for assigning a gap to the appropriate class was as follows: if the gap occupied the entire space between, say, the second and fourth scale division marks, it was classed as a "two

† Hodgson (1950) (Ref. 65).

‡ O'Ceallaigh (1953) (Ref. 66).

division gap", but if any part of the grains at either end of the gap protruded on to or over the scale division lines, the gap was included in the category of one division gaps. This distance between the edges of the grains bordering the gap was chosen rather than the distance between the centres of these grains, because of the difficulty of determining the position of the centre of the last grain of an unresolved cluster. All gaps greater than the minimum gap length (or gap lengths) in successive 50 μ sections of a track were recorded, and from these measurements the gap density in the track was determined. The minimum gap length was chosen according to the grain density of the track, and varied from 0.5 μ, in the case of heavily ionised tracks, to 4 or 5 μ for the very thin tracks.

Recently another method of measuring ionisation in emulsions has been reported by Alvial et al. (1956). Measurements are made of the thickness of a track at known distances from the end, and the interpretation of the results is based on the assumption that the thickness is a function only of the ionisation, that is, of the velocity and charge of the particle. This method is similar to that employed in cloud chambers for the purpose of discriminating between very low energy particles of different mass, and may be of considerable use in the regions near the end of a track where grain

This relation (12) is derived from the probability function of a rare statistical distribution. The probability of obtaining m events in a distance d, when on the average n occur in that distance, is

$$p_1 = e^{-n} \frac{n^m}{m!}$$

In a distance x where the mean number of events is

$$k = \frac{xn}{d} ,$$

the probability of obtaining no events is

$$p_2 = e^{-\frac{xn}{d}} .$$

Now, if we take the number of "events" as the number of developed grains in the track, p_2 is the probability of obtaining a gap of length x, and $\frac{d}{n}$ is the mean separation of the developed grains ($= \lambda$, say). Thus in a distance ℓ, since the number of gaps of all sizes is equal to the number of developed grains ($= \frac{\ell}{\lambda}$), the number of gaps $g(>x)$ is

$$g(>x) = \frac{\ell}{\lambda} e^{-\frac{x}{\lambda}}$$

counting is impossible, and gaps are few in number.

In the present work, a particular study was made of the gap count technique, and it was found that this method of determining grain density was applicable to even the heaviest tracks, where the high degree of clogging made direct grain counting and blob counting impossible. The variations of gap density with grain density, the methods of determining grain density from gap counts, and the results obtained from these measurements will now be considered in detail.

V.1. Estimation of grain density from gap density measurements.

In a length ℓ of the track of a charged particle in a photographic emulsion, the number of gaps $g(>x)$, greater than some chosen minimum length x, diminishes rapidly as x increases. This variation of $g(>x)$ with x is in fact exponential, and may be expressed mathematically by the relation, which is derived as shown opposite :

$$g(>x) = \frac{\ell}{\lambda} e^{-x/\lambda} \qquad (12)$$

where λ is the mean separation of the developed grains, and x is the total gap length measured between grain centres.

Experimental proof of the validity of this expression was obtained by [redacted] Williams (1955) from measurements of the gap density of fast electron tracks, for different values of the minimum gap length. A

graph of gap density as a function of gap length indicated an exponential relation between the two quantities, and [redacted] it was shown that when $\log \frac{1}{g(>x)}$ was plotted as a function of x, the graph was a straight line. The equation of this line, obtained from equation (12), is

$$\log_e \frac{1}{g(>x)} = \frac{1}{\lambda} \cdot x + \log_e \frac{\lambda}{l} \qquad (13)$$

and since λ, the mean free path of the grains, varies inversely with the grain density, the slope of the graph will depend upon the grain density. Thus, for tracks of the same grain density, the slopes will be equal within the experimental error, and as the grain density increases the slope will also increase. This has been confirmed by [redacted] Williams from measurements on the tracks of a number of particles. It may therefore be assumed that the variation of gap density with gap length and with λ, is described by equation (12).

In practice, the grain density is usually expressed as the number of grains per 50μ of track, and so

$$\frac{1}{\lambda} = \frac{n}{50}$$

Substitution in equation (12) gives

$$g(>x) = \frac{ln}{50} \; e^{-\frac{nx}{50}}$$

or, expressing g(> x) as the number of gaps per 50 of track, ($l = 50\mu$)

† Log $\frac{1}{g(>x)}$ is better written $-\log g(>x)$

$$g(>x) = ne^{-\frac{nx}{50}} \qquad (14)$$

Henceforth, the symbol $g(>x)$ will be replaced by g_x which will be assumed to represent the number of gaps in a given length (in this case 50μ) of track, which are greater than $x\mu$ in length.

From this equation (14) it follows that

$$\frac{nx}{50} = \log_e n + \log_e \frac{1}{g_x}$$

or, taking logarithms to the base 10, and rearranging the equation,

$$\log_{10} \frac{1}{g_x} = \frac{n}{115.2} \cdot x - \log_{10} n \qquad (15)$$

For the tracks of particles whose velocity does not change appreciably over the region in which the gap density is measured, the grain density will be reasonably constant, and n may be regarded as a constant in equation (15). Thus a graph of $\log \frac{1}{g_x}$ as a function of x will be a straight line, and from the slope of this line, $\frac{n}{115.2}$, the grain density may be determined.

In all the equations (12 to 15) above, the quantity x represents the total gap length, that is, the distance between the centres of the developed grains which define the gap. The measured gap length, on the other hand, is the distance between the inside edges of these grains, and the two lengths differ in size by an amount equal to the diameter, d, of the grains. If $\bar{x}$ represents the

measured gap length,

$$x = \bar{x} + d$$

all lengths being measured in microns (μ). Replacing x by $\bar{x} + d$ in equation (15) we have

$$\log \frac{1}{g_{\bar{x}}} = \frac{n}{115.2} (\bar{x} + d) - \log n ;$$

since d is constant for a given microscope under given optical conditions, and n is a constant for the measured part of the track,

$$\log \frac{1}{g_{\bar{x}}} = A\bar{x} + C$$

where $A = \frac{n}{115.2}$ and $C = \frac{n}{115.2} d - \log n.$ (16)

Thus the grain density may be determined from the density of gaps greater in length than $\bar{x}\mu$. In practice $\bar{x}$ was measured in terms of the scale divisions of the eyepiece graticule of the Cooke, Troughton and Simms microscope, where 1 scale division = 1.036μ for the eyepiece separation used, but all calculations were made with x converted to microns. A and C were determined from the least squares solution of the equation of the straight line graph of $\log \frac{1}{g_{\bar{x}}}$ as a function of $\bar{x}$, and the grain density and grain diameter were calculated from the equations (16).

When the grain density is determined by this method, an exact value of the grain size is not required for the calculation. However, this parameter is implicit in the formula, and variations in the size of d would result

in variations in the calculated grain density. What is really seen when a grain is observed in the field of view of a microscope is the diffraction pattern of the grain. The size of this pattern will vary from one microscope to another, and will be changed if the optical conditions of the microscope are in any way altered. It is therefore important that the optical system of the microscope should remain unchanged throughout the period of measurement of a track or series of tracks.

An illustration of the application of this method to the determination of grain density and grain diameter is given by the following results (Table VII) which were obtained from long straight tracks associated with cosmic ray stars in the plates. Gap measurements were made in successive 50 μ sections over the lengths of the tracks indicated, and from these results the mean gap densities for gaps greater than $\bar{x}$ scale divisions in length were determined for different values of $\bar{x}$, as shown in the table.

Table VII.

Track	Track Length (μ)	Gap size (scale divisions)						
		1	2	3	4	5	6	7
1	3000	6.8	2.05	0.61	0.14	0.05		
2	1000	9.3	5.4	3.1	1.8	0.9	0.5	0.3
3	1000	8.8	6.4	4.8	3.4	2.6	1.9	1.3

The graphs of $\log \frac{1}{g_{\bar{x}}}$ as a function of $\bar{x}$ for the three tracks are shown in figure 3. From the least squares solution of the equation of each of these lines, A and C were calculated, and the grain density n, and the grain diameter d, were obtained as shown in Table VIII. The uncertainties in the values of n were calculated from the errors in the slopes of the graphs.

Table VIII.

Track	A	C	n grains/50μ	d μ
1	0.524 $\pm$ 0.011	- 1.3833	60.4 $\pm$ 1.3	0.73
2	0.248 $\pm$ 0.007	- 1.2366	28.6 $\pm$ 0.8	0.82
3	0.128 $\pm$ 0.001	- 1.0747	14.7 $\pm$ 0.1	0.62

It was found that in all the plates of the first expedition the grain densities of minimum ionisation tracks, formed by relativistic particles, were equal within the experimental error, and had a value of approximately 13 grains/50μ. Grain diameter measurements on these tracks and on heavy tracks showed that there were no significant variations in the values of d for lightly and heavily ionising particles, nor were there variations from plate to plate. The distribution of values of d shown in figure 4 was obtained from 47 tracks in the first expedition plates. In each of the tracks, gap

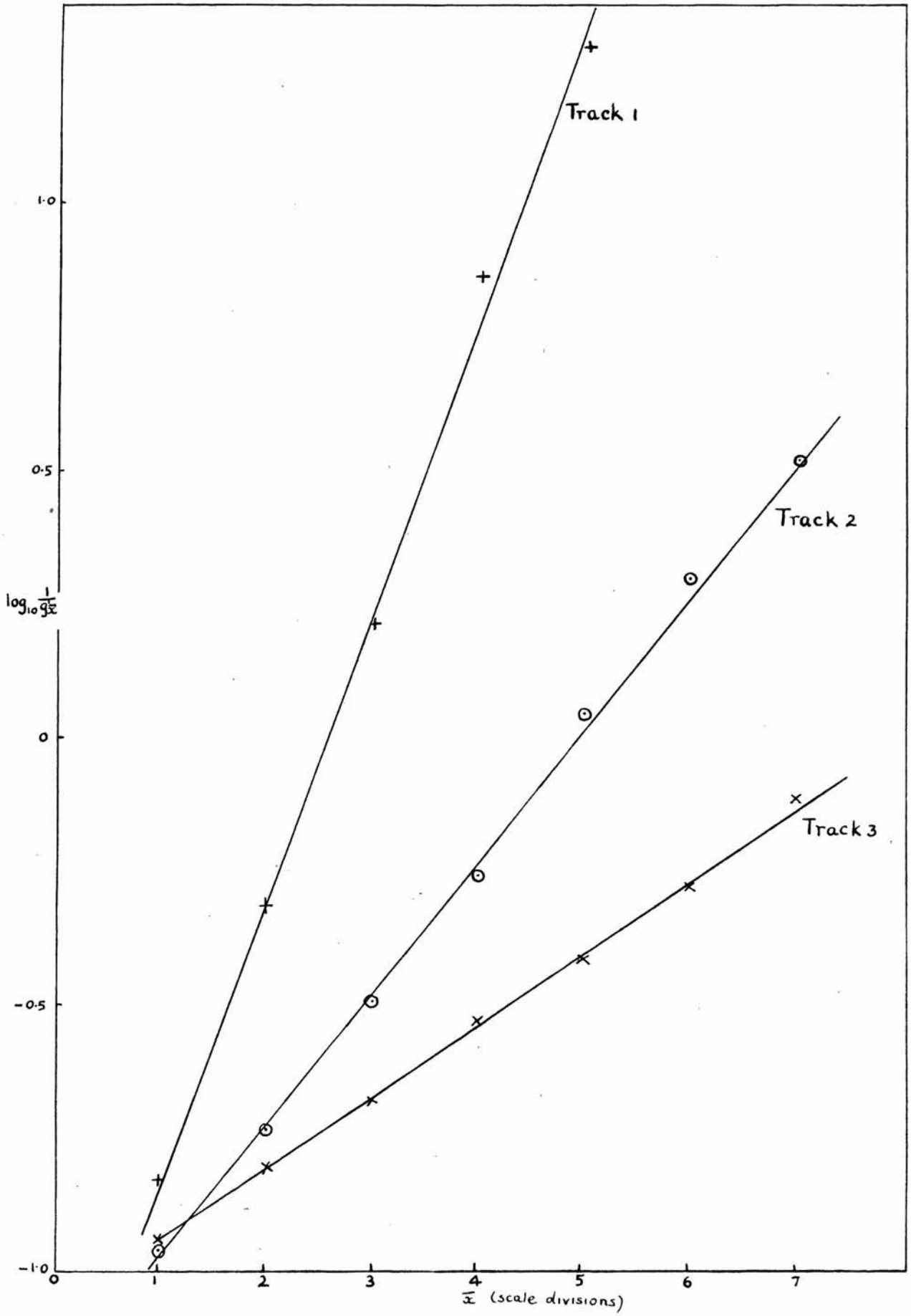

FIGURE 3. Log $\frac{1}{g\bar{x}}$ v. gap length ($\bar{x}$ in scale divisions) for the tracks of three particles in Ilford G5 emulsions.

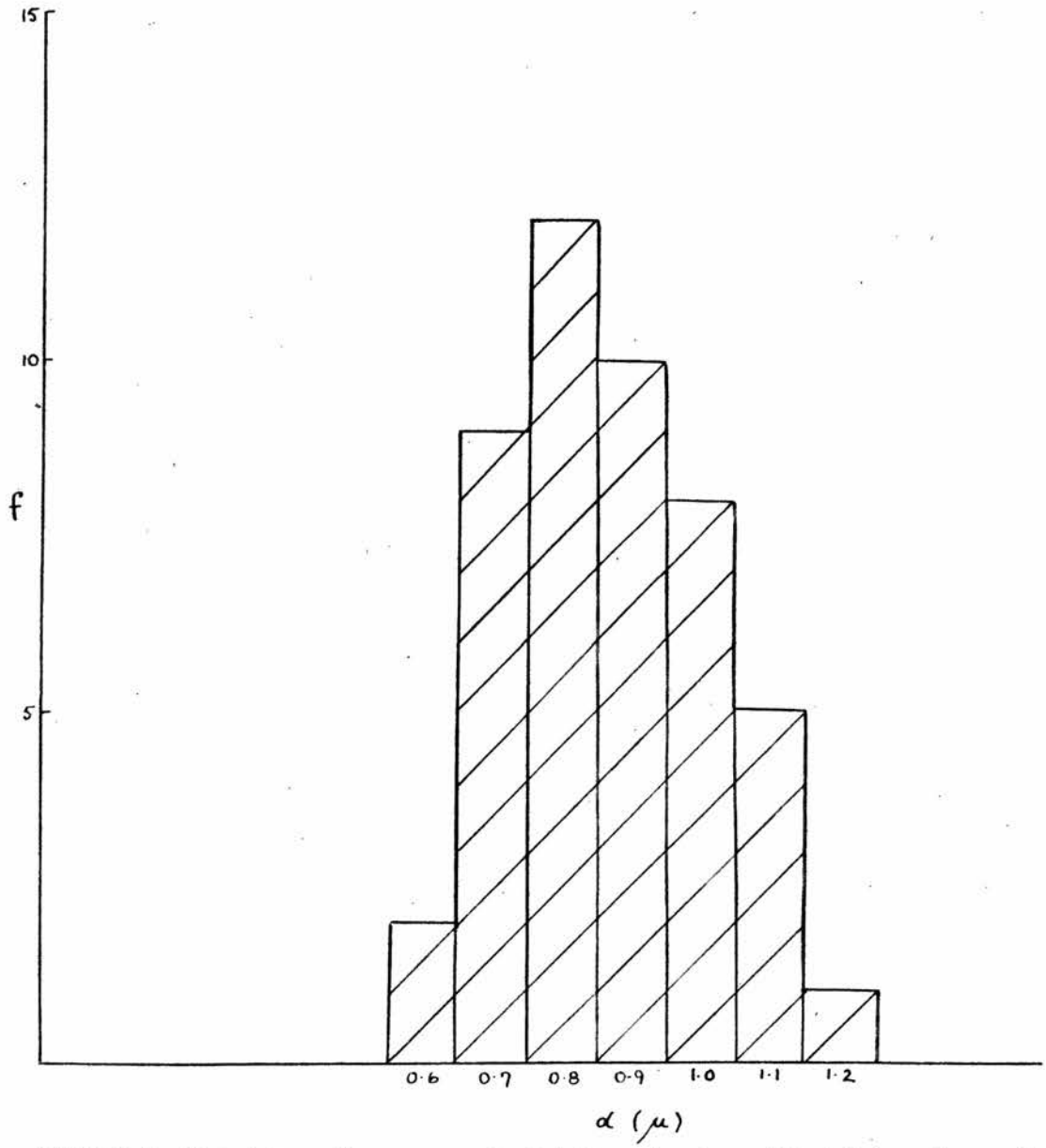

FIGURE 4 Distribution of grain sizes for fortyseven tracks in Ilford G5 emulsion. f is the number of tracks, and d the grain diameter in microns.

measurements were made over at least 1 mm., and in none of them was there evidence of a change in grain density over the measured region.

From these values of d it was calculated that the mean grain diameter for these Ilford G5 emulsions is

$$d = 0.87 \pm 0.02 \mu.$$

This result was confirmed by visual examination of well-resolved grains in thin tracks, whose mean grain diameter was found to be 0.9μ. Background grains in the emulsion, which were not associated with tracks, were found, on the whole, to be much smaller in size with a mean diameter less than 0.7μ.

V.2. Variation of gap density with grain density and gap size.

Given the mathematical relationship between grain density and gap density, and the experimentally determined value of the grain diameter, it is now possible to calculate the average densities of gaps of different sizes which will be present in tracks of different grain density. These calculations were carried out using the equation (14), namely

$$g_x = ne^{-\frac{nx}{50}}$$

in the form in which the total gap length is replaced by the measured gap length $\bar{x}$, and $g'_{\bar{x}}$ is expressed in units

of gaps/300 μ:

$$g'_{\bar{x}} = 6ne^{-\frac{n}{50}(\bar{x} + d)} \qquad (17).$$

The results are shown in Table IX and in figures 5 and 6 which have been drawn to show the variation of gap density with grain density and with gap size.

(i) In figure 5, gap density is plotted as a function of gap size ($\bar{x}$ in scale divisions) for different values of the grain density. From this graph it is clear that, except in the case of the very heavy tracks, the numbers of small gaps do not vary significantly over a considerable range of grain density, and it would not be possible to distinguish between a track with n = 12 grains/50 μ and another with n = 20 grains/50 μ by comparing only the numbers of gaps greater than 1 or 2 scale divisions, in a given length of each track. Thus, the lower the grain density the greater the gap length which must be considered. At very low grain densities, where n is between 12 and 15 grains/50 μ, it may be seen that a considerable proportion of the gaps are large ones. In this case the ratio of the density of gaps greater than 5 scale divisions in length to the density of those greater than 2 scale divisions in length is 0.48; at higher grain densities, for example at n = 50 grains/50 μ, the ratio is 0.045, more than 10 times smaller than before because of the preponderance of

Table IX.

Grain Density	Gap Size							
	½	1	2	3	4	5	6	7
12	51.4	45.2	35.3	27.5	21.4	16.7	13	10.2
14	56.8	48.8	36.6	27.4	20.5	15.3	11.5	8.6
16	61.3	51.6	37.1	26.6	19.1	13.7	9.8	7.1
18	65.2	53.7	37.1	25.5	17.6	12.1	8.4	5.8
20	68.5	55.2	36.6	24.1	15.9	10.5	6.9	4.6
22	71.3	56.2	35.7	22.6	14.3	9.1	5.7	3.6
24	73.5	56.8	34.6	21	12.8	7.8	4.8	2.9
26	75.3	57	33.3	19.4	11.4	6.7	3.9	2.3
28	76.7	56.7	31.9	17.8	10	5.6	3.2	1.8
30	77.7	56.2	30.3	16.2	8.7	4.7	2.5	1.4
35	78.8	54	26.3	12.8	6.2	3.0	1.5	0.7
40	78.3	50.9	22.3	9.7	4.3	1.9	0.8	0.4
45	76.6	47.1	18.7	7.4	2.9	1.2	0.5	
50	74	43.1	15.4	5.4	1.9	0.7	0.3	
60	67.1	35.1	10.2	2.9	0.9	0.3		
70	59.2	27.8	6.6	1.5	0.4			
80	51.1	21.5	4.2	0.8				
100	36.5	12.4	1.6	0.2				
130	20.5	4.9	0.4					
160	10.9	1.9						
200	4.4	0.5						

(Grain density in grains/50μ,
Gap density in gaps/300μ,
Gap size in scale divisions.)

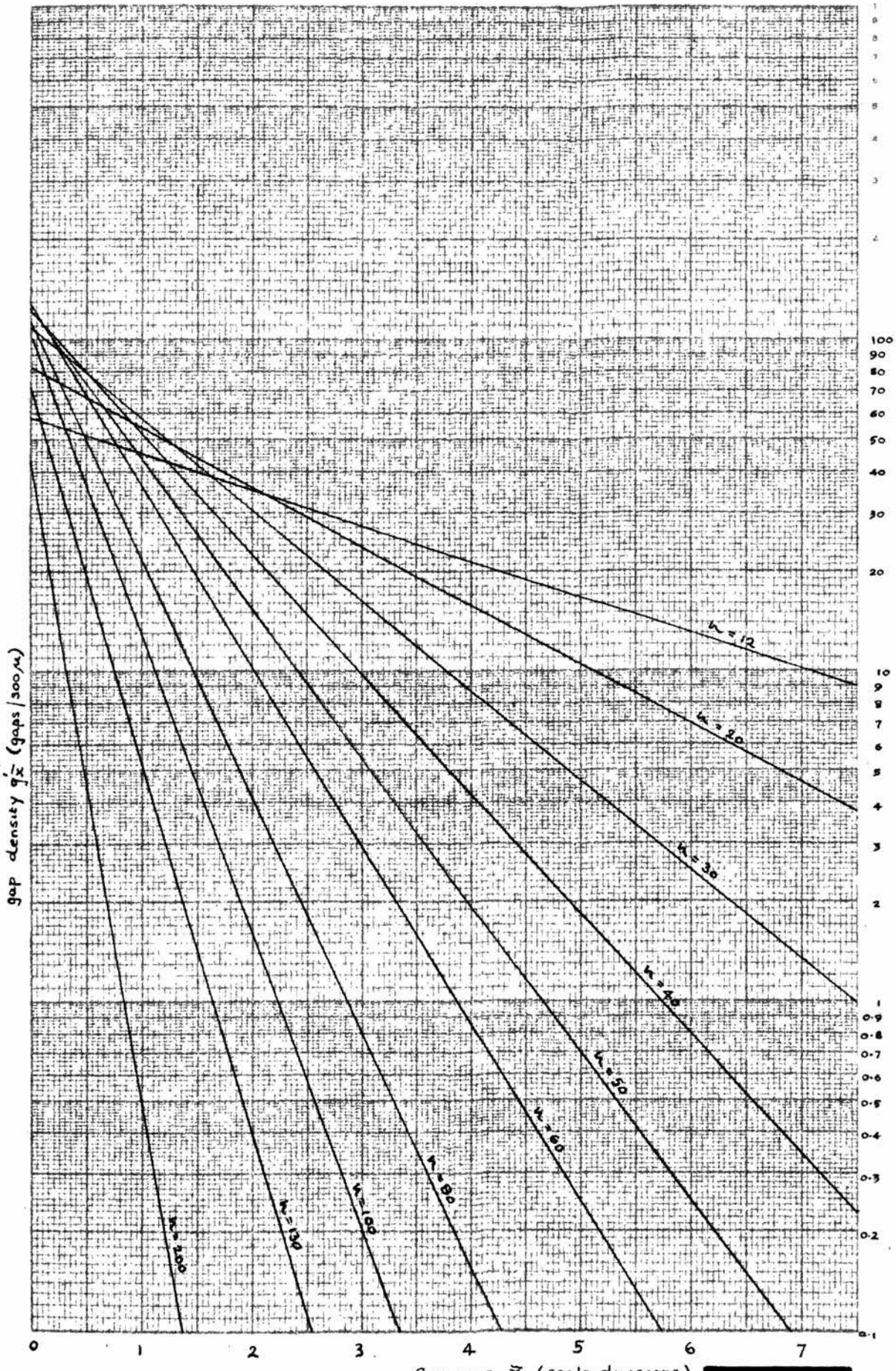

FIGURE 5 Gap density $g'_{\bar{x}}$ (in gaps/300μ) v. gap size, $\bar{x}$ (in scale divisions) for different

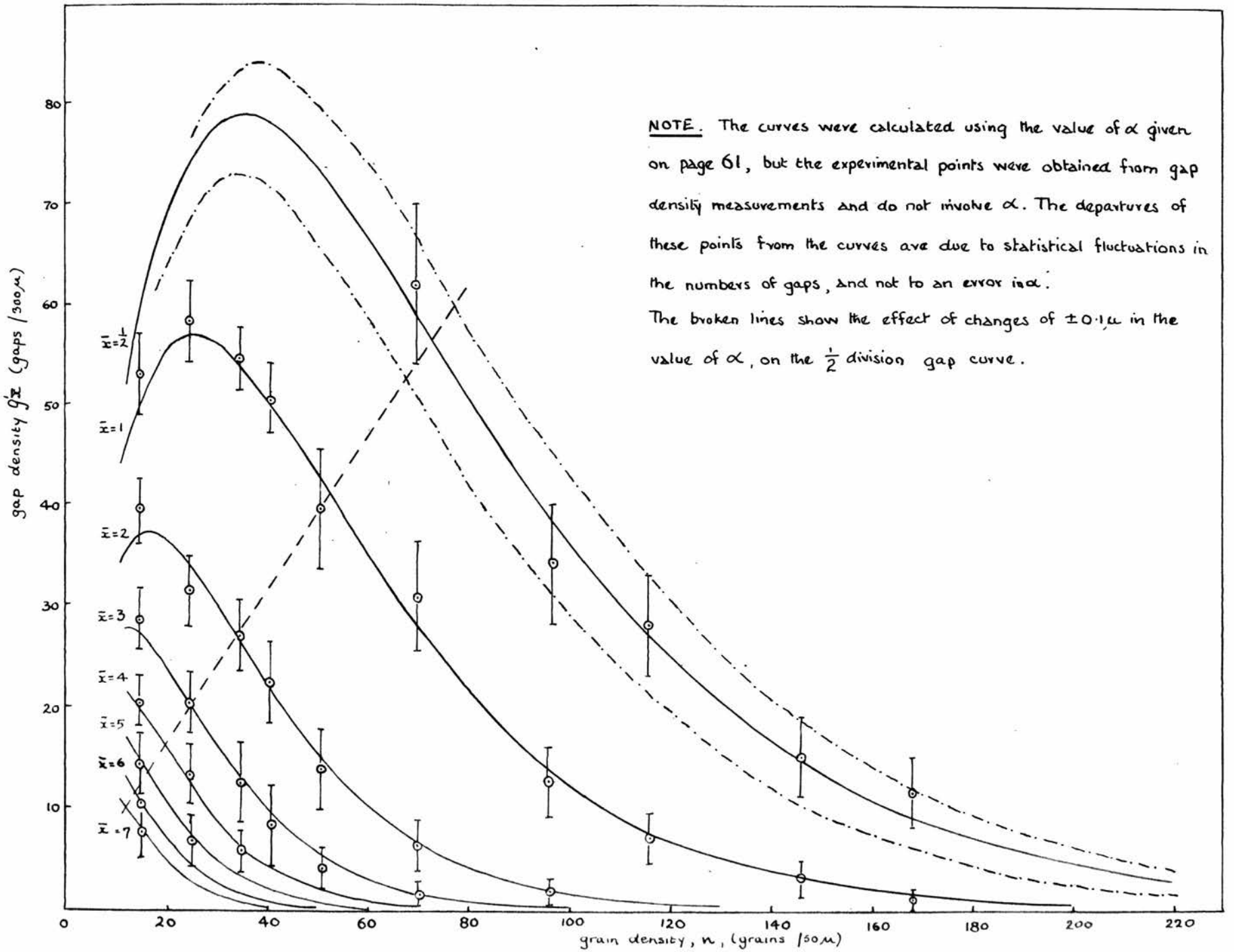

FIGURE 6 Gap density $g'_{\bar{x}}$ (in gaps /300μ) v. Grain density n, (in grains per 50μ) for different gap sizes

small gaps.

(ii) In figure 6, gap density is plotted as a function of grain density for different measured gap sizes $\bar{x}$. The solid lines represent the results obtained from the equation (17) and Table IX, and the points were obtained from gap counts on a number of tracks in the plates. The grain density of each track was calculated by the method described on page 58. For each point, the standard error in the gap density was calculated from the experimental results, but since the errors in the corresponding values of the grain density are very small (1 or 2 per cent.) they have not been shown. It will be seen that the experimental points lie very close to the curves, and it is in fact possible to use these curves to determine approximate values of the grain density when the gap densities are known. Inspection of this graph again shows that the small gaps are unreliable as a means of estimating the grain density of a track, because for each $\bar{x}$ there is more than one value of n for a given value of g_x in the low grain density region.

When this graph is used for finding the grain density of a track, it is not necessary to determine the numbers of gaps of all sizes, unless an exact value of the grain density is required, as a reliable estimate can be obtained from measurements made on one size of gap only. The choice of the best gap length for any given track is governed by the grain density of the

track and by the behaviour of the curves shown in figure 6. At the point of inflexion of one of these curves, the gap density changes more rapidly with grain density than at any other point, and consequently the number of gaps is sensitive to small changes in n. It is therefore reasonable to assume that the best gap length is that one whose curve is at or near a point of inflexion at the grain density under consideration.

Using the equation relating gap density (per 300μ) and grain density, for a total gap length x,

$$g_x = 6ne^{-\frac{nx}{50}},$$

the points of inflexion may be calculated for different values of x. For a point of inflexion we require

$$\frac{d^2g}{dn^2} = 0.$$

Now,

$$\frac{dg}{dn} = 6e^{-\frac{nx}{50}}\left(1 - \frac{nx}{50}\right)$$

and

$$\frac{d^2g}{dn^2} = 6e^{-\frac{nx}{50}}\left(\frac{nx^2}{(50)^2} - \frac{2x}{50}\right).$$

Therefore, at the point of inflexion

$$6e^{-\frac{nx}{50}}\left(\frac{nx^2}{(50)^2} - \frac{2x}{50}\right) = 0$$

and so,

$$\frac{nx^2}{(50)^2} = \frac{2x}{50}$$

thus $x = 2 \times \frac{50}{n} = 2\lambda$ where λ is the mean separation. The point of inflexion for each curve is therefore at the point where

$$\bar{x} + d = 2\lambda \quad \text{where } d = 0.87\mu .$$

In Table X and figure 7 the values of the grain density corresponding to the points of inflexion for different gap sizes are shown, and in figure 6 the dotted line represents the locus of these points.

Table X.

Measured gap size (scale divisions)	Total gap size (μ)	Grain density (grains/50μ)
0.5	1.39	72.9
1	1.91	52.8
2	2.94	34.0
3	3.98	25.2
4	5.01	20.0
5	6.05	16.5
6	7.09	14.1
7	8.12	12.3

The procedure for determining the grain density of a track using only one gap size is then as follows. First, the grain density of the track must be roughly estimated by grain counting, so that the best or optimum

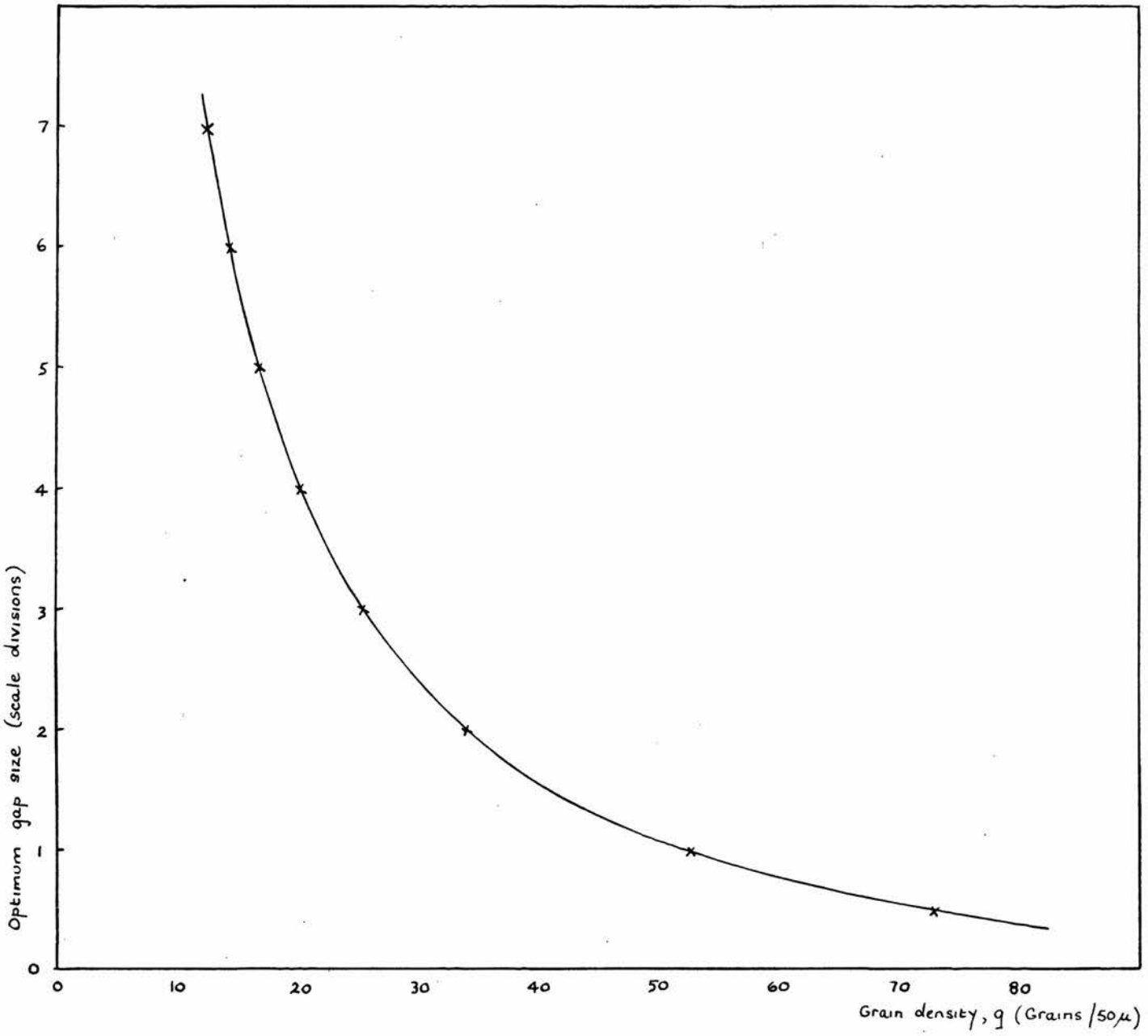

FIGURE 7. Optimum gap size (in scale divisions) v. grain density (in grains per 50μ)

gap length may be determined from figure 7. Then the average number of gaps of this length in 300 μ of track is found, and the grain density read directly from the graph in figure 6. This method has the advantage of being very rapid as it involves the counting of a relatively small number of gaps, and it yields values of the grain density which are comparable with those obtained from all the gaps by the "least squares method". A few examples of the applications of both of these methods to tracks of different grain density are shown in Table XI. As the optimum gap length appropriate to each grain density is not necessarily a whole number, the procedure was to use the measured gap size nearest to this value.

Table XI.

Track	n_1 (grains/50μ)	Optimum gap size (S.D.)	Gap density (gaps/300μ)	n_2 (grains/50μ)	Track length (μ)
1	13.3 ± 0.1	7	8.5	13	3500
2	14.2 ± 0.2	6	10.4	15	2000
3	15.5 ± 0.3	5	15.1	14.5	1500
4	19.7 ± 0.5	4	15.5	20.5	1000
5	27.0 ± 0.1	3	18.8	26.5	9000
6	36 ± 1	2	25.4	36	1200
7	54 ± 3	1	41	53	1000
8	74 ± 2	0.5	59.5	70	1200

n_1 is the grain density calculated from all gaps.
n_2 is the grain density calculated from gap density of optimum gaps.

V.3. Change in gap size with inclination of the track.

All the experimental results which have been quoted in this chapter were obtained from tracks which were parallel to the x-y plane of the emulsion or inclined to it at a very small angle. However it was often necessary to measure the grain density of the tracks of particles which had passed obliquely through the emulsion, and the gap counting technique had to be adapted for this purpose.

In a track which is not parallel to the emulsion surface, the projected lengths of the gaps measured in the eyepiece scale are smaller than the true distances between the edges of the grains which define the gaps. In principle the total distance could be determined if the depth difference across the gap were also measured, but in practice this procedure is impossible because of the limitations imposed on the accuracy of depth measurements by the mechanical precision of the microscope fine adjustment. However, the difficulty of estimating the total gap length was overcome by making allowance for the inclination of the track to the x-y plane of the emulsion.

If this inclination is θ, if $\bar{x} + d$ is the true gap length and $\bar{x}' + d$ the projection of the true gap length in the x-y plane, as shown in the diagram of figure 8, then

$$\bar{x}' + d = (\bar{x} + d) \cos\theta$$

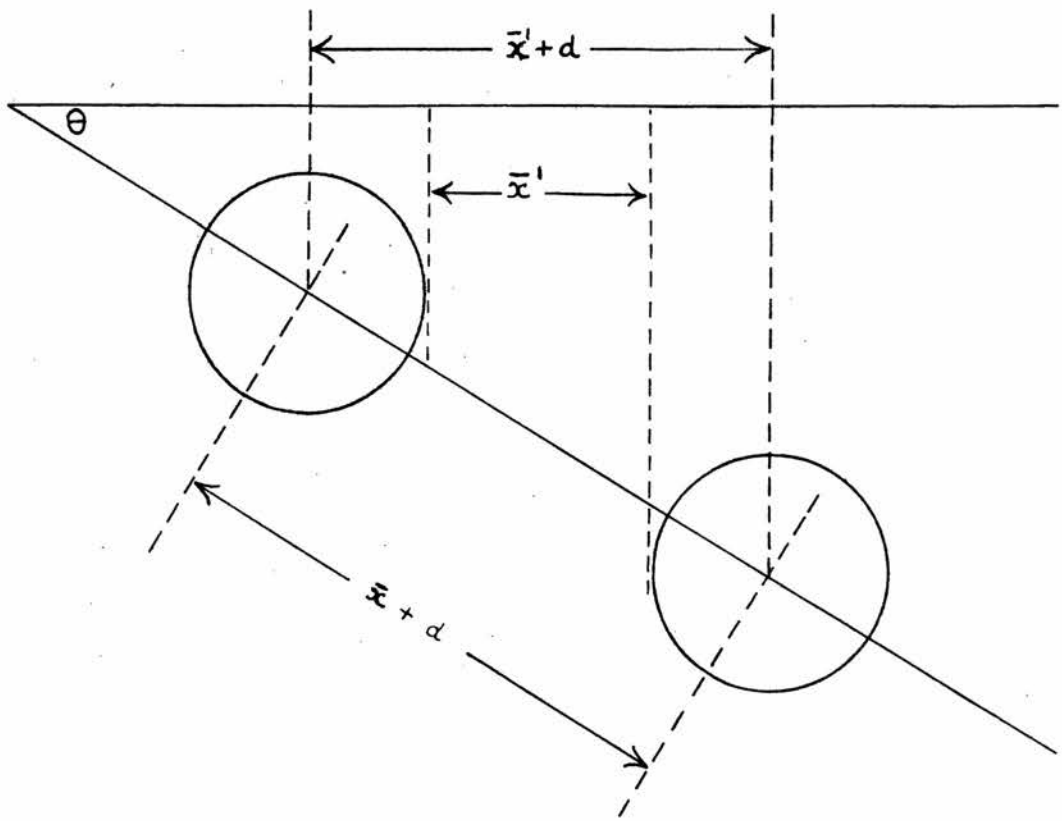

FIGURE 8

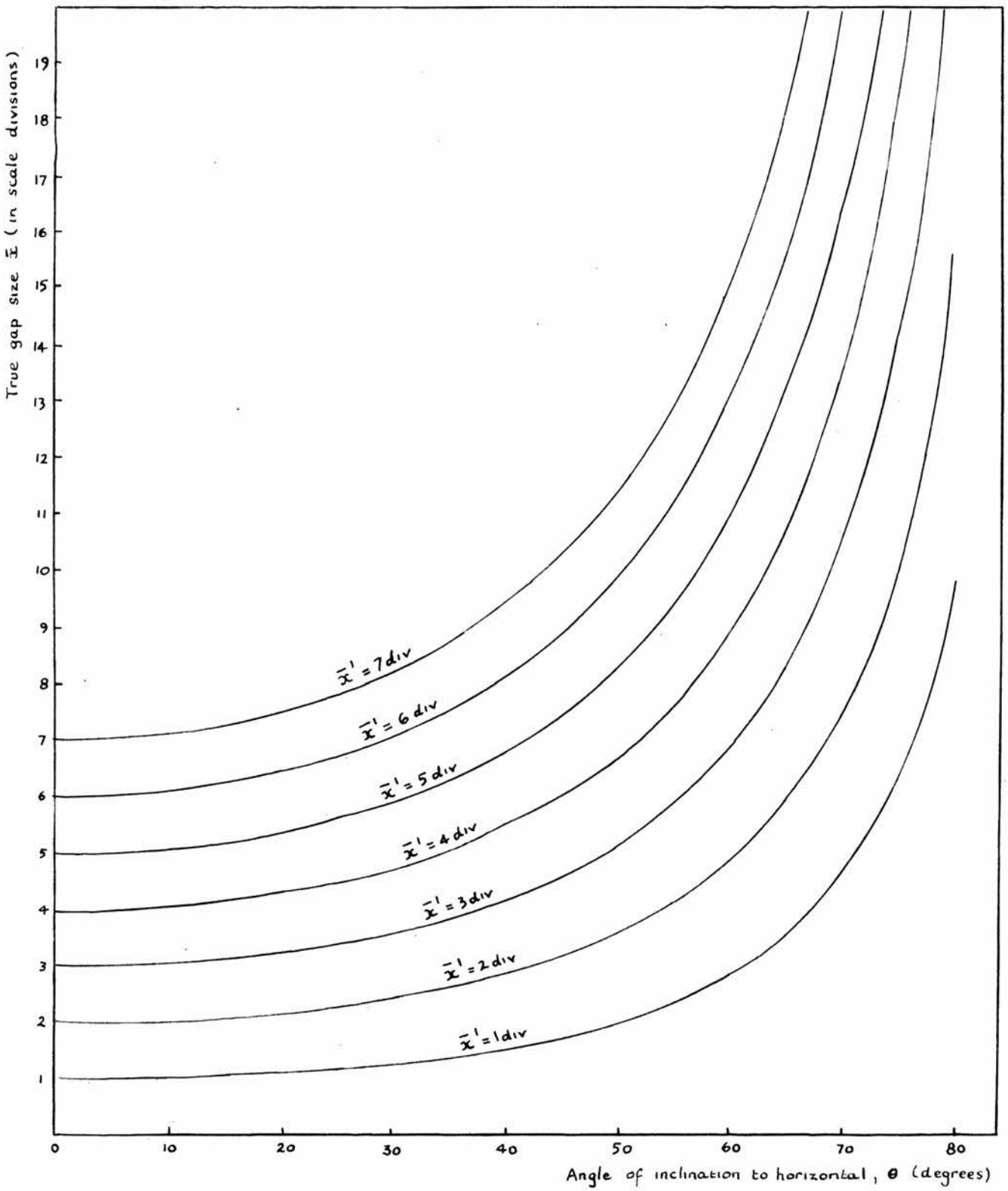

FIGURE 9 True gap size $\bar{x}$ (in scale divisions) v. θ the angle of inclination of the track to the plane of the emulsion (in degrees), for different values of $\bar{x}'$, the projected gap length (scale divisions).

$$\therefore \bar{x} = \frac{\bar{x}' + d}{\cos\theta} - d$$

where $d = 0.87\mu = 0.84$ scale divisions.

Values of $\bar{x}$ have been calculated for different inclinations θ, and these are shown in figure 9 where $\bar{x}$ is plotted as a function of θ for a number of different values of the projected gap length.

From this graph it may be seen that the projected lengths of the small gaps (1 and 2 scale divisions) are approximately equal to the true lengths so long as the angle of inclination is less than 30°, but for the longer gaps, the true gap length increases rapidly as the inclination increases. Tracks used for calibration purposes were therefore acceptable only if their angles of inclination to the horizontal were less than 15°.

The procedure for determining the grain density of a steep track emerging from a cosmic ray star was to carry out gap counts in exactly the same way as for a horizontal track, and then to determine the true lengths of the measured gaps from the graph of figure 9. These results were subsequently used in the construction of the graph of $\log \frac{1}{g_{\bar{x}}}$ as a function of $\bar{x}$, and the grain density was calculated in the usual way from the slope of the graph.

Any determination of the grain density of a steeply inclined track from gap count results will tend to be

an over-estimate of the actual value, because no allowance has been made for an increase in the size of the diffraction patterns of the grains, which reduces the observed gap size. Conversely, grain and blob counting would yield values of the grain density which were smaller than the true one, because of the difficulty of resolving the clusters of grains, and the masking of one grain by another. The problem of resolving clusters of grains occurs in grain counts on any track, and it accounts for the marked discrepancy between the values of the grain density obtained by direct grain counting and by the gap count method, which will now be discussed.

V.4. Comparison of the results from grain and gap counting.

Gap counts and grain counts were carried out on a number of long tracks in the plates. The grain density was determined from the gap counts using either the optimum gap size as described above, or the gaps of all sizes, and from the grain counts by calculating the average number of grains present in 50 μ sections of track. These results are shown in Table XII and in figure 10, where it may be seen that, although the results obtained from the two methods are comparable when the grain density is small, as the grain density increases so the discrepancy between the values increases. This discrepancy can be explained in terms of clogging in the

track.

Table XII.

Track	n_1 grain density from gap counts (grains/50 μ)	n_2 grain density from grain counts (grains/50 μ)	Track length (μ)
1	13.3 ± 0.1	12.6 ± 2.8	2000
2	15.4 ± 0.1	14.4 ± 3.5	9000
3	19.7 ± 0.5	17.5 ± 3.7	4500
4	23.0 ± 0.7	21.4 ± 3.9	1000
5	28.3 ± 0.3	25.4 ± 3.9	9000
6	30.0 ± 0.4	27.5 ± 4.4	1500
7	36.1 ± 0.5	29.2 ± 3.7	3000
8	32.6 ± 0.6	30.0 ± 2.8	1000
9	48.8 ± 1.5	34.0 ± 2.9	3000
10	52.3 ± 0.9	37.5 ± 3.5	3000
11	58.2 ± 1.4	44.0 ± 4.4	6250
12	65 ± 3	51 ± 5	2000
13	69 ± 3	56 ± 3.5	3000
14	76 ± 4	56.5 ± 4	3000
15	85 ± 4	59 ± 3	3000
16	100 ± 5	61 ± 3	3000
17	118 ± 6	64 ± 3	1500
18	142 ± 7	67 ± 3	1500

At high velocities, the energy lost by a particle

Error in n_2 : standard deviation of grain counts.

Error in n_1 : calculated from the least squares formula for a linear graph.

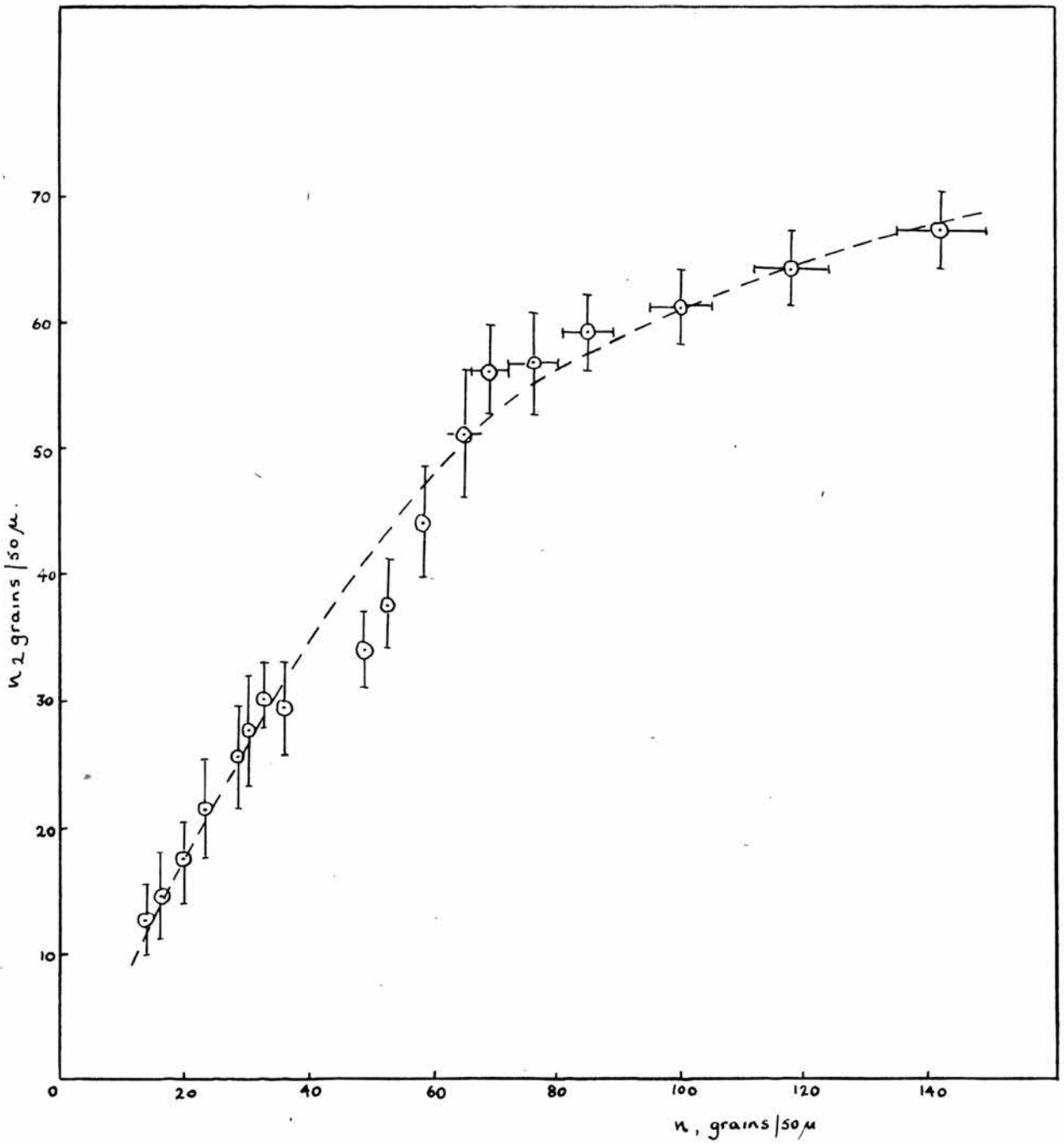

FIGURE 10 n_2, grain density calculated from grain counts v. n_1, grain density calculated from gap counts, for 18 tracks.

per centimetre of its path is small, and only a few of the grains in the emulsion become developable. Under these conditions, the developed grains are separated from each other by large gaps, and are clearly resolved. As the velocity decreases, however, the rate of loss of energy increases, and more grains become developable, with the result that in the developed plate the grain spacing is small, and the grains tend to overlap and to form clusters. For grain densities greater than 30 grains/50μ, only a very small number of the individual grains is resolved, and most of the track is made up of clusters. In such circumstances, direct grain counting becomes highly subjective, and on the whole very inaccurate. Although it is sometimes possible to estimate the number of grains in a cluster by counting the number of bright diffraction centres obtained by mis-alignment of the microscope, this method cannot be applied to heavy tracks where there is considerable overlapping of the grains.

From the results quoted above, it will be seen that the maximum grain density, which could be obtained from grain counting in these plates, was approximately 70 grains/50μ, but in fact there are many more grains in a heavy track. If it is assumed that at very low particle velocities all the grains lying along a track are ionised, then the average number of developed grains per 50μ of track is equal to the average number of grains

present per 50μ of the unprocessed emulsion. This number may be calculated from Jdanov's formula for the average number of grains per micron, namely

$$c = \frac{3}{2}\frac{C}{d\rho}$$ (Jdanov, 1935) (Ref. 54)

where C = concentration of silver bromide in the emulsion = 3.521 gm./cm.^{3}

d = mean diameter of the undeveloped grains = 0.18μ

ρ = density of silver bromide = 6.47 gm./cm.^{3}.

From this equation it follows that

$$c = 4.54 \text{ grains}/\mu = 227 \text{ grains}/50\mu,$$

which is nearly $3\frac{1}{2}$ times the estimated number.

Gap counts, on the other hand, may be made regardless of the degree of clogging in the track, since they depend only on the number and size of the spaces between the grains and clusters of grains. It is significant that the maximum value of the grain density calculated from gap numbers is 220 grains/50μ, which is very close to the theoretical maximum value. Also, at low grain densities, the results obtained by this method are in agreement with those of direct grain counting, which further suggests that gap counting is an accurate and reliable method of determining grain density.

While no mention has yet been made of the errors involved in gap and grain measurements, the conclusion which may be drawn from the results already given is that grain counting is applicable only to thin tracks,

up to approximately 25 grains/50 μ, although gap counting may be employed over the entire range of grain density and particle velocity. However, before any final conclusions can be reached, it is necessary to consider the accuracy with which the grain density may be calculated using gap and grain measurements.

V.5. Errors involved in gap and grain measurements.

Although the main sources of uncertainty in the grain density calculations were found to be the statistical fluctuations in the measured gap and grain numbers, other possible sources of error must be considered, as for example uneven processing of the emulsion, the presence of background grains, and errors of measurement.

V.5.1. Errors due to uneven processing of the emulsions.

One of the problems associated with the use of thick emulsions is that of achieving uniform development throughout each emulsion, and the same degree of development in all the plates. In order to test the uniformity of development in any one plate, gap counts were made on a number of tracks of comparable grain density, which passed through the plate from the upper to the lower surface of the emulsion, and which were not too steeply inclined to the plane of the emulsion. Each track was divided into three equal lengths, and the total numbers

of gaps formed in each of the three horizontal layers of emulsion were measured and compared.

Thin tracks, usually with n = 20 grains/50 μ approximately, were chosen for this purpose, because these must have been formed by fast particles whose velocity would not change appreciably during their passage through the emulsion. Consequently their grain densities and gap densities should be constant for all the layers of the emulsion, unless uneven development has taken place.

The results which are shown in Table XIII were obtained from a total track length of 2.7 cm. in one plate, and are representative of all the plates. In the three layers of emulsion, the numbers of 4, 5 and 6 division gaps are the same to within a few per cent., thus confirming that uniform development has taken place.

Table XIII.

	Total gap count			Track length (mm.)
	$\bar{x} > 4$	$\bar{x} > 5$	$\bar{x} > 6$	
Top layer	480	319	213	9
Middle layer	474	310	222	9
Bottom layer	487	315	209	9

In order to test the degree of development in different plates, gap counts were made on tracks formed

by particles of two kinds:

(1) relativistic particles: in most cases the electron resulting from the decay of a μ-meson,

(2) slow particles: protons and mesons which came to rest in the emulsion.

It was found that the gap density of the tracks formed by the fast particles was approximately the same in all the plates, and gave a value of 13 grains/50μ for the grain density at minimum ionisation. Measurements of the numbers of very small gaps (0.5 scale division), which occur over the first few millimetres of proton and meson tracks, showed little variation from plate to plate, apart from the expected statistical fluctuations.

From these results it was concluded that for this set of Ilford G5 emulsions the degree of development was the same in each layer of every plate, and consequently gap and grain measurements made in one plate could be compared with those in another plate, without correction.

V.5.2. Errors in measurement.

One of the advantages of this gap method of determining the grain density of a track is that no serious error arises in the measurement of the lengths of the gaps except when these are very small or the track very steeply inclined. Only those gaps which have a length nearly equal to an integral number of scale divisions present any difficulty, but provided the criterion

mentioned earlier for the classification of gaps is strictly adhered to, few gaps will be wrongly assigned. It was found that the results obtained by different observers, and by the same observer at different times, were consistent except in the case of the very short gaps and the gaps in steep tracks, where the results were affected by personal judgment.

The smallest gap which was measured was 0.5 scale division in length (0.52μ), and as the eyepiece scale was marked in half divisions, the criterion could still be applied. For these small gaps, however, errors in measurement did occur because of the lack of definition at the edges of the grain diffraction patterns. In heavy tracks where even these small gaps were few in number, this introduced a considerable error into the gap density measurements, and consequently caused a greater uncertainty in the value of the grain density. This lack of definition at the edges of grains seemed to become more marked when the gaps were small, and was one of the main sources of error in the measurements made on steep tracks where the projected gap lengths were much shorter than the true gap lengths.

Measurement errors in grain counting arise chiefly from the difficulty of estimating the number of grains in a cluster. These errors become evident when the results of different observers are compared, or even

when the results obtained by a single observer at different times are considered, and cannot therefore be included under the heading of statistical fluctuations which are a property of the emulsions themselves. Because of the discrepancy in the values of the grain density determined from grain counts by different observers, all measurements of this kind reported in this thesis have been made by a single observer. However, as gap measurements are not subject to these personal errors, these results can be taken from observations made by more than one observer.

V.5.3. Statistical fluctuations in gap and grain measurements.

If it is assumed that the distribution of the developed grains along the track of a charged particle is random, then there will be a fluctuation in the numbers of gaps in successive sections of the track. In order to assess the magnitude of this fluctuation and its dependence on grain density, measurements were made on a number of tracks in the plates.

A typical example of the distribution of the numbers of gaps in successive sections of a thin track is shown in figure 11a. These results were obtained from gap measurements over 18 mm. of the track, and represent the number of gaps greater than 2 scale divisions in length, per 100 μ of track. From this distribution it

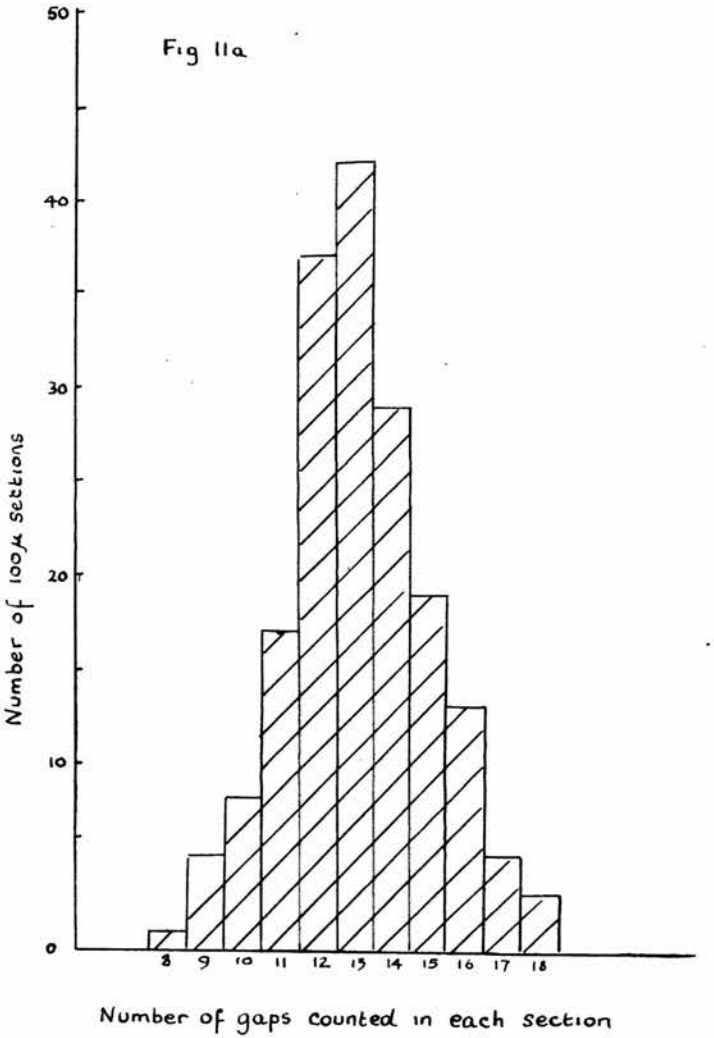

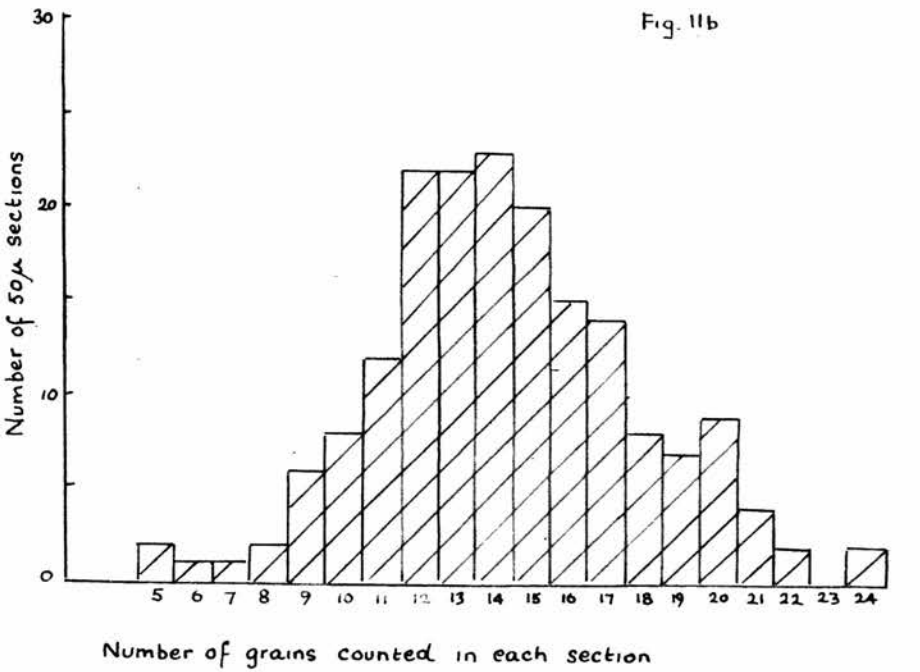

FIGURE 11 Distribution of grains and gaps (of length $\bar{x} > 2$ scale divisions) along a straight track in the emulsion, of grain density approximately 14 grains / 50 μ.

was found that g_2, the mean density of the 2 division gaps, was 13.1 per 100μ, and that σ, the standard deviation of the distribution, was equal to $\pm$ 1.8. This standard deviation is equal to half that expected for a rare statistical [redacted] distribution, namely the square root of the mean. Gap measurements on the other tracks of different grain density showed that provided the length of track measured is greater than 1 mm., the ratio $\frac{\sigma}{\sqrt{g_x}}$ is always approximately equal to 0.5 for small gaps (1 and 2 scale divisions), although it increases to 0.7 or 0.8 for the longer gaps which are fewer in number. From these results it may be concluded that the errors due to fluctuations in the numbers of gaps are always less than would be expected if the gaps were distributed at random along the track. A further discussion of these errors is contained in the Appendix (attached inside back cover).

The assumption that the developed grains in a track are randomly distributed implies that the numbers of grains in equal, successive sections of the track will be normally distributed about the mean value n, and that the standard deviation of the distribution will be $\pm\sqrt{n}$. In order to test this assumption, the numbers of grains in 50μ sections of all the tracks mentioned above were determined, and the distribution of grain counts for each track was examined.

The distribution of the grain numbers in 9 mm. of the thin track is shown in figure 11b where the number

of observations is the same as in figure 11a. These grain numbers have a mean value of 14.4 and the standard deviation of the distribution is 3.5, or $0.9\sqrt{n}$, which suggests that the distribution is very nearly normal. However, it was found that the ratio $\frac{\sigma}{\sqrt{n}}$ tended to decrease with increasing grain density, as is shown in the graph of figure 12 where the standard deviation is plotted against the square root of the mean grain number for 19 tracks whose grain densities (calculated from the grain counts) ranged from 12.6 grains/50μ to 67 grains/50μ. The values of σ and $\sqrt{n}$ used in the construction of this graph, and the value of $\delta\sigma$, the error in σ which was calculated from the formula

$$\delta\sigma = \frac{\sigma}{\sqrt{2(r-1)}} \qquad (r = \text{the number of observations})$$

are given in Table XIV.

In the graph of figure 12 it will be seen that the ratio $\frac{\sigma}{\sqrt{n}}$ does not vary regularly with grain density and that tracks of the same grain density may yield quite different values of $\frac{\sigma}{\sqrt{n}}$. It was thought that this inconsistency might arise from the fact that some of the tracks lay near the bottom of the emulsion where the visibility of the grains is sometimes poor, and the counting procedure difficult. However, no evidence could be found to support the view that differences in the positions of the tracks accounts for the variations in the values of $\frac{\sigma}{\sqrt{n}}$ for tracks of the same grain density.

Table XIV.

Track	n	$\sqrt{n}$	σ	$\delta\sigma$	$\frac{\sigma}{\sqrt{n}}$
1	12.6	3.6	2.8	0.3	0.78
2	14.7	3.8	3.6	0.2	0.95
3	17.5	4.2	3.7	0.3	0.88
4	22.5	4.7	4.0	0.3	0.85
5	22.7	4.8	3.6	0.2	0.77
6	25.4	5.0	3.9	0.2	0.78
7	26.5	5.1	3.1	0.5	0.61
8	27	5.2	4.3	0.3	0.83
9	29.2	5.4	3.7	0.3	0.68
10	30.6	5.5	4.1	0.4	0.75
11	33.5	5.8	3.0	0.3	0.52
12	37.5	6.1	3.5	0.3	0.57
13	41.7	6.5	3.0	0.3	0.46
14	44	6.6	4.4	0.3	0.67
15	44	6.6	3.7	0.3	0.56
16	51	7.1	5.0	0.55	0.70
17	56	7.5	3.5	0.3	0.47
18	61	7.8	3.0	0.3	0.38
19	67	8.2	3.0	0.4	0.37

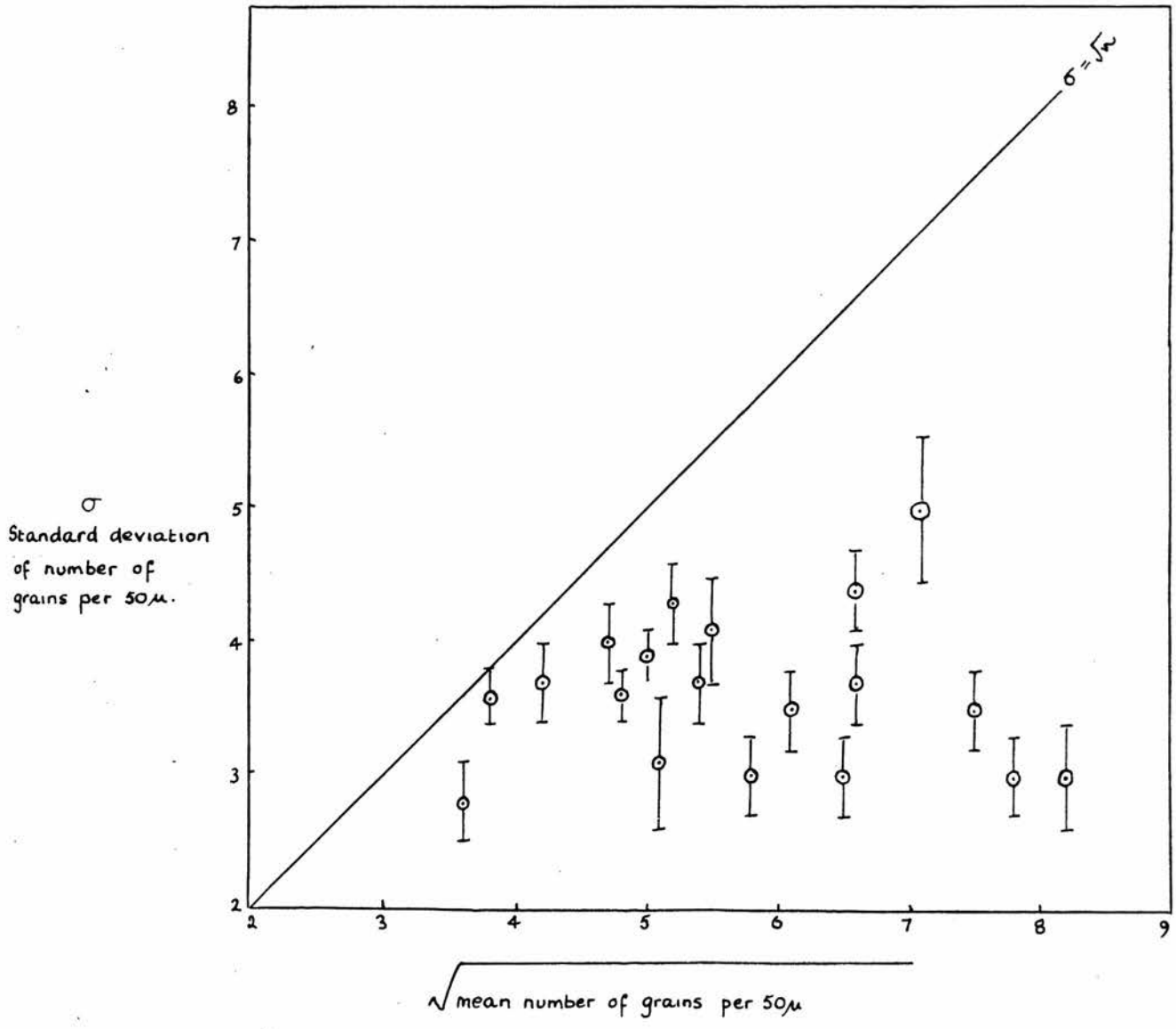

FIGURE 12 σ, the standard deviation of the grain density distribution $v\sqrt{n}$, the square root of the mean grain density, for values of n between 12·6 and 67 grains/50μ. The straight line passes through the points for which $\sigma = \sqrt{n}$.

The smallest value of σ obtained from these tracks was in the densest track where the grain density was 67 grains/50μ and $\sigma = 0.37\sqrt{n}$. This is considerably smaller than the lowest value ($\sigma = 0.75\sqrt{n}$) obtained by Hodgson (1952) who explained the departure from the normal distribution in terms of the lack of resolution of the clusters in a heavy track. Inevitably an underestimate will be made of the number of grains in a cluster, because it is impossible to account for grains which are completely hidden by others, and consequently a true grain count cannot be obtained. An indication of the magnitude of this under-estimation may be seen by comparing the grain count and gap count values of the grain density of this track for which $\sigma = 0.37\sqrt{n}$:

Gap measurements: 142 grains/50μ

Grain measurements: 67 grains/50μ

and from these results it appears that more than half the grains were missed in the grain counts.

For thin tracks, however, with the exception of the first one in the Table XIV, the standard deviation of the distribution approaches $\sqrt{n}$. This implies that the distributions for low grain densities are nearly "rare statistical distributions", as might be expected from the fact that nearly all the individual grains in these tracks are clearly resolved.

However, there is a further source of error, namely

the background grains, which may contribute to the increased spread of the distributions at low grain densities. These background grains are the very small grains which appear in the emulsion, and which, because of their size, are often recognisable, together with the grains associated with other tracks. Where two thin tracks cross each other, it is not always possible to assign a given grain to one track, unless there is a depth difference between this track and the other. Also, Coulomb scattering of the particle may result in some of its track grains lying away from the main line of the track and appearing to be background grains. Thus errors may occur because of the exclusion of some track grains and the inclusion of some background grains. While these errors will be negligible when the grain density is high, they may be appreciable in thin tracks. At low grain densities, gap counts will also be affected, especially when only the optimum gap size is used, because background grains may cause a single long gap to be counted as two or more short gaps.

A re-estimation of the grain densities of the tracks was made, taking care to exclude all possible background grains, and it was found that the values of the mean grain density obtained from grain counts were unchanged, as were the general features of the grain number distributions. It was therefore concluded that

the grains are in fact randomly distributed along the track and that the change in the distribution at high grain densities is due to the lack of resolution of the clusters of grains. Gap numbers, on the other hand, are not have statistically distributed, and the statistical fluctuations in the numbers of gaps are smaller than the corresponding fluctuations in the grain numbers. Consequently the error involved in a determination of gap density is smaller than that involved in a determination of grain density.

In view of the statistical fluctuations in the numbers of gaps and grains in a track, it is of interest to determine the minimum length of track required to give a reasonably accurate estimate of the grain density using either the gap count or the grain count technique.

Grain counts were made on several long, straight tracks in the emulsion, and the grain density (per 50μ) of each track was calculated using first the readings from the first 100μ of track measured, then the readings from the first 300μ, and so on until finally the mean grain density (per 50μ) of the whole track was determined. These results are shown in Table XV.

Gap counts were made over the same tracks, using only the optimum gap length which varied with the grain density as was shown before. The average numbers of

gaps (in units of gaps per 300μ) calculated for the first 100μ, 300μ, 500μ, etc. are shown in Table XVI, and in Table XVII the grain densities appropriate to these gap densities are given, having been determined from the graph of figure 6.

Table XV.

Track	Track length (μ)								Probable error in final mean value
	100	300	500	1000	1500	2000	3000	5000	
1	16	12.8	13.8	13.3	13.6	13.6	13.6	13.4 (± 3.4)	0.2
2	25	25.1	26.3	26.3	25.8	25.2	25.5	25.6 (± 4)	0.3
3	28	29.2	29.2	28.7	29.5	29.2	29.2 (± 4)		0.35
4	34.5	34.5	35.1	34.4	34.0	33.9	34.0 (± 3)		0.3
5	43	41.3	42.2	41.6	41.9	40.6	41.7 (± 3)		0.3

Figures in brackets in the second last column are the standard deviations of the grain count distributions.

Table XVII.

Track	Track length (μ)								Probable error in final mean value
	100	300	500	1000	1500	2000	3000	5000	
1	15	16	16	15	15	15	15	14 (± 2)	0.15
2	23	27	30	28	26.5	25	25.5	26 (± 2.5)	0.2
3	38	32	35	31	33	33	33 (± 3)		0.3
4	59	59	58	57	54	55	55 (± 4)		0.35
5	71	65	62	59	61	61	62 (± 4.5)		0.4

Figures in brackets in the second last column have been estimated from the graph of figure 6, taking account of the standard deviations of the gap count distributions.

Table XVI.

Track	Grain density from grain counts (grains/50μ)	Optimum gap size (scale divisions)	Track length (μ)							
			100	300	500	1000	1500	2000	3000	5000
1	13.6	7	8.0	7.4	7.3	7.7	7.5	7.7	7.7	8.4
2	25.5	3	21.5	18.7	16.5	18.0	19.0	20.2	19.7	19.5
3	29.2	3	10.8	14.5	12.5	15.4	14.2	14	14.1	
4	34.0	2	11.0	10.7	11.4	11.6	12.6	12.4	12.4	
5	41.7	1	27	31.5	34.1	36.0	34.7	34.3	33.8	

The uncertainties shown in the last columns of Tables XV and XVII have been calculated from the data obtained from the entire track lengths, those in the second of these tables being approximate values determined from the graph of figure 6.

From these results it appears that the values of the grain density obtained from measurements on any length of track greater than 300μ are the same to within a few per cent. as those which are obtained from 3 or 5 mm. of track. This indicates that it is possible to find a reasonably accurate estimate of the grain density of any track which has a range in the emulsion of more than 300μ.

V.6. Applications of the gap count method.

The purpose of this study of gap counting was to establish a quick, reliable method of determining the grain density of a track, with a view to using this parameter in the identification of particles associated with cosmic ray stars. Some of the applications of this method to the tracks of particles will now be considered, but the most important application to the present work, namely the identification of singly charged particles from the variation of their ionisation with range, will be discussed in the next chapter.

V.6.1. The mass of slow particles.

It was stated in Chapter IV that the grain density along the track of a singly charged particle is proportional to the rate of loss of energy of the particle, and this in turn is a function only of the velocity,

$$n = f_1(v).$$

Also, for a given velocity, the residual range of the particle is

$$R = mf_2(v)$$

and two singly charged particles of masses m_1 and m_2, travelling with the same velocity, have residual ranges R_1 and R_2 in the ratio

$$\frac{R_1}{R_2} = \frac{m_1}{m_2}.$$

Since the velocities of the particles are equal, the grain densities of the two tracks will also be equal, and it is therefore possible to determine the mass ratio, m_1/m_2, of two particles which end in the emulsion by comparing their ranges at equal ionisation densities, assuming that

$$n = \phi_1\left(\frac{R}{m}\right).$$

To reduce the effects of statistical fluctuations, it is customary to use the "integrated ionisation", that is, the total number of developed grains N in the track up to residual range R, or, since the ionisation may also be determined from the gap count, the total

number of gaps G in the track up to range R. n, the grain density, may be written in the form $\frac{dN}{dx}$ where dN is the number of developed grains in an element of track of length dx, and so

$$\frac{dN}{dx} = \phi_1\left(\frac{R}{m}\right)$$

and the total number of grains up to range R may be obtained by integration:

$$N = \int_0^N dN = m\int_0^{R/m} \phi_1\left(\frac{R}{m}\right) d\left(\frac{R}{m}\right) = m\phi_2\left(\frac{R}{m}\right)$$

[redacted]

Similarly, the cumulative gap total G [redacted] may be expressed in the form

$$G = \int_0^G dG = m\phi_3\left(\frac{R}{m}\right)$$

The mass ratio of the two particles may be found using the graphical procedure suggested by Perkins (Lattes et al., 1948). A graph of G for a given gap size as a function of R is plotted on a double logarithmic scale for each particle, and a line at 45° to the axes is drawn to intersect the two curves. The mass ratio $\frac{m_1}{m_2}$ is then obtained from the ratio of the intercepts on

either axis of the points of intersection of this line with the curves.

This method of determining the mass ratio of two particles can only be applied if gaps of the same size are counted in both tracks. The equation of the line expressing log G as a function of log R is

$$\log G = c_1 \log R + \log c_2$$

where c_1 is the slope of the line, and c_2 is a constant. While c_2 depends on the mass of the particle, as will be shown in figure 14, the slope of the graph varies according to the gap size. This is illustrated by the graph of figure 13, where the cumulative totals for gaps of different sizes are plotted as a function of residual range, using the results shown in Table XVIII, which were obtained from a long track in one of the plates.

Using this method of determining mass ratios, it was found that a value of the mass of a particle, correct to within a few per cent., could be obtained from gap counts on a single track. To illustrate this, results are given below for four particles which came to rest in the plates, namely a μ -meson and a π -meson, both identified by their decay products, a proton recoil, and a particle heavier than a proton but singly charged, and later identified by this method as a deuteron.

Gap counts ($\bar{x} > 1$ scale division) were made over the entire length of each of the tracks. The cumulative

Table XVIII.

Residual Range (mm.)	Cumulative gap totals			
	$\bar{x}$ > 1 div.	$\bar{x}$ > 2 div.	$\bar{x}$ > 3 div.	$\bar{x}$ > 4 div.
1.2	2			
1.5	3			
2.1	5			
2.4	6			
2.7	8			
3.0	14			
3.3	17			
3.9	24			
4.5	34	1		
4.8	40	2		
5.4	51	3		
6.0	60	4		
6.9	83	7		
7.5	98	7	1	
9.0	138	15	2	
10.5	187	21	3	
12.0	263	32	4	
13.5	327	42	4	
15.0	398	55	8	1
16.5	486	69	10	2
18.0	605	99	13	3
19.5	706	122	17	5
22.5	918	182	33	7
25.5	1187	257	54	14
28.5	1473	355	84	27
31.5	1797	458	117	34
34.5	2138	584	167	52

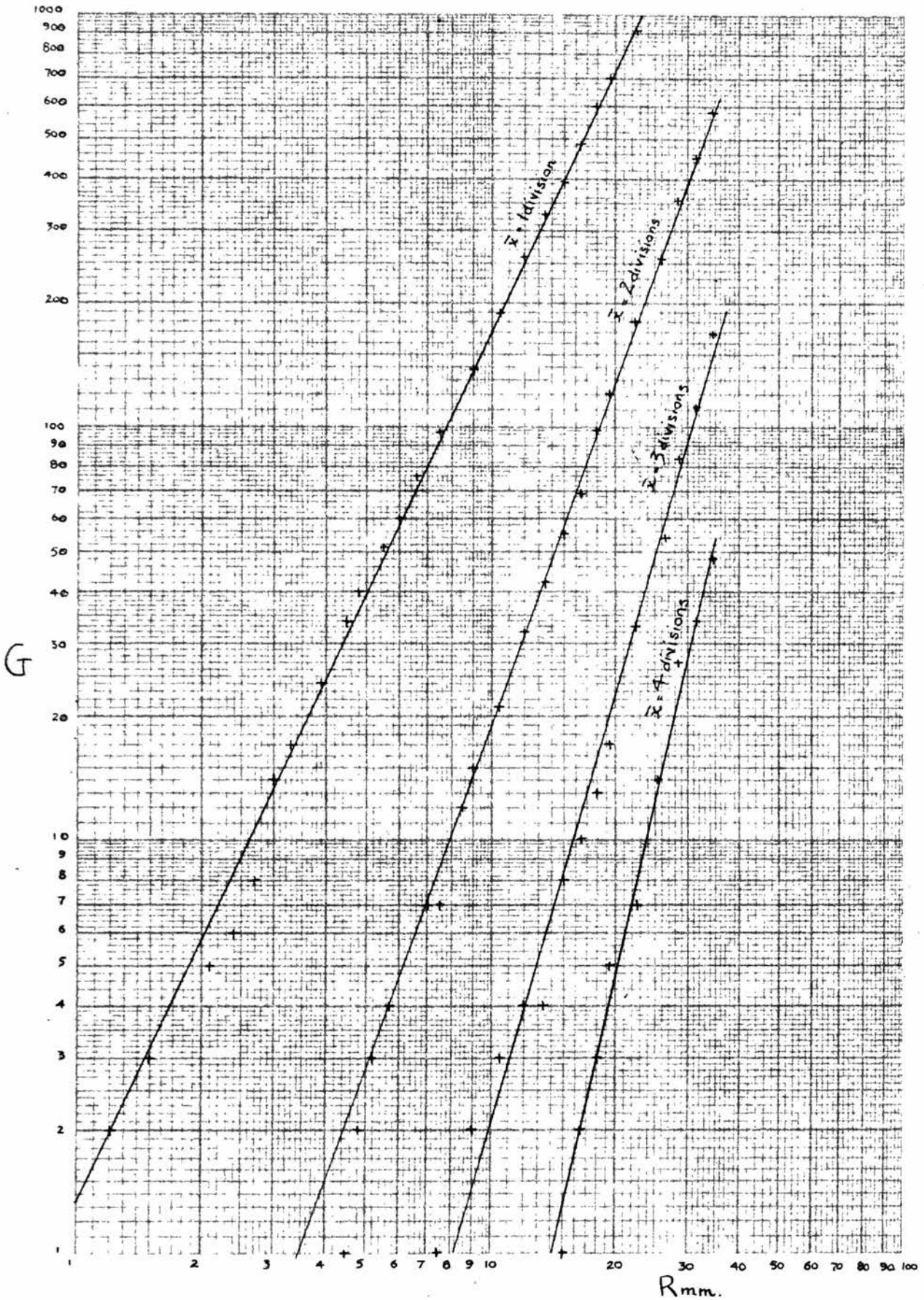

FIGURE 13 Cumulative gap count, G, v. Residual range (mm.) for gaps greater than 1, 2, 3 and 4 scale divisions in length.

gap totals G, for different values of the residual range R, were calculated from these readings as shown in Table XIX, and the graphs of G as a function of R were plotted as shown in figure 14.

Table XIX.

Range (mm.)	Cumulative gap totals ($\bar{x}$ > 1 div.)		Range (mm.)	Cumulative gap totals ($\bar{x}$ > 1 div.)	
	Proton	Deuteron		μ -meson	π -meson
2.1	11		1	31	20
2.7	25	8	1.2	45	35
3.8	48	24	1.5	75	62
5.2	82	42	1.8	107	86
6.0	127	60	2.1	154	116
7.5	205	98	2.2	170	129
9.0	299	138	2.4	211	
10.5	421	187	2.7	265	
12.0	537	263	3.0	319	
15.0	840	399			
17.5	1180	600			
21.0		834			
24.0		1046			
27.0		1317			
33.0		1954			

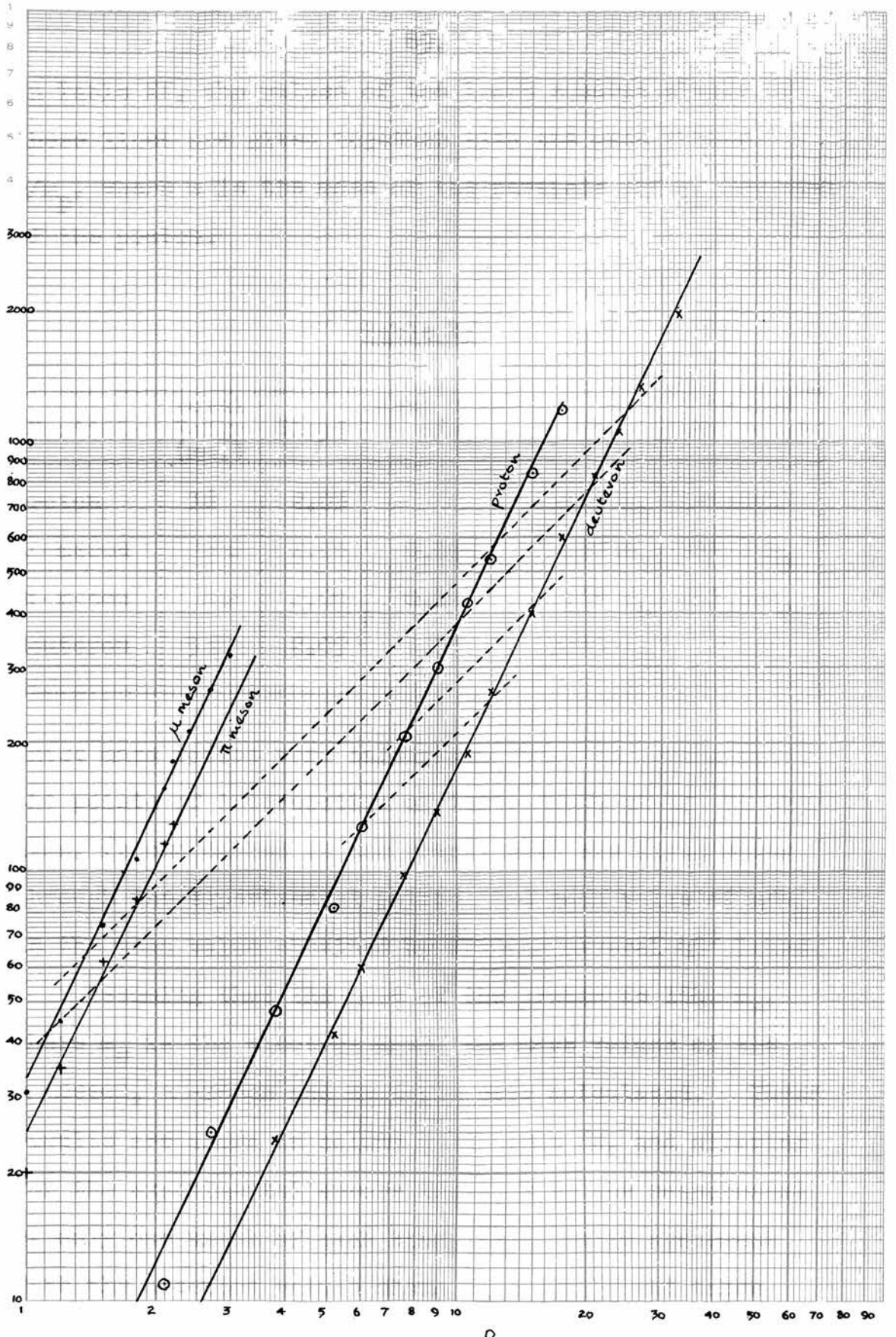

FIGURE 14. Cumulative gap count G v. Residual range R (in mm.) (for gap length $\bar{x} > 1$ scale division) for 4 particles — μ and π mesons, proton and deuteron — in G5 emulsions. The broken lines are at 45° to the axes.

In Table XX, the values of the least squares slopes of these lines are given together with the mass ratios m/m_p, where m is the mass of the particle and m_p the mass of the proton.

Table XX.

Particle	Total Range (mm.)	Slope	Mass ratio m/m_p	Mass	Standard mass value
proton	18	2.03		1840 m_e	(assumed)
μ-meson	3·0	2.06	0.096	177 m_e	206.7 m_e
π-meson	2·2	2.04	0.14	258 m_e	273.1 m_e
deuteron	33	2.09	1.95	3588 m_e	

These mass ratios were calculated from the ordinates of the points of intersection of lines drawn at 45° to the axes, (shown dashed in the graph) with the lines drawn through the experimental points, and each value of m/m_p is the mean value obtained by drawing several 45° lines.

Assuming that the mass of the proton is 1840 m_e, where m_e is the electron mass, the mass values of the μ-meson, π-meson and deuteron were calculated. These results are shown in column 5 of Table XX, and allowing for the experimental errors involved in the measurement of only one track of each kind, they are in agreement with the accepted values shown in column 6 and taken

from Shapiro (1956).

It will be seen from figures 13 and 14 that, for a given gap size, the graphs of log G v. log R are straight lines over the ranges of the particles considered. In the following paragraph, it will be shown how use was made of this straight line relationship in the determination of the residual range of a particle. The particular application of this procedure was to the "joining" of two tracks.

V.6.2. Joining tracks. A. The residual range method.

One of the main problems encountered during the study of the gap count technique was that of finding tracks which were long enough to show the variation of gap density over a range of several centimetres in the emulsion, and which could be used as standards for calibration and comparison. Although a large area of the plates was searched, no suitable tracks could be found, and it was decided that the only means of securing the desired range of observations was by combining the results from two or more tracks.

This decision was prompted by the fact that two long tracks had been found: one which came to rest in the emulsion and had a range of 14.15 mm., and another formed by a particle which entered the emulsion from the upper surface, and travelled 31.5 mm. before leaving the lower surface. Gap counts on the first track showed that it

was formed by a particle heavier than a proton, (later identified as a deuteron by the method described in V.6.1), and towards the high energy end of the track the gap density was the same as that of the other track at its low energy end near the glass. An attempt was then made to "join" these two tracks by finding the point at which the gap density of the faster track was equal to the gap density in the stopping track, and by comparing the densities in the overlapping region.

The method of joining the tracks was based on the following consideration. From the graph of figure 14, it follows that for singly charged particles and a given gap size

$$\log G = c_1 \log R + \log c_2$$

where, as before, c_1 is the slope of the line, and c_2 a constant, and so

$$G = c_2 R^{c_1}.$$

Differentiating this equation with respect to R, we have

$$\frac{dG}{dR} = c_1 \times c_2 R^{(c_1 - 1)} \qquad (18).$$

Now, $\frac{dG}{dR}$ is the rate of change of the cumulative gap total with range, therefore,

$$\frac{dG}{dR} = \text{gap density.}$$

Thus using equation (18), the gap density for a given gap size may be calculated for different values of R. The constant c_1 will vary according to the size of gap,

and c_2 will vary with the mass of the particle. If the gap density along a track is known, it should then be possible to calculate the residual range.

The cumulative total graphs for gap sizes of 1, 2 and 3 scale divisions were drawn, and have already been shown in figure 13. From the least squares solutions of these lines, the values of the constants c_1 and c_2 given in Table XXI were calculated.

Table XXI.

Gap size (scale divisions)	c_1	c_2
1	2.09	1.43
2	2.77	3.21×10^{-2}
3	3.85	2.03×10^{-4}

Thus the equations of gap density $\frac{dG}{dR}$, which will now be denoted by $g'_{\bar{x}}$, as a function of R, are

$$\left.\begin{aligned} \bar{x} = 1 \text{ scale division} &: g'_1 = 2.99R^{1.09} \\ \bar{x} = 2 \text{ scale divisions} &: g'_2 = 0.089R^{1.77} \\ \bar{x} = 3 \text{ scale divisions} &: g'_3 = 7.82 \times 10^{-4} R^{2.85} \end{aligned}\right\} \quad (19).$$

In the second track, the numbers of gaps per 3 mm. of track were calculated for successive 3 mm. sections, and the residual ranges corresponding to these gap densities were calculated. Using these ranges, the residual range R_o, of the particle at the point where it

entered the emulsion, was calculated by subtracting from each value the appropriate distance from the glass, measured along the track. In the latter part of the track, it was found that the density of 1 division gaps began to decrease with increasing range. No explanation can be offered for this anomaly, except perhaps a change in the inclination of the track which would account for the decrease in value of R_o obtained from the part of the track nearest the surface.

From these results, shown in Table XXII, the mean value of the residual range, at the point where the particle entered the emulsion, was found to be

$$R_o = 11.9 \pm 1.4 \text{ mm.}$$

In the Table XXII, the 3 mm. sections are numbered in order, starting with the section nearest the glass.

It was then possible to combine the observations from the two tracks, and to construct the graph of log G v. log R for a deuteron as shown in figure 13 where gaps of up to 4 scale divisions have been included.

It must be noted that this method of joining tracks is applicable only if the tracks are formed by the same kind of particle. An earlier attempt to combine the results from the stopping track with those of another which did not come to rest were unsuccessful because in this case the second track was actually formed by a proton, and consequently the equation (19) did not apply.

Table XXII.

Section	$\bar{x}$ > 1 division			$\bar{x}$ > 2 divisions			$\bar{x}$ > 3 divisions		
	g'_1 (gaps/ 3 mm.)	Residual Range (mm.)	R_o (mm.)	g'_2 (gaps/ 3 mm.)	Residual Range (mm.)	R_o (mm.)	g'_3 (gaps/ 3 mm.)	Residual Range (mm.)	R_o (mm.)
1	135	12.0	12.0	23	12.3	12.3	4	13.7	13.7
2	207	17.8	14.8	44	18.0	15.0	5	14.1	11.1
3	218	18.6	12.6	57	20.7	14.7	14	21.1	15.1
4	223	19.1	10.1	67	22.7	13.7	16	21.9	12.9
5	271	22.7	10.7	76	24.5	12.7	25	26.0	14.0
6	310	26.0	11.0	114	30.6	15.6	35	29.2	14.2
7	327	27.0	9.0	104	29.2	11.2	36	29.5	11.5
8				116	30.9	9.9	43	31.3	10.3
9				127	32.4	8.4	48	32.5	8.5
10				148	35.5	8.5	55	34.3	7.3
	Mean R_o = 11.4 ± 1.9 mm.			Mean R_o = 12.2 ± 2.6 mm.			Mean R_o = 11.9 ± 2.6 mm.		

V.6.2. Joining tracks. B. The χ^2 test.

In order to check the value R_o = 11.9 mm. obtained by the method A, a second method of joining the tracks was employed. Since gap density varies with residual range, it is possible to determine the residual range of the second track by finding the portion of this track whose gap density is most nearly equal to the gap density at the high energy end of the stopping track.

For the stopping track, the numbers of gaps greater than 1 and 2 scale divisions in length in the last 3 mm. section were

Table XXIII.

Gap size (scale divisions)	1	2
Gap density per 3 mm.	186	27

and the χ^2 test was applied to find the 3 mm. section of the other track which had the same gap density. This test consists of finding the section of track for which χ^2 is a minimum, where

$$\chi^2 = \sum \frac{x^2}{m}$$

and m = expected value (in this case, the gap density of the stopping track)

m_o = observed value (the gap density of the second track)

$x = m - m_o$.

The numbers of gaps greater than 1 and 2 scale divisions in length in overlapping 3 mm. sections of the second track are shown in Table XXIV, where the distances are measured from the point at which the track starts to the beginning of each 3 mm. section. Also shown in this table are the values of x, $\frac{x^2}{m}$ and χ^2, and the suffixes 1 and 2 refer to the 1 and 2 division gaps respectively.

In figure 15, a graph of χ^2 v. distance has been drawn, and this shows that χ^2 has a minimum value for the section beginning 1.8 mm. from the glass. This section therefore corresponds to the last 3 mm. section of the stopping track, and since the total range of this track was 14.15 mm. it follows that the residual range of the second track at the glass is

$$R_o = (14.15 - 3) - 1.8 \text{ mm.} = 9.35 \text{ mm.}$$

While this value is rather smaller than that obtained by the other method, the agreement between the results is regarded as satisfactory, considering the experimental error involved (approximately 25% in the case of the 2 division gaps alone), and the small changes in gap density which occur in tracks of this grain density (90 grains/50μ).

In an attempt to define the residual range of this second track more accurately, the χ^2 test was applied using successive 3 mm. sections starting 300μ and 100μ apart. However, statistical fluctuations in the gap numbers were such that no further information could be obtained from these results.

Table XXIV.

Distance (mm.)	Gap size > 1 scale division			Gap size > 2 scale divisions			$\chi^2 = \frac{x_1^2}{m_1} + \frac{x_2^2}{m_2}$
	Number of gaps	x_1	$\frac{x_1^2}{m_1}$	Number of gaps	x_2	$\frac{x_2^2}{m_2}$	
0	135	51	14.0	23	4	0.6	14.6
0.6	148	38	7.8	29	2	0.1	7.9
1.2	161	25	3.4	25	2	0.1	3.5
1.8	165	21	2.4	30	3	0.3	2.7
2.4	186	0	0	37	10	3.7	3.7
3.0	207	21	2.4	44	17	10.7	13.1
3.6	217	31	5.2	48	21	16.3	21.5

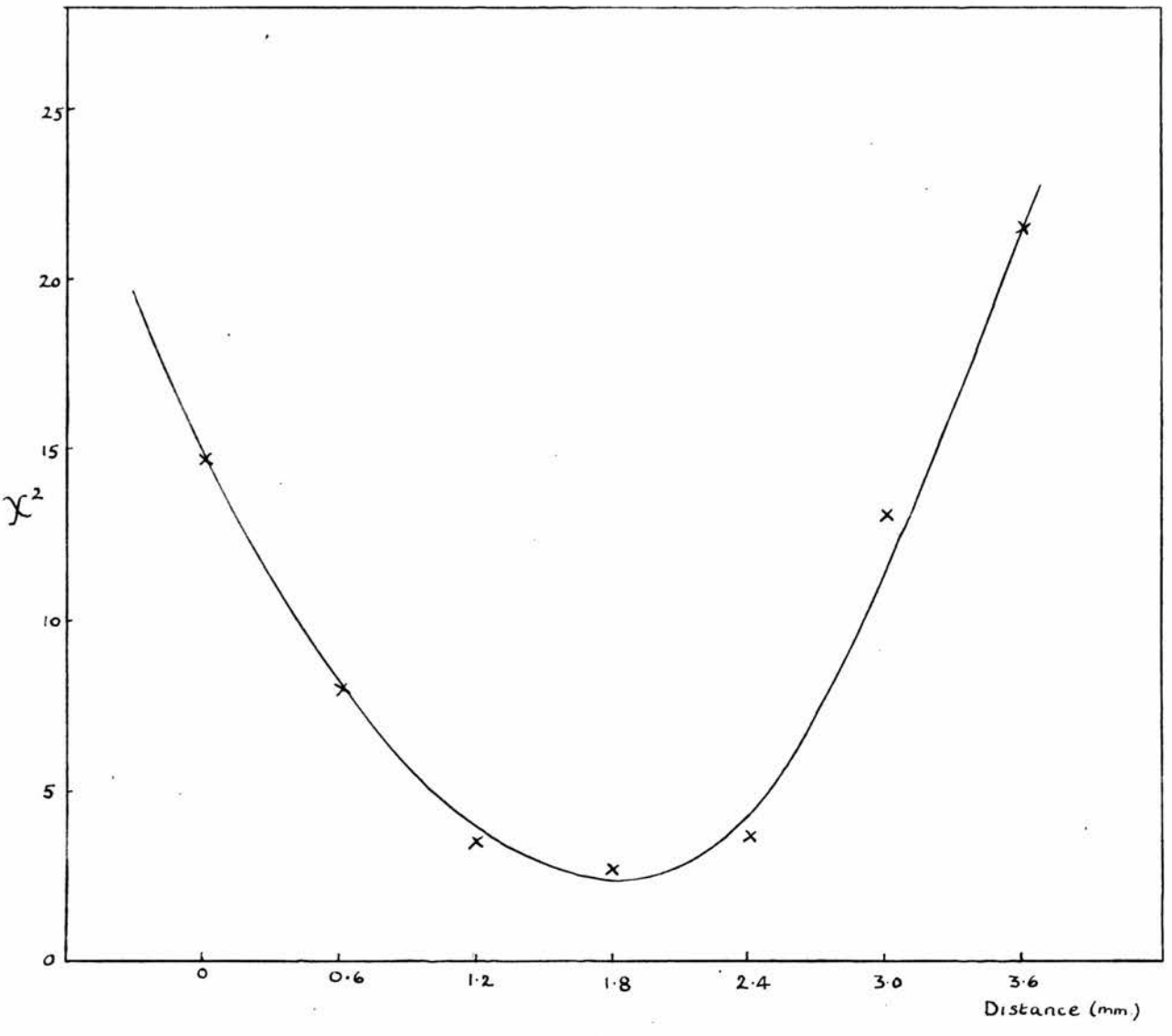

FIGURE 15 χ^2 v. Distance for overlapping 3mm. sections of track. Distances are measured in mm. from the end of the track to the beginning of the 3mm. sections.

While neither of these methods can give an exact value of the point of overlap of these two tracks, the first has the advantage that it can only be applied to the tracks of identical particles. Using the second method, it is possible to relate, apparently successfully, the tracks of different particles, and the results must therefore be verified by the construction of a graph of log G v. log R from the combined gap numbers in the two tracks. If the tracks have in fact been formed by different particles, there will be a change in the slope of the graph. On the other hand, this second method is applicable when neither of the tracks stops in the emulsion, but the method A may be used only when one particle comes to rest, as it is otherwise impossible to determine the equations relating G and R.

V.6.3. Wet tracks.

A further application of the procedure of plotting G as a function of R was to the tracks of particles which passed through the emulsion in the early stages of processing, while the emulsions were wet but before development was complete. The problem of these so-called "wet tracks" was first encountered during the systematic searching of the plates, when occasionally a star was seen to consist of a number of thin tracks, some of them ending in the emulsion. While it is possible that a secondary particle from a star may decay in

flight, producing a track which ends abruptly in the emulsion, the probability that more than one such particle will be ejected from a nuclear disintegration is very small. It was therefore concluded that these events could only be explained if it was assumed that they took place while the emulsion was wet, that is, during the 4 hours when the plates were soaked in ice-cold developer, or near the beginning of the half-hour development time in the warmed space. Events of this kind were rare, as is to be expected since the development time is very short compared with the total exposure time of approximately 100 days, and only three were observed in all the plates.

In order to study the differences in the behaviour of the tracks of particles passing through wet and dry emulsions, a number of Ilford G5 plates were exposed to the 15 MeV neutron flux produced by deuteron bombardment of a solid lithium target in the Edinburgh one million volt Cockcroft and Walton cascade generator, and measurements were made on the tracks of the proton recoils produced in the emulsions by the incident neutrons. Some of these plates had been soaked in ice-cold developer for 4 hours before the exposure which lasted only for 10 minutes, and were returned to the warmed space for development immediately afterwards. During the exposure they were maintained at the low temperature to

prevent development taking place. The other plates were not processed until after the exposure and the neutrons therefore passed into dry emulsions. Proton tracks in these two sets of plates will be referred to as "wet" and "dry" tracks respectively.

Gap counts were made on a number of these wet and dry tracks, straight tracks parallel to the emulsion surface being used wherever possible. Unfortunately, the overall range of the protons was never more than approximately 1 mm. in the dry emulsion, corresponding to an energy of about 14 MeV, and this restricted the gap measurements to those greater in length than 0.5 scale divisions. From the measurements made on 12 wet tracks and 12 dry tracks, the mean gap densities (in gaps per 100μ) for different values of the residual range were determined, and the cumulative totals of the gaps were calculated as shown in Table XXV.

The graphs of log G as a function of log R were plotted (figure 16), and the equations of the lines were found to be:

$$\text{Dry protons: } \log_{10} G = 1.26 \log_{10} R + \log_{10} 0.0027 \qquad (20)$$
$$\text{Wet protons: } \log_{10} G = 1.11 \log_{10} R + \log_{10} 0.05$$

where R is in microns. While the slopes of these lines are not exactly equal, the difference in the values is probably due only to the experimental errors involved. These errors, which are reflected in the values of the

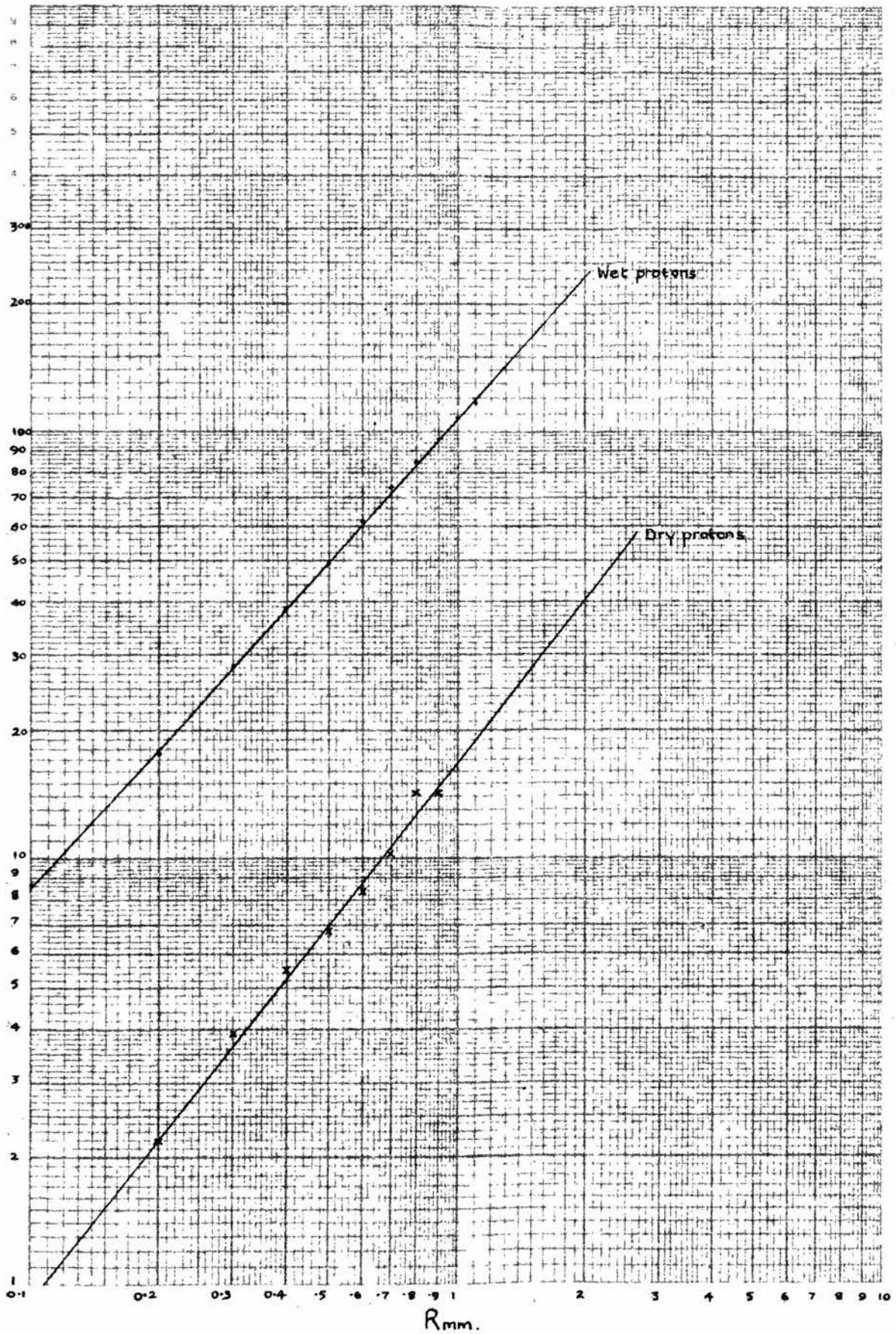

FIGURE 16 Cumulative gap count G v. Residual range R (in mm.) for gaps greater than 0·5 scale divisions in length in wet and dry proton tracks.

Table XXV.

Residual Range (mm.)	Wet protons		Dry protons	
	Mean gap density, $g'_{\frac{1}{2}}$ (gaps/100 μ)	$G_{\frac{1}{2}}$	Mean gap density, $g'_{\frac{1}{2}}$ (gaps/100 μ)	$G_{\frac{1}{2}}$
0 - 0.1	8.6	8.6	0.9	0.9
0.1 - 0.2	8.9	17.5	1.3	2.2
0.2 - 0.3	10.8	28.3	1.7	3.9
0.3 - 0.4	10.3	38.6	1.6	5.5
0.4 - 0.5	11.0	49.6	1.3	6.8
0.5 - 0.6	11.9	61.5	1.6	8.4
0.6 - 0.7	12.9	74.4	1.8	10.2
0.7 - 0.8	10.6	85	4	14.2
0.8 - 0.9	11.5	96.5	0	14.2
0.9 - 1.0	12.0	108.5		
1.0 - 1.1	9.0	117.5		

gap density shown in Table XXV, are due to poor statistics because of the small number of observations available, and to the large error involved in the measurement of these very small gaps. A more accurate estimation of the variation of gap density with residual range may however be obtained from the equations (20), since the use of the cumulative gap count tends to reduce the effect of statistical fluctuations in the numbers of gaps. From these equations, expressions for the gap

density, $\frac{dG}{dR}$ or $g'_{\frac{1}{2}}$, were derived as described in V.6.2, and the gap density in units of gaps/300μ was calculated for different values of the residual range. The grain density appropriate to each gap density was also determined, using the graph of fig. 6, and all these results are shown in Table XXVI.

Table XXVI.

Range (mm.)	Wet proton tracks		Dry proton tracks		
	Gap density $g'_{\frac{1}{2}}$ (gaps /300μ)	Grain density n_w (grains /50μ)	Gap density $g'_{\frac{1}{2}}$ (gaps /300μ)	Grain density n_d (grains /50μ)	$\frac{n_d}{n_w}$
0.05	25.1	120	2.8	220	1.833
0.15	29.1	112	3.9	206	1.840
0.25	30.8	109	4.4	200	1.835
0.35	32.0	107	4.8	197	1.841
0.45	32.9	105	5.2	194	1.848
0.55	33.7	104	5.5	192	1.846
0.65	34.3	103	5.7	190	1.845
0.75	34.9	102.5	5.9	188	1.834
0.85	35.3	101.5	6.1	186	1.832
0.95	35.9	101	6.3	185	1.832

In the last column of this table the values of the ratio of the grain density in a dry track to that in a wet track for the given ranges are also shown. Over

the length of track considered these values are approximately constant, and this implies that the rate of change of grain density with range is the same for both wet and dry tracks. The mean value of the ratio is

$$\frac{n_d}{n_w} = 1.839 \pm 0.002$$

and this must be a measure of the degree of swelling in the wet emulsion, that is, a measure of the change in the number of grains per unit volume of emulsion. The value of the ratio $\frac{n_d}{n_w}$ depends on the volume of water in the emulsion and is therefore a constant under given conditions, at least for the tracks of slow particles. Unfortunately it was not possible to compare the grain densities of thin tracks in wet and dry emulsions as the wet plates did not contain any tracks produced by fast particles of known energy.

Another set of Ilford G5 plates, exposed at the same time and under the same conditions as those already considered, was examined to find the effect of underdevelopment on the grain density of the tracks. These plates of which a number had been soaked in ice-cold developer for 4 hours before exposure, were removed from the warmed space after 15 minutes, exactly half the time normally allowed for development. Gap counts on the wet and dry tracks in these plates, when analysed in the same manner as before, gave almost exactly the same results as those on the tracks in the fully developed plates. This suggests that development of the latent

image is in fact complete after only 15 minutes in the warm development stage.

The results obtained from this study of the differences between tracks formed in wet and dry emulsions were of use in the identification of events which had taken place during the development process, and not during the time of exposure of the plates on the mountain. Gap counts made on thin tracks which stopped abruptly in the emulsion were used to show whether these were produced by unstable particles which decayed in flight, or by particles passing through the emulsion while it was wet. For a particle of the second kind, a graph of log G v. log R constructed from measurements of gaps of a given size was a straight line parallel to the corresponding line for a track in a dry emulsion. Where the line was not parallel to that of the dry track, it could be assumed that the particle had decayed in flight.

V.7. Conclusions.

From the work described in this chapter it may be concluded that the gap count method provides a convenient and accurate means of determining the grain density produced by a charged particle during its passage through a nuclear emulsion, and that it may be used for the determination of the mass of a particle which stops in the emulsion, for the "joining" of tracks and for the

identification of events which have taken place while the emulsion is wet.

The advantages of this method over the direct grain counting method are:

(1) the gap count method may be used for all tracks regardless of their grain density, and, with certain limitations, for tracks which are inclined to the plane of the emulsion.

(2) when gaps of all sizes are measured, the error in the calculated value of the grain density is smaller than that obtained by grain counting.

(3) when only one gap size, the optimum or best gap length, is used, the gap counts may be obtained more quickly than the corresponding grain count, and the standard deviation of the distribution of gap numbers is smaller than that of grain numbers.

(4) the criterion for selecting gaps is less subjective than that for grains or even for blobs, and the values of gap density do not vary from one observer to another.

This particular method of classifying gaps has also the advantage over some other gap counting techniques that the exact lengths of the gaps are not required, and consequently serious errors in measurement do not arise.

Chapter VI.

PROTON ENERGY LOSS AND GRAIN DENSITY.

Having established the gap counting method as a suitable means of measuring the grain density of a track, the next problem was to determine the relations between the grain density and the velocity, kinetic energy and residual range of the particle which produced the track. In this chapter, these relationships are derived for a proton, starting from the expression derived by Bethe for the rate of loss of energy of a charged particle during its passage through matter, and using the experimental results obtained from a number of proton tracks.

VI.1. Energy loss as a function of velocity, kinetic energy and residual range.

A charged particle travelling with a velocity $v\ (=\beta c)$ through a medium of atomic number Z, containing N atoms per cm.^{3}, loses energy at a rate which is expressed by:

$$-\frac{dE}{dx} = \frac{4\pi e^4 z^2}{mc^2\beta^2} NZ\left[\log_e \frac{2mc^2\beta^2}{I(1-\beta)^2} - \beta^2\right] \qquad (21)$$

where ze = the charge of the incident particle

m = the electronic mass

I = the average excitation potential of the atoms of the stopping material.

The formula (21) is valid under the conditions that

(1) $\frac{z}{137\beta} \ll 1$

and (2) $v > v_s$ for all s, where v_s is the Bohr orbital velocity of the sth electron in the stopping material. For a proton, the condition (1) is satisfied for the whole range of energies under consideration.

The condition (2) may also be expressed in terms of the energy E of the incident particle which has a mass M, and the ionisation potential E_s of the electrons of mass m, in the sth orbit:

$$E > \left(\frac{M}{m}\right) E_s.$$

Now, for silver and bromine, the ionisation potentials of the K electrons are respectively 25.6 keV and 13.5 keV; therefore the formula (21) is valid only when the energy of the incident proton is greater than 47 MeV in silver, and 25 MeV in bromine. For a proton of energy less than 47 MeV, the K electrons become less effective in stopping, and below 7 MeV, the contribution to the stopping effect of the L_I electrons of silver, which have an ionisation potential of 3.8 keV, also decreases. In the lighter elements of the emulsion, where the K ionisation potentials are smaller than those of silver and bromine, the condition (2) is satisfied for all except the very smallest velocities.

In order to take account of this change in the effective number of stopping electrons in the atoms of the medium, a correction term must be included in the formula (21), (Livingston and Bethe, 1937), which then

becomes:

$$-\frac{dE}{dx} = \frac{4\pi e^4 z^2}{mc^2\beta^2} N \left[Z \left\{ \log_e \frac{2mc^2\beta^2}{I(1-\beta^2)} - \beta^2 \right\} - \sum_s C_s \right]$$

where C_s is the correction for the non-participating electrons in the sth shell. However, for heavy elements, the contribution of the K electrons to the stopping of a heavy particle (for example, a proton) is small, and the correction term in the expression for the energy loss is also small. Consequently the formula may be applied, without correction, to the stopping of heavy particles down to velocities which are lower than those of the atomic electrons in the stopping medium (Livingston and Bethe, 1937).

In the calculations which follow, the corrections have been neglected even at the lowest proton energies, since it was found that there was a difference of only a few per cent. in the values of $\frac{dE}{dx}$ calculated with and without the correction terms. For the very small values of β, the estimated energy loss is in fact greater than the true value, but the effect of this error on the subsequent calculations of the residual range was found to be small.

When the stopping medium consists of a number of different elements, as in the present case of a nuclear emulsion, the contribution of the atoms of each constituent element to the stopping power must be determined, and the total stopping power obtained by the method

described by Cuer, from the sum of these contributions. In Table XXVII the values of N and Z are given for the elements in an Ilford G5 emulsion (taken from Rotblat†), together with the values of I, the mean ionisation potential per atom for each element. The values of I which were used in these determinations are rather higher than those used in earlier work (for example, Vigneron, 1953), and are calculated from the experimental results quoted by Caldwell (1955) and Sternheimer (1956) who found:

$\frac{I}{Z}$ = 13 eV for light elements (H, C, N, O and S)

and $\frac{I}{Z}$ = 14 eV for heavy elements (Ag, I).

A value of $\frac{I}{Z}$ = 13.5 eV was used for bromine, since the elements lighter and heavier than bromine have mean ionisation potentials of 13Z eV per atom, and 14Z eV per atom respectively.

† Ref. 24.

Table XXVII.

Element	Atomic number	Number of atoms/cm.^{3} (x 10^{22})	I eV/atom
H	1	2.93	13
C	6	1.51	78
N	7	0.31	91
O	8	0.75	104
S	16	0.02	208
Br	35	1.17	472.5
Ag	47	1.17	658
I	53	0.12	742

Using the values of N, Z and I quoted in Table XXVII, the total energy loss of a proton ($z = 1$) in each element of the emulsion was calculated in units of MeV/mm. from the formula (21), neglecting the correction term. Values of β between 0.05 and 0.99 were used. From the sum of the contributions of all the elements, the total energy loss due to collisions, $-(\frac{dE}{dx})_{total}$ MeV/mm., was obtained for each value of β, and the corresponding kinetic energies were determined from the relation

$$E = Mc^2\left[\frac{1}{(1-\beta^2)^{1/2}} - 1\right] \qquad \text{where } Mc^2 = 938 \text{ MeV.}$$

The next step was to find the equation relating the residual range R(E), of a proton, with its kinetic energy E, and this was carried out by graphical evaluation of the integral

$$R(E) = \int_0^R dx = \int_0^E \frac{1}{\frac{dE}{dx}}\, dE$$

where dE is the energy lost in a length dx of the track. Graphs of $(-\frac{dE}{dx})^{-1}$ as a function of kinetic energy were plotted to include all the values of the total energy loss already determined, and the residual range R_1 mm. for a given kinetic energy E_1 MeV was calculated from the total area under the graph from E = 0 to E = E_1 MeV. These results are shown in figure 17 where the values of R have been plotted on a logarithmic scale as a function of kinetic energy. Over a large region, the graph is a

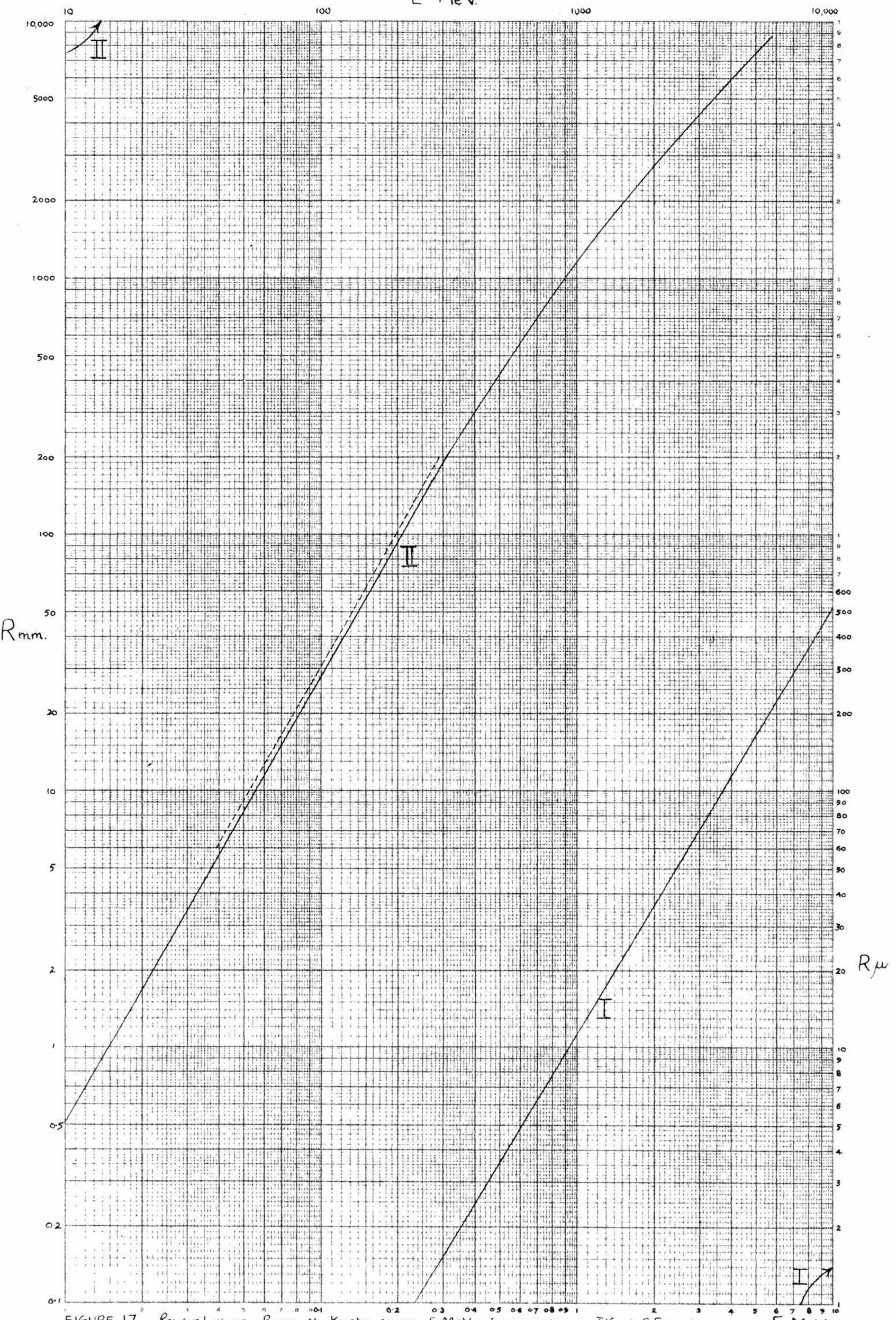

FIGURE 17. Residual range, R mm v. Kinetic energy, E MeV, for a proton in Ilford G5 emulsion.
The dotted line represents the values of R calculated from Vigneron's equation.

straight line which may be expressed by the equation

$$E = aR^{\gamma} \qquad (a, \gamma \text{ constants}).$$

Between 6 mm. and 200 mm., a and γ were found by the method of least squares to have the values

$$a = 0.259$$

$$\gamma = 0.581.$$

Thus

$$E = 0.259R^{0.581} \qquad (22).$$

These values may be compared with those obtained by other workers, from theoretical considerations and by experiment, as, for example, those shown in Table XXVIII. Of these, the first was derived by Fay, Gottstein and Hain (1954) from experimental values given by Bradner et al. (1950), Rotblat (1951) and Catala and Gibson (1951), taking into account the difference in stopping power between Ilford C2 and G5 emulsions. The other follows from calculations by Vigneron (1953), similar to those described above, but making allowance for the change in the number of stopping electrons at low proton velocities.

Table XXVIII.

Reference	a	γ	
Fay et al.	0.281 ± 0.005	0.568 ± 0.003	experimental
Vigneron	0.2806	0.568	calculated
Present work	0.259	0.581	calculated

Although there is apparently a considerable discrepancy between the present values of a and χ, and those derived by other authors, there is in fact little difference between the values of R calculated from the present results, and from those obtained by Vigneron. This is illustrated in figure 17 where the solid line refers to the present work and the dashed line to Vigneron's values of R between 6 mm. and 200 mm. It is most probable that the discrepancy has arisen from the choice of values for the constants I in the original equation: the mean ionisation potentials of the atoms used by Vigneron were all considerably smaller than those used in the present work.

The rate of loss of energy calculated from the formula (21) gives a measure of the total energy loss, including the rare large energy transfers which are responsible for the formation of delta-rays, and do not contribute to the ionisation produced along the actual path of the particle. Since the grain density of the track is a measure of this ionisation only, it is necessary to subtract from the total energy loss the contribution of these large energy transfers, before determining the relation between the grain density and the energy loss (now to be referred to as the "net energy loss").

The shortest identifiable delta-ray has a range of approximately 1 μ, which corresponds to an energy of

5 keV, and thus all single energy transfers greater than 5 keV may be assumed to produce delta-rays without contributing to the ionisation along the track. With this value of the cut-off, the correction to be applied to the total energy loss is (using the same notation as before),

$$\left(\frac{dE}{dx}\right)_{\epsilon>5keV} = \frac{2\pi e^4 z^2}{mc^2\beta^2} NZ\left[\log_e \frac{W_{max}}{W}\right] \qquad (23)$$

where W = 5 keV and W_{max} = the maximum energy which can be transferred to a free electron by the primary. If the total energy of the primary particle is E (including in this case the rest mass energy), and its mass M, it can be shown by applying the conservation laws that

$$W_{max} = 2mc^2 \frac{E^2 - M^2c^4}{2Emc^2 + M^2c^4 + m^2c^4} \qquad (24)$$

and if M >> m, as in the case of a proton, (24) can be replaced by

$$W_{max} = \frac{2mc^2\beta^2}{1-\beta^2} \qquad \text{if } E \ll Mc^2 \frac{M}{m} \quad (25).$$

This value of W_{max} was substituted in the equation (23) and the correction to the total energy loss was calculated for each value of β by summing the values of $(\frac{dE}{dx})_{\epsilon>5keV}$ for all the elements of the emulsion. For very small velocities, this correction is zero, since the logarithmic term vanishes when

$$\frac{2mc^2\beta^2}{1-\beta^2} = W = 5 keV.$$

that is, when $\beta = 0.07$.

Table XXIX has been compiled to show the results obtained from the calculations described in the first part of this chapter. Columns 1 and 2 show the values of β and the corresponding proton kinetic energies: in 3, 4 and 5 are listed respectively the total energy loss calculated from equation (21) neglecting the correction for the change in the effective number of stopping electrons, the correction for large energy transfers calculated from equation (23), and the net energy loss obtained by subtracting the values in column 4 from those in column 3. In the last column, 6, the values of the residual range of a proton are given, having been derived from the equation (22), and the graph of figure 17.

VI.2. Grain density as a function of velocity, kinetic energy and residual range.

In the preceding paragraph, the variation of the velocity, the residual range, the kinetic energy and the net energy loss of a proton have been determined, and it now remains to find the connections between these parameters and a fourth, the grain density of the proton

Table XXIX.

1	2	3	4	5	6
β	E(MeV)	$-\left(\frac{dE}{dx}\right)_{total}$ (MeV/mm)	$-\left(\frac{dE}{dx}\right)_{\epsilon>5keV}$ (MeV/mm.)	$-\left(\frac{dE}{dx}\right)_{net}$ (MeV/mm.)	R
0.05	1.22	44.66		44.66	15.5 μ
0.08	3.01	26.22	1.28	24.94	71
0.09	3.86	22.46	1.89	20.57	107
0.1	4.73	19.44	2.16	17.28	147
0.15	10.7	10.79	2.05	8.74	593
0.2	19.3	6.93	1.60	5.33	1.62 mm.
0.25	30.7	4.86	1.25	3.61	3.57
0.3	45.3	3.62	1.00	2.62	7.25
0.35	63.3	2.84	0.82	2.02	12.89
0.4	85.4	2.26	0.68	1.57	21.62
0.45	112	1.86	0.58	1.28	34.43
0.5	145	1.55	0.50	1.05	53.70
0.55	185	1.33	0.44	0.89	81.68
0.6	235	1.15	0.39	0.76	123.3
0.7	375	0.89	0.32	0.57	265
0.8	625	0.73	0.28	0.45	590
0.85	843	0.67	0.26	0.41	900
0.9	1214	0.63	0.25	0.38	1480
0.92	1455	0.62	0.25	0.37	1850
0.94	1811	0.61	0.25	0.36	2430
0.96	2413	0.61	0.25	0.36	3400
0.98	3776	0.62	0.26	0.36	5640
0.985	4496	0.64	0.27	0.37	6780
0.99	5713	0.66	0.28	0.38	8630

track. For this purpose, use was made of the experimental results obtained from several of the longer tracks observed during the systematic searching of the emulsion. In one plate, a proton was seen to have entered the emulsion from the glass and travelled 15 mm. before coming to rest. Gap counts on the track of this particle made it possible to determine its grain density at different distances from the low energy end, making use of the graph of gap density as a function of grain density (figure 6) in the manner described in Chapter V. From these results and the relationship already established between the residual range and the net energy loss, the results in Table XXX were obtained.

Further results were obtained from a number of tracks formed by fast protons which were among the secondary particles of cosmic ray stars. Their grain densities were determined by the gap count method as above, their kinetic energies were obtained from the scattering parameters as described in Chapter IV, and the corresponding energy losses from a graph of energy loss as a function of kinetic energy. These results are shown in Table XXXI.

An attempt was then made to fit these experimental results into the theoretical relations between the grain density and the specific energy loss of a particle, proposed by Demers (1947) and by Blau (1949).

Table XXX.

Residual Range (mm.)	Gap density, $g'_{\frac{1}{2}}$ (gaps/300 μ)	Grain density (grains/50 μ)	$-\left(\frac{dE}{dx}\right)_{net}$ (MeV/mm.)
0.15	3.0 ± 0.9	215 ± 10	17.1
0.25	3.8 ± 1.0	206 ± 10	13.4
0.35	4.7 ± 1.1	197 ± 10	11.4
0.45	5.6 ± 1.2	191 ± 9	10.0
0.55	6.3 ± 1.3	186 ± 9	9.1
0.7	7.3 ± 1.4	179 ± 9	8.05
0.9	9.0 ± 1.5	168 ± 8	7.2
1.1	10.1 ± 1.6	163 ± 7	6.55
1.3	12.2 ± 1.8	154 ± 7	6.0
1.5	13.6 ± 1.9	149 ± 7	5.6
1.7	15.3 ± 2.0	144 ± 6	5.25
1.9	17.0 ± 2.0	139 ± 5	5.0
2.2	18.6 ± 2.1	135 ± 5	4.65
2.6	21.5 ± 2.3	128 ± 5	4.3
3.0	22.7 ± 2.4	125 ± 5	4.0
3.8	27.3 ± 2.6	115 ± 5	3.58
4.5	31.2 ± 2.8	108 ± 5	3.29
5.5	36.1 ± 3.0	100 ± 4	2.96
7.0	43.1 ± 3.3	90 ± 4	2.65
9.0	51.0 ± 3.5	80 ± 4	2.35

Table XXXI.

E (MeV)	n grains/50μ	$-\left(\frac{dE}{dx}\right)_{net}$ MeV/mm.
80	62 ± 3	1.65
140	49 ± 5	1.07
139	36 ± 2	1.08
288	24.5 ± 2	0.67
1195	13.5 ± 1	0.378

(1) It was suggested by Demers that the probability of development of a grain through which an ionising particle has passed may be expressed in terms of ℓ, the length of the path of the particle in the grain, and E_ℓ, the energy lost by the particle in the grain. Assuming that the grains are spherical in shape, the path length will vary between 0 and d, the grain diameter. If E is the maximum energy spent in the grain (ℓ = d), and I_1 is the mean energy loss per unit length, then

$$E_\ell = I_1 \ell = \frac{E\ell}{d}$$

and the probability that the grain will be developed after receiving an amount of energy E_ℓ is expressed by Demers as

$$P(E_\ell) = 1 - e^{-E_\ell/E_0} \qquad (26)$$

where E_0 is a constant of the dimensions of energy,

which depends on the sensitivity and development of the emulsion.

In general, however, the particle will pass through the grain at random, and for the probability of development in this case Demers has obtained the expression

$$P_1(x) = \frac{\int_0^d \left(1 - e^{-El/E_0}\right) \frac{2l\,dl}{d^2}}{\int_0^d \frac{2l\,dl}{d^2}}$$

$$= 1 - \frac{2}{x^2}\left(1 - e^{-x} - xe^{-x}\right) \qquad (27)$$

$$= \frac{2x}{3} - \frac{x^2}{4} + \frac{x^3}{15} - \frac{x^4}{72} + \cdots \qquad (28)$$

where $x = \frac{E}{E_0} \approx \frac{I}{I_0}$

and I is the specific energy loss of the particle in the emulsion ($\left(\frac{dE}{dx}\right)_{net}$ of Table XXIX).

I_0 is a constant analogous to E_0.

(2) Using the same notation as in (1), the expression proposed by Blau for the probability of development is

$$P_2(x) = 1 - e^{-\sqrt{x}} \qquad (29)$$

The number of developed grains in unit length of the track of an ionising particle (n' grains per micron) can then be expressed in terms of the probability of development:

$$n' = cP(x)$$

where c is a constant depending on the composition of the emulsion, and is equal to the number of grains traversed by the particle per unit length of its path. I_o and c are treated as adjustable parameters.

A comparison between the experimental results and the theoretical relations (27) and (29) above, was made by employing exactly the same technique as Zajac (1949), who compared the experimental results from electron tracks with the Demers and Blau relations. In figure 18 the functions $\log_{10} P_1(x)$ and $\log_{10} P_2(x)$ have been plotted against $\log_{10} x$, together with the experimental values $\log_{10} n'$ as a function of $\log_{10} \frac{dE}{dx}$, using the results of Tables XXX and XXXI. By moving this experimental line (shown dotted in the diagram) parallel to the x-axis, the parameter I_o may be adjusted, and by a similar shift along the y-axis to bring the experimental line into coincidence with the appropriate theoretical curve, the value of c may be determined.

It may be clearly seen from figure 18 that the slope of the experimental line is not comparable with that of the curve obtained from Blau's expression, and consequently the experimental results cannot be fitted to an expression of this form. However, the position of the experimental curve can be adjusted so that it fits Demers' curve, and consequently the grain density per

† However, in 1949 Blau (Univ. of Bristol) reported that all the experimental curves then published for α-particles, tritons, protons, π and μ-mesons, could be represented by this expression.

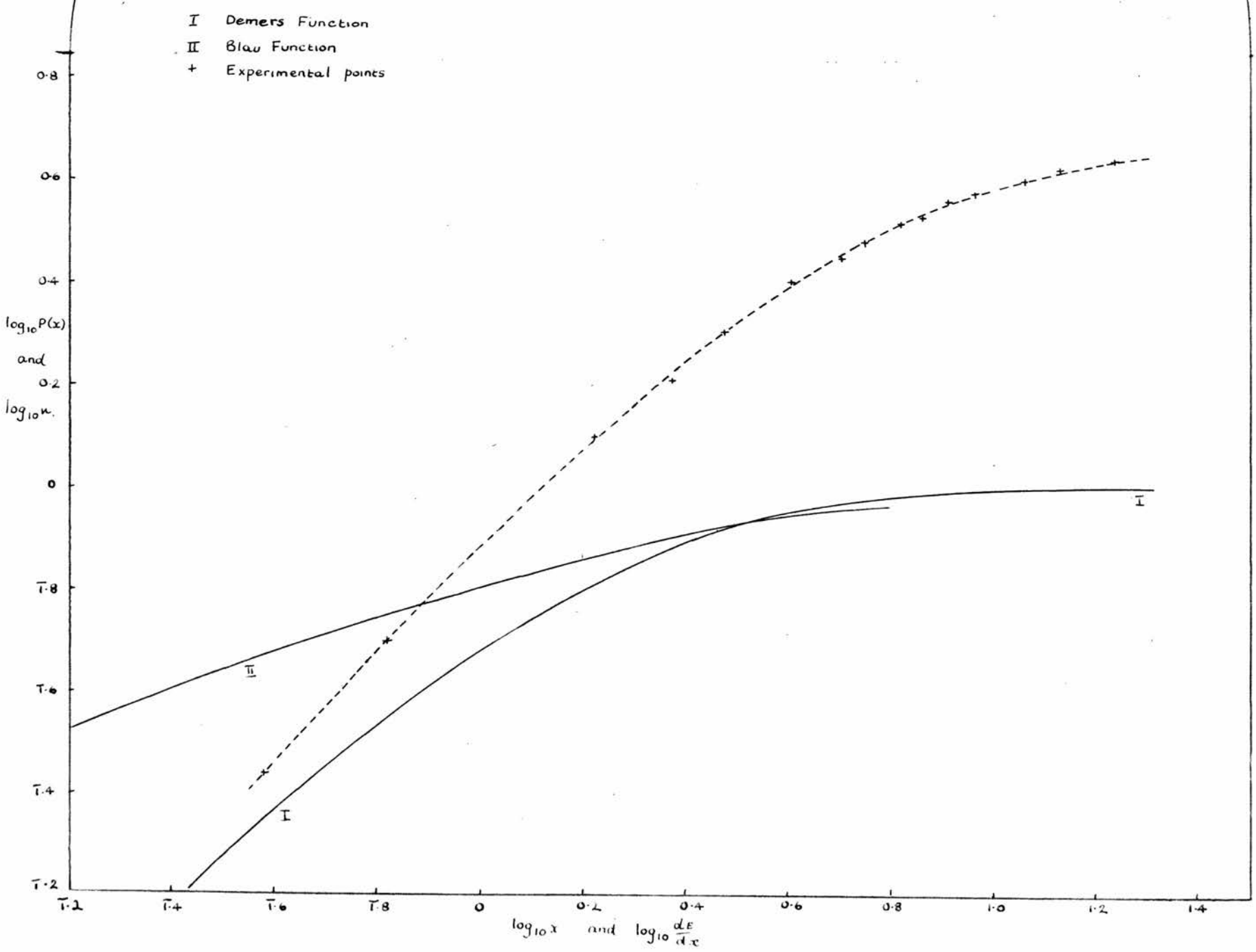

FIGURE 18 $\text{Log}_{10} P(x)$ v. $\log_{10} x$ where $P(x)$ is the probability of development calculated from: I Demers' formula II Blau's formula for different values of x; and $\log_{10} n$ v. $\log_{10} \frac{dE}{dx}$ net drawn for the experimental values of n, the grain density (in grains/50μ) and $\frac{dE}{dx}$ net, the rate of loss of energy (in MeV/mm. or keV/μ)

micron may be expressed as

$$n' = c\left[1 - \frac{2}{x^2}(1 - e^{-x} - xe^{-x})\right] \qquad (30).$$

From the change in the ordinate and in the abscissa required to make the experimental curve coincide with Demers' curve, it was found that the parameters had the values

$$C = 4.68 \text{ grains/micron}$$

$$I_o = 3.47 \text{ keV/micron.}$$

The equation (30) was subsequently used to determine the grain density along a track as a function of the specific energy loss ($\frac{dE}{dx}$ or I) of the particle. As the grain density was usually calculated as the number of grains per 50 of track, the constant c was replaced by

$$n_o = 50 \cdot c = 234 \text{ grains/50}\mu$$

and since $x = \frac{I}{I_o} = 0.288I$

the form of the equation used was

$$n = n_o\left[1 - \frac{2}{(0.288I)^2}(1 - e^{-0.288I} - 0.288Ie^{-0.288I})\right]$$

grains/50μ. (31)

where for convenience I has been used in place of $\frac{dE}{dx}$. For the very small values of I ($\frac{dE}{dx}$) between 0.1 MeV/mm. and 2.0 MeV/mm., more accurate values of the grain density were obtained by inserting the appropriate constant in equation (28).

From the results of these calculations, the graph

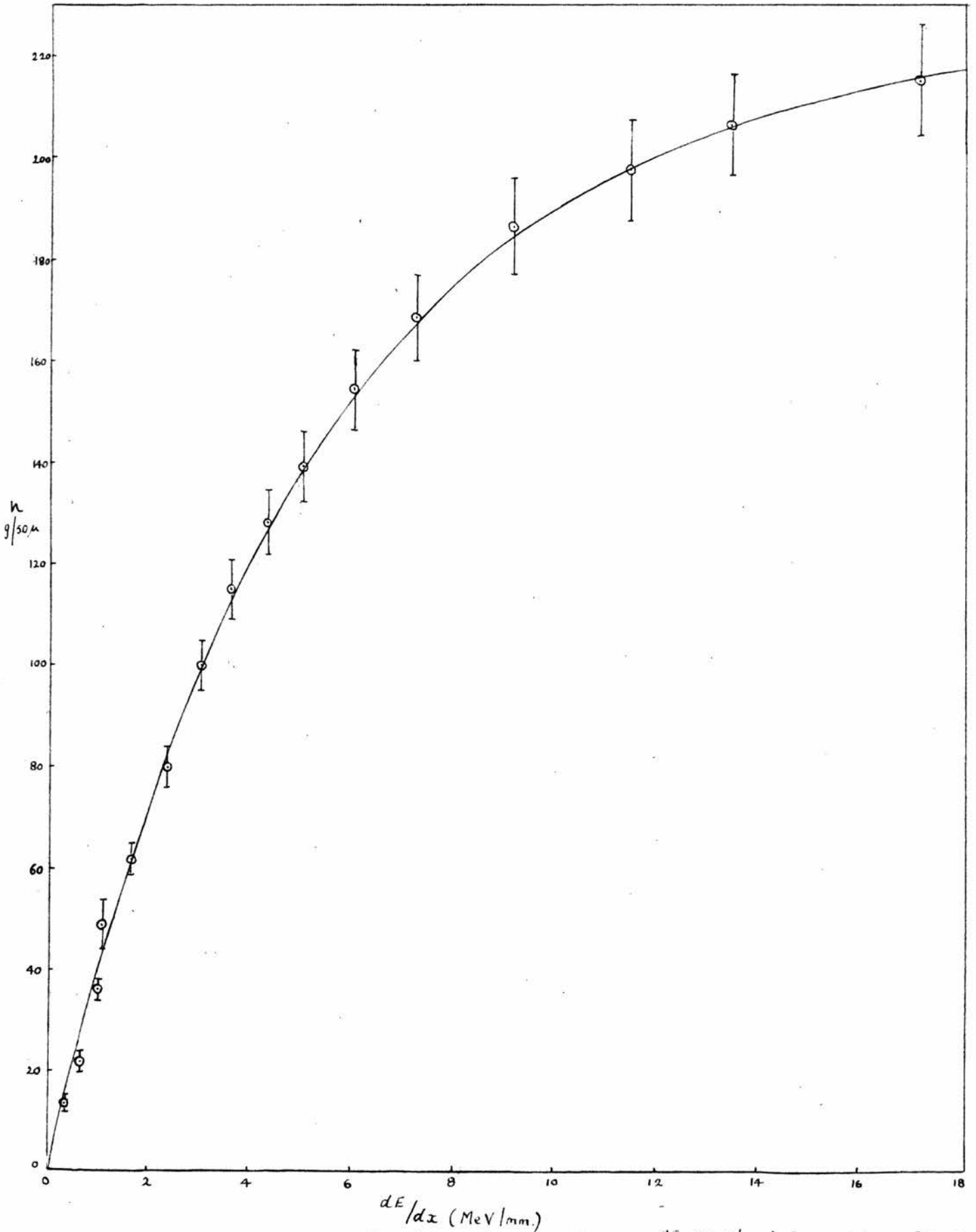

FIGURE 19 Grain density n, (grains/50μ) v. rate of loss of energy, $\frac{dE}{dx}$ (MeV/mm.) for particles in Ilford G5 emulsion. The solid line represents the relation calculated from Demers' expression; the experimental points are taken from the proton tracks.

of figure 19 was drawn, in which the experimental values of the grain density shown in Tables XXX and XXXI, and already used in the determination of the parameters c and I_o, have also been shown. It will be seen that there is close agreement between the experimental results and the theoretical values obtained from equation (31), which are represented by the solid line of the graph.

Even for high values of the grain density, where the experimental errors are large, there is no evidence of a discrepancy between the results obtained from the proton tracks in the emulsion, and those derived by theoretical calculations. This suggests that in the range of values of $\frac{dE}{dx}$ included in this graph, the exclusion from the energy-loss equation of the correction term, which is applicable when the velocity of the incident particle is comparable with the velocity of the atomic electrons in the stopping material, does not introduce an appreciable error.

Using the relations between $\frac{dE}{dx}$ and velocity (β) and $\frac{dE}{dx}$ and grain density, established in this chapter, it was possible to determine the variation of grain density with velocity for a proton. This is illustrated in figure 20 which is in fact applicable to all singly charged particles. Since the kinetic energy and residual range of a proton with a given velocity are

known, the variation of grain density with each of these parameters was also obtained.

Finally, from these relationships for a proton, the corresponding variations in grain density with kinetic energy and residual range for other singly charged particles were determined. It was stated earlier that the grain density along the track of a particle travelling through a given medium is a function of the rate of loss of energy of the particle, and this in turn depends only on its velocity and charge. Thus two particles of mass M and m, with equal charges, and travelling with velocity v, will produce tracks of the same grain density, but since their masses are unequal their kinetic energies will not be the same, and they will travel different distances before coming to rest. Under these conditions it may be shown that

$$\frac{R_M}{R_m} = \frac{E_M}{E_m} = \frac{M}{m} \qquad \text{when } v_M = v_m.$$

Thus, for a given grain density, the residual range and kinetic energy of a singly charged particle of known mass may be determined from the corresponding proton values, using the expression above. The results for a proton are shown in the table overleaf, and illustrated by the graphs of figures 21 (a, b) in which the curves have also been drawn for π and μ-mesons, and for deuterons.

Table showing variation of grain density (n grains/50μ) and $\frac{dE}{dx}$ (MeV/mm.) with velocity (in terms of β), kinetic energy (E MeV) and residual range (R mm.), for a proton in Ilford G5 emulsion.

β	E MeV	R mm.	$\frac{dE}{dx}$ MeV/mm.	n grains/50μ
0.86	900	1020	0.4	17.2
0.75	490	405	0.5	22.0
0.68	345	230	0.6	25.3
0.63	266	147	0.7	29.0
0.58	215	104	0.8	33.0
0.51	155	59	1.0	40.4
0.41	90	23.5	1.5	57.6
0.35	63.5	12.8	2.0	73.1
0.31	48.5	7.8	2.5	87.0
0.28	39	5.4	3.0	101
0.24	27.4	3.0	4.0	121
0.21	20.7	1.9	5.0	139
0.18	16.6	1.3	6.0	153
0.17	13.9	0.94	7.0	165
0.16	11.9	0.71	8.0	175
0.14	9.2	0.45	10.0	190
0.13	7.4	0.31	12.0	200
0.12	6.2	0.23	14.0	208
0.11	5.4	0.18	16.0	213
0.10	4.6	0.135	18.0	217
0.09	3.8	0.1	21.0	222

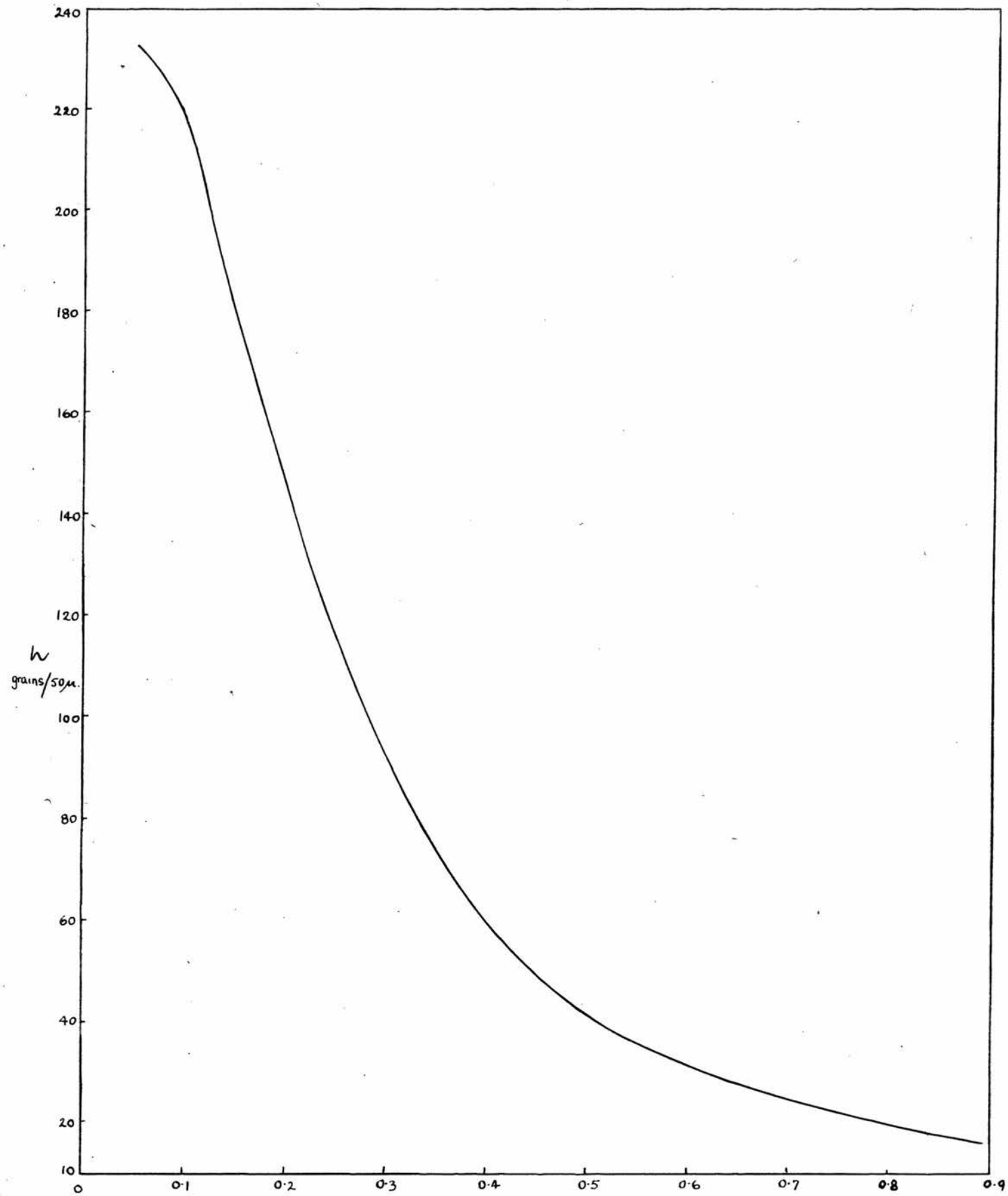

FIGURE 20 Grain density n, (grains/50μ) v. β $(=\frac{v}{c})$ for a singly charged particle in Ilford G5 emulsion.

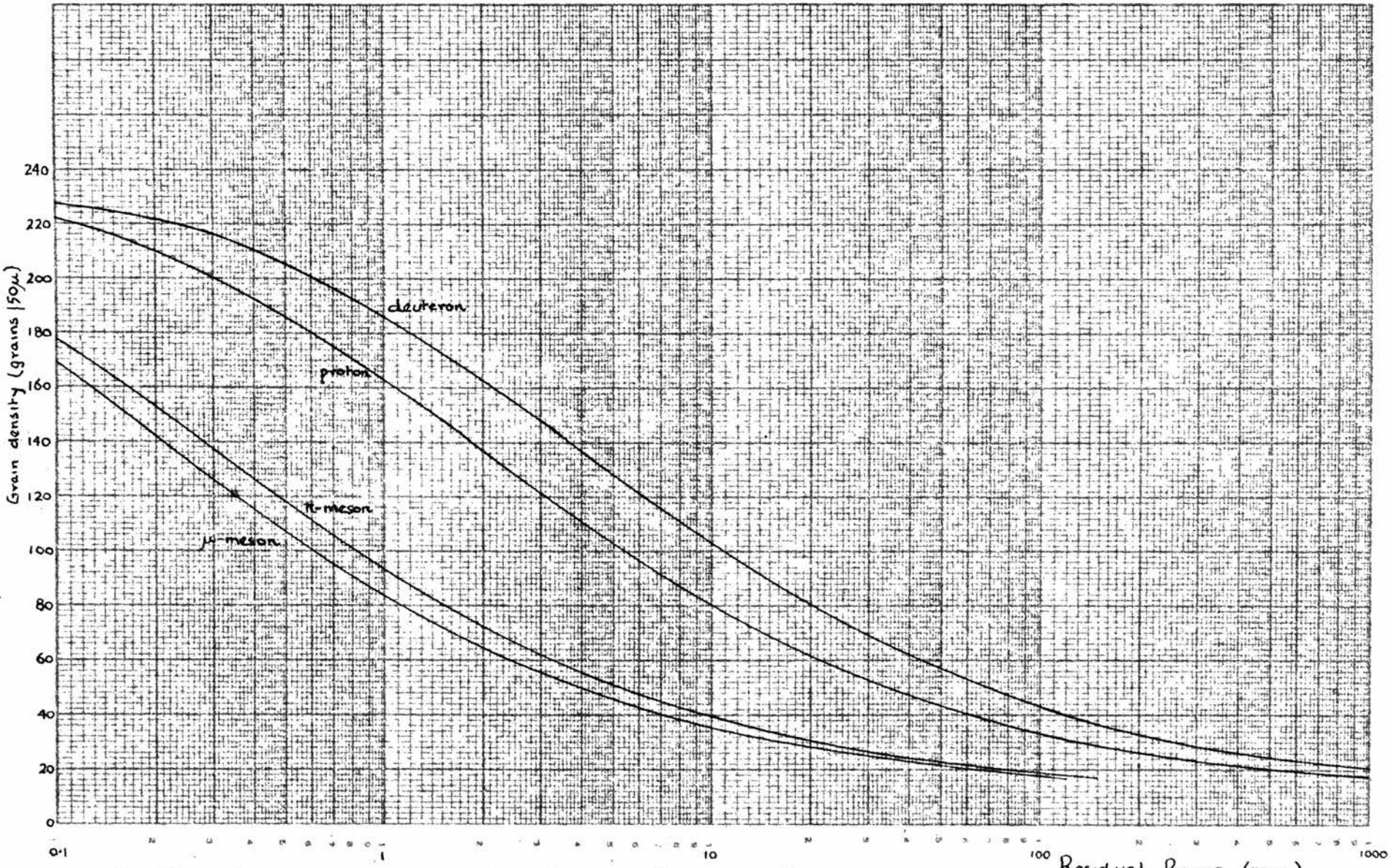

FIGURE 21a. Grain density (grains/50μ) v. Residual Range (mm) for singly charged particles in Ilford G5 emulsions.

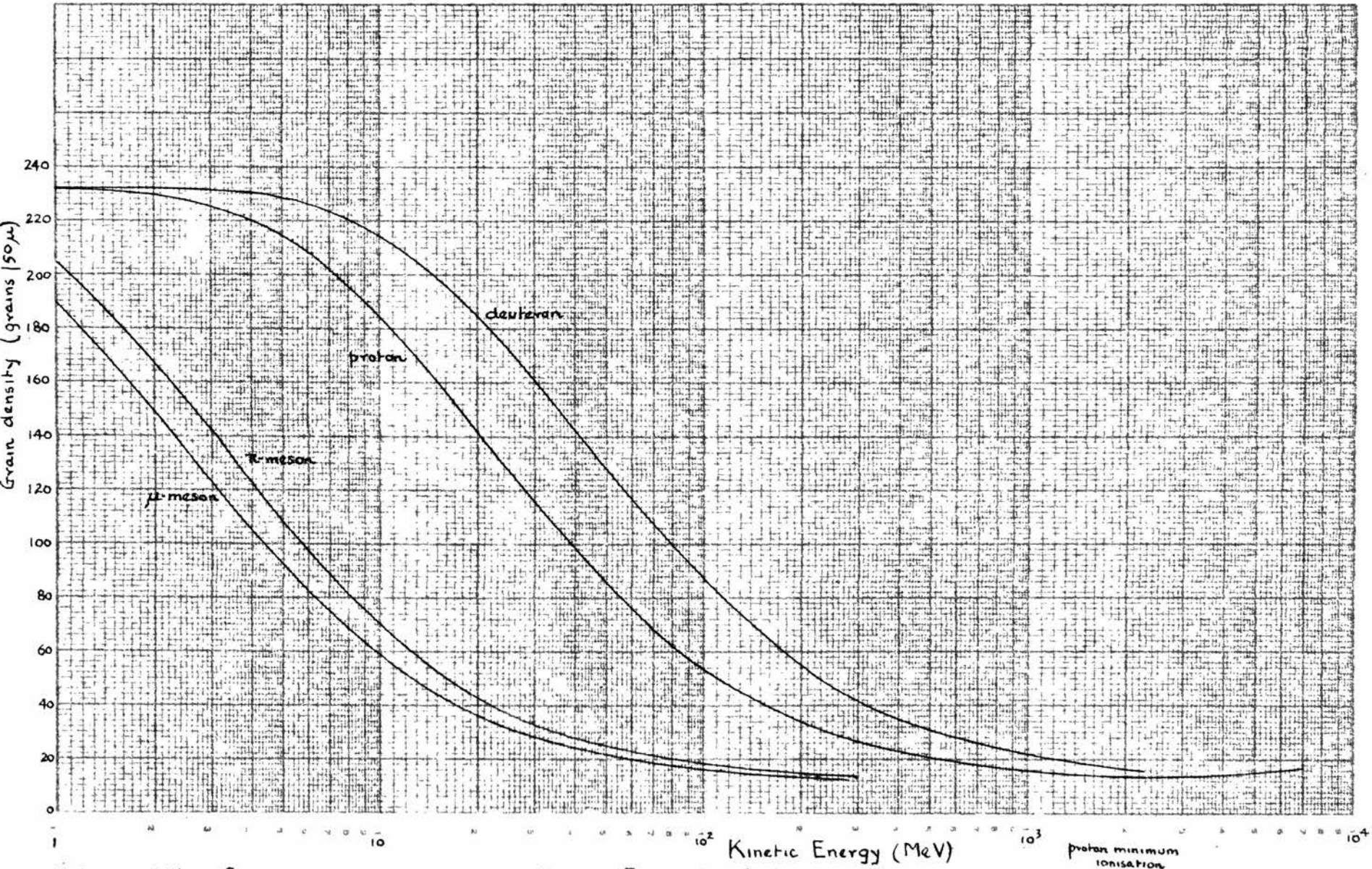

FIGURE 21b Grain density (grains/50μ) v. Kinetic Energy (Mev) for singly charged particles in Ilford G5 Emulsions.

In order to identify a particle which does not come to rest in the emulsion, the procedure is to determine the grain density in two regions of its track, which are separated by a known distance. These grain densities and their distance of separation along the track will then fit only one of the curves of figure 21a, and thus the identity of the particle may be established. Near the low energy end of a particle, the length of track which is required for identification is comparatively small. Assuming that a 10% change in grain density would be detectable, it may be shown that, in the case of a proton, a change of this order of magnitude would take place over less than 2 mm. for grain densities down to approximately 100 grains/50μ, but for thinner tracks a much longer distance is required, as the grain density changes more slowly with range.

VI.3. Some remarks on the constants in Demers' function.

In an analysis of the grain density of electron tracks in Kodak NT4 emulsions, similar to that described earlier in this chapter, Zajac (1949) found that while it was impossible to express the experimental results by Blau's function, they could be fitted satisfactorily to Demers' function with

$$c = 2.2 \text{ grains/micron}$$

$$I_o = 2.22 \text{ keV/micron.}$$

It is of interest to compare the values obtained experimentally from proton and electron studies, with those estimated from Jdanov's formula (Jdanov, 1935) namely:

$$c = \frac{3}{2}\frac{C}{d\rho}$$

where C = concentration of silver bromide in the emulsion

d = mean diameter of the undeveloped grains

ρ = density of silver bromide.

For Kodak NT4 and Ilford G5 emulsions, these constants have the values:

		Kodak NT4	Ilford G5
C		3.408 gm./c.c.	3.521 gm./c.c.
d		0.35 μ	0.18 μ
ρ		6.47 gm./c.c.	6.47 gm./c.c.
c	Jdanov formula	2.26 grains/μ	4.54 grains/μ
	Experimental	2.22 grains/μ	4.68 grains/μ

These results show that the experimental values of c for NT4 and G5 emulsions are in good agreement with those determined from Jdanov's formula. The small difference in the values, which is more noticeable in the case of G5 emulsions, may be accounted for by an uncertainty in the mean grain diameter. From the value of c = 4.68 grains/micron, it may be deduced, using Jdanov's formula, that d = 0.175μ.

Using these results it is possible to determine the minimum amount of energy which a grain must receive before it becomes developable. In the calculations of the total energy lost per centimetre of its path, by a proton travelling through a nuclear emulsion, it was found that nearly 80% of the total energy loss takes place in the silver bromide grains, whatever the kinetic energy of the proton. By calculation, it may also be shown that the specific energy loss in the silver bromide grains is approximately 1.43 times the specific energy loss in the emulsion. In the notation of pages 115 and 116 these were denoted by I_1 and I respectively, therefore

$$I_1 = 1.43I.$$

From this relation, the maximum energy E spent in the grain may be calculated, using the value of the grain diameter (0.175 μ) calculated from the experimental results:

$$E = I_1 d = 1.43I \times 0.175 = 0.25I.$$

Consequently, the parameter E_o in the equation (26) may be determined, since I_o = 3.47 keV/micron for the emulsion:

$$E_o = 0.25I_o = 0.87 \text{ keV}.$$

Substituting this value in the equation (26), we have

$$P(E_\ell) = 1 - e^{-E_\ell/0.87}$$

when an amount of energy E_ℓ keV is transferred to the

grain.

Now, from the value of 4.68 grains/micron obtained earlier, it follows that the maximum possible grain density is 234 grains/50μ, which would correspond to a probability of 1. When the probability of development is equal to $\frac{1}{2}$, it may be shown from the equation above that the energy transferred to the grain is 0.6 keV. At minimum ionisation, the grain density is 13 grains/50μ, from which it follows that approximately 1 in 18 grains has been developed, and the average energy transferred to each grain is 0.05 keV. Assuming a value of 10 grains/50μ for the minimum grain density required for a recognisable track, in Kodak NT4 emulsions, Zajac found that the corresponding minimum energy transfer to each grain by an electron was 0.125 keV, approximately twice that for Ilford G5 emulsions.

A grain in a photographic emulsion will only become developable provided a sufficient number of ion pairs has been formed in the grain during the passage of the ionising particle through it. The number of ion pairs produced depends upon the energy transferred to the grain, and this in turn is a function of the velocity and charge of the particle, and its path length through the grain. When the particle has a high velocity, it will spend only a short time in the vicinity of an atom in the grain, and will be less likely to produce

ionisation of the atom than a slow particle. Also, in an emulsion the grains are distributed at random about the path of the particle, and consequently the path length through the grains is variable. If the particle passes through the edge of a grain, there will be fewer atoms along this path than along a path through the centre of the grain, with the result that a smaller number of ions will be produced, and the grain may not become developable.

Thus, at high velocities, the number of ions produced by the particle during its passage through the grain will not, on the average, be sufficient to allow the formation of a latent image unless the particle passes through the longest possible path length (that is, unless it travels along the diameter of the grain), with the result that only a small number of grains will become developable. As the velocity decreases, however, a greater number of atoms in each grain will be ionised, until, at very low velocities, all the grains including those in which the path of the particle is short contain at least the minimum number of ions required to render them developable.

The effect of the passage of particles of different velocity on the spacing of the developed grains is shown in a much simplified manner by the schematic diagram overleaf. Below each grain is shown the velocity of

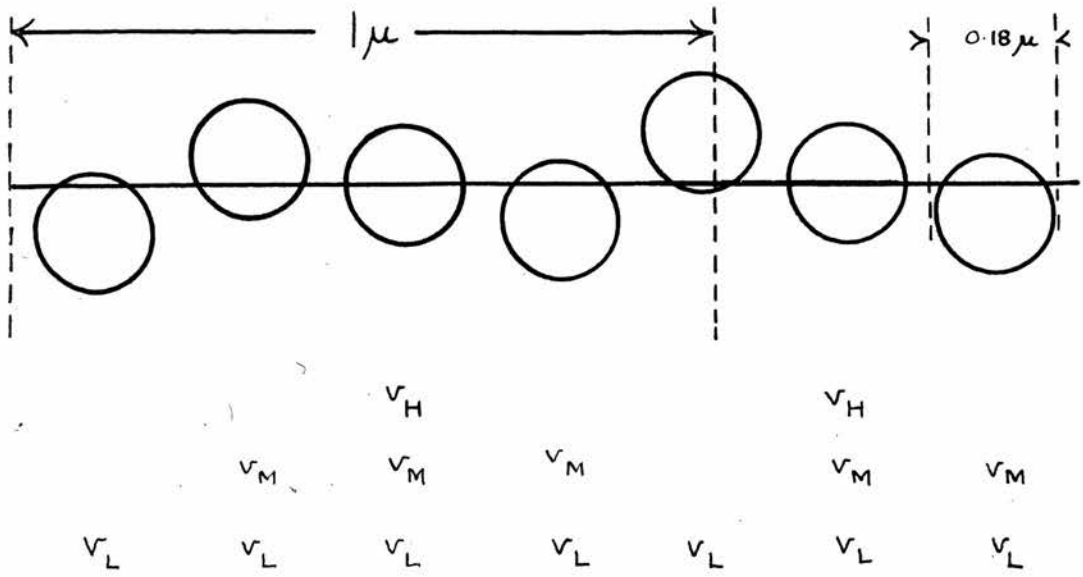

Schematic diagram showing the effect of the passage of particles of different velocity, on the spacing of the developed grains (H, M, L denote high, medium and low velocities respectively.). This two-dimensional diagram does not take account of the fact that the grains are not all in the same plane.

the particle which will, on the average, allow the formation of sufficient ions to make the grain developable. The suffixes H, M and L, refer to high, medium and low velocities respectively. In the earlier calculations it was shown that in an Ilford G5 emulsion the average number of grains is 4.68 per micron, and the mean grain diameter is approximately 0.18μ, but the diagram has not been drawn to scale.

Chapter VII.

EXPERIMENTAL RESULTS.

In the course of the systematic searching of the plates, 1378 cosmic ray stars of all kinds were observed, with prong numbers ranging from 1, in the case of stars produced by very low energy particles, to 43 for a star which represents the complete disintegration of a silver nucleus. The contribution of the first series of plates to the total number of stars was 1029, and that of the second series, of which a smaller area was searched, was 349. Each event was examined and classified in the manner already described, and from the results information has been obtained concerning the ratio of charged to uncharged particles in the star-producing radiation present in the atmosphere, and the rate of absorption of the neutral star-producing radiation in air and in ice. The integral star size distribution in the plates is also considered and a possible interpretation of the shape of the curves in terms of the energy spectrum of the incident particles is given.

In the latter part of this chapter, which is concerned with the properties of the neutral star-producing radiation, the information obtained from the second expedition plates has been omitted, not only because the number of events observed in each plate is small, and the statistical errors involved are correspondingly

large, but also because of an uncertainty arising from the conditions under which the plates were exposed. During the time that the plates were at the mountain top, the ice in which some of the plates were buried melted and was replaced by ice heaped on top of the boxes in the shape of a cone. Thus, although the depth of each box below the top surface of the ice was maintained, the actual thickness of the layer of ice separating the box from the atmosphere was much less than the specified distance, and varied as the ice melted and was replaced. However, although the number of events was subject to large errors arising from these sources, neither the size of the stars nor the identity of their primaries was affected, and in the earlier part of the chapter results from both expeditions have been used.

VII.1. Cosmic ray stars.

VII.1.1. Properties of stars.

Diagrams illustrating the size-frequency distributions of all the stars observed in the plates of the two expeditions, exposed at sea level, on the mountain top and under the ice cap, are shown in figure 22 (a, b and c respectively). Stars produced by ionising particles have been separated from those produced by neutral particles, and their size distributions are shown in the shaded diagrams. While these histograms do not yield

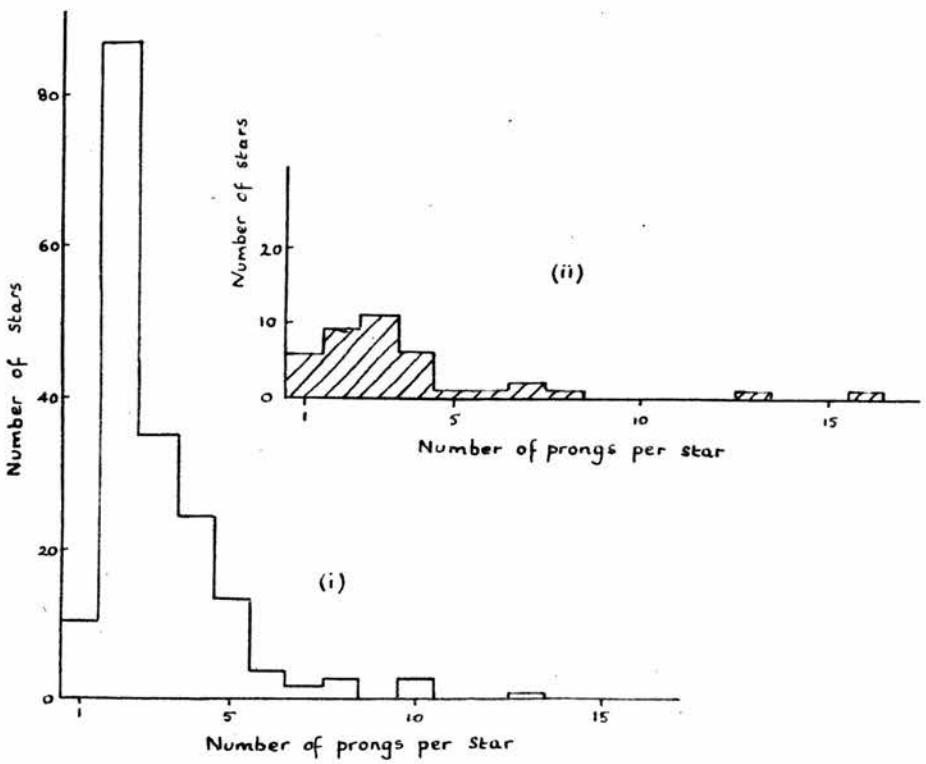

FIGURE 22a Distribution of prong numbers for stars produced by (i) non-ionising primaries (ii) ionising primaries in plates exposed (a) at sea level, (b) on the mountain top, (c) under the ice cap.

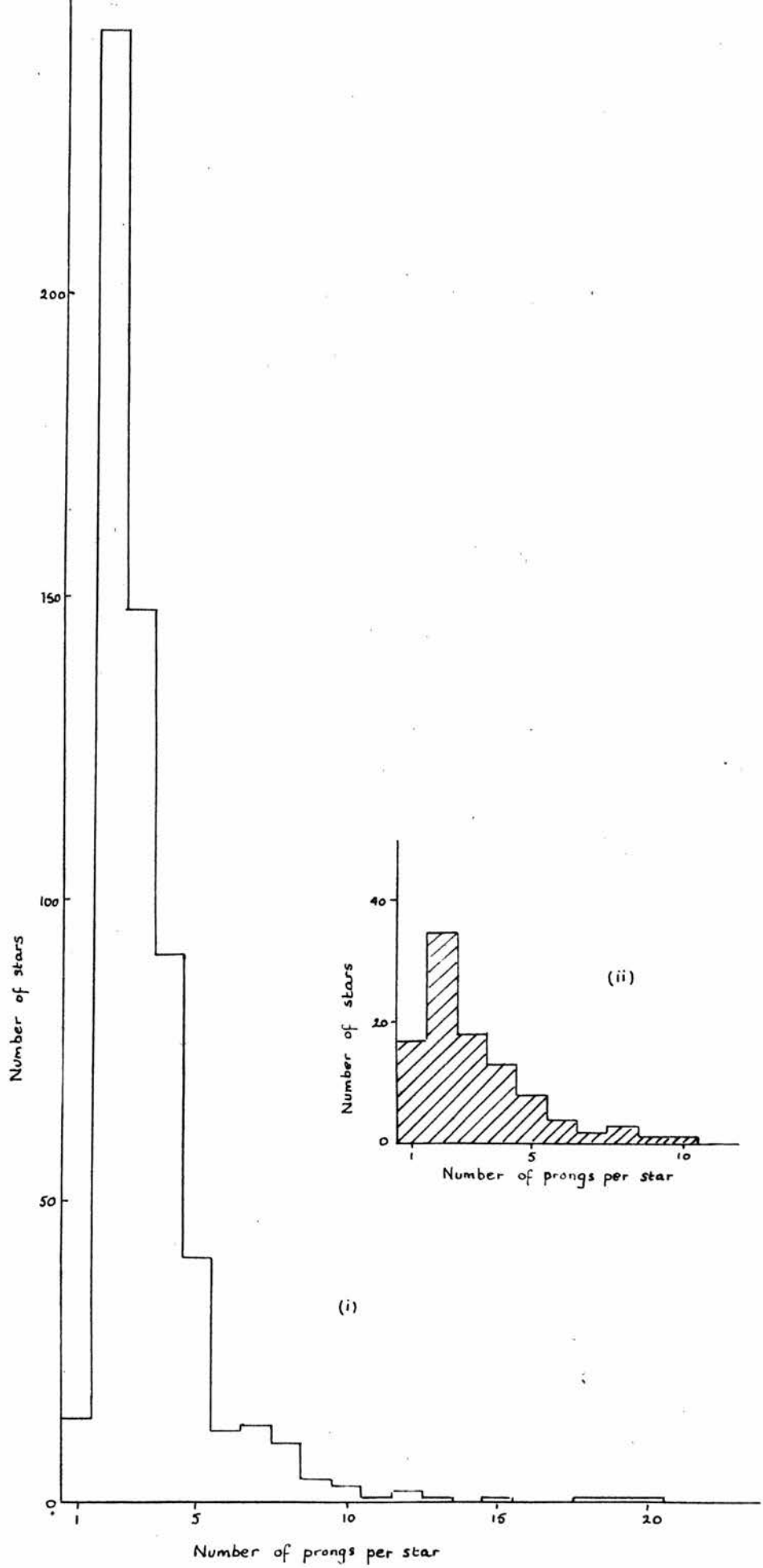
200
150
100
50
0
Number of stars
1
5
10
15
20
Number of prongs per star
(i)
40
20
0
Number of stars
(ii)
1
5
10
Number of prongs per star

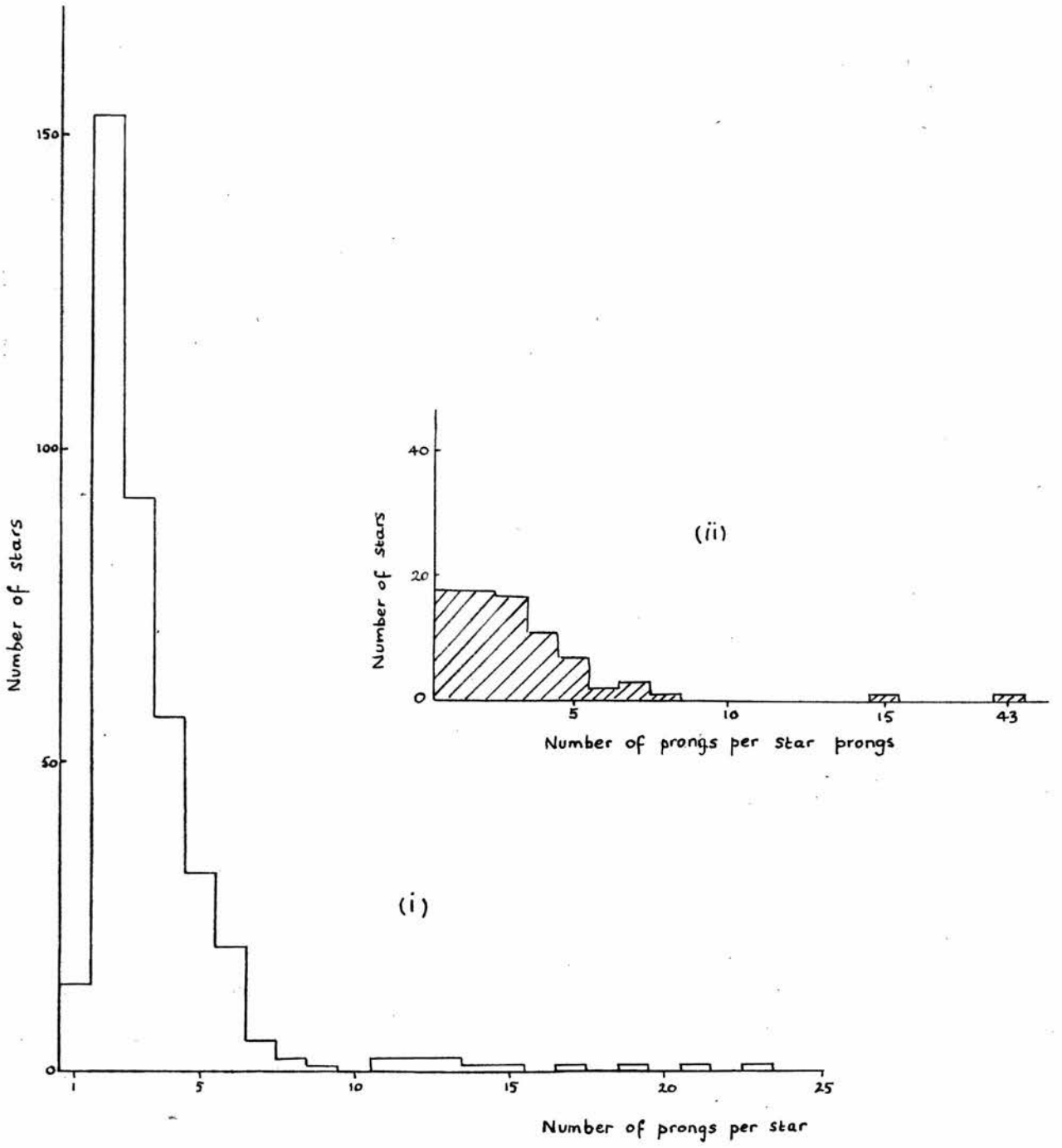
150
100
50
0
Number of stars
1
5
10
15
20
25
Number of prongs per star
(i)
40
20
0
Number of stars
(ii)
5
10
15
43
Number of prongs per star prongs

FIGURE 22c

any information regarding the relative intensity of the cosmic radiation at the different levels, as each represents a different volume of emulsion, they do show the predominance of small stars over stars with a large number of prongs, at all levels.

In all the histograms of neutron induced stars, it will be noted that the number of stars which have only one secondary track is only a small fraction of the total number, and is much smaller than the number of two prong stars. This deficiency of n = 1 events, which is also evident in the case of stars produced by charged particles, may be explained as a combination of various effects.

In the first place, the criterion for selecting one prong stars leads to an expected deficiency in the number of these stars. When a neutral particle passes through a nucleus, imparting enough energy to allow the emission of an evaporation particle, this event will not be recognised as a star unless the excitation energy has been sufficient to produce a nuclear recoil. On the other hand, a similar star initiated by a charged particle will be classed as an n = 2 event. Secondly, it is probable that some of the events classed as n = 2 stars with neutral primaries, are in fact single prong stars with slow ionising primaries, not identified as such. A further type of event which may be excluded

is an inelastic collision between a primary proton and a nucleus which, under certain circumstances, may have the appearance of a deflection. If one nucleon receives most of the energy of the colliding particle and escapes from the nucleus without further collisions, the residual nucleus can have only a very small excitation energy, which will be insufficient to allow the emission of other particles.

It is evident from these results that only a small proportion of the stars produced in the lower atmosphere are initiated by ionising particles. The ratio of the number of stars produced by ionising particles, N_I, to the total number, $N_I + N_N$, where N_N is the number produced by neutral particles, was calculated for each plate, and the mean value determined for the plates at sea level, on the mountain top and under the ice, taking the results for both expeditions together (Table XXXII).

Table XXXII.

Position	Sea level	Mountain top	Under ice	Mean
Ratio $\frac{N_I}{N_I + N_N}$	0.15 ± 0.04	0.13 ± 0.03	0.14 ± 0.03	0.14 ± 0.01

Although Brown (1954) found evidence of an increase in the ratio of the number of ionising primaries to the total number of star primaries, between sea level and an altitude of 3240 metres, in the present work the ratio was found to be approximately constant for the range of altitude under consideration. The mean value of 0.14 ± 0.01 is comparable with the results obtained by other workers; for example, Page (1950) found that for emulsions exposed at 3450 metres above sea level, the ratio was 0.17 ± 0.03, and Brown (loc. cit.) gave a value of 0.18 ± 0.02 for the star producing flux entering a cloud chamber at sea level. Assuming that the average cross-section for star production is the same for neutral and charged particles, it follows that ionising particles account for only 14% of the star producing radiation present in the lower atmosphere at 66°N.

Of the 220 stars produced by the charged component of the cosmic radiation, only 45 or 20% resulted from the capture of slow negative π-mesons, which thus accounted for only 3% of the total number of star primaries. Since no energy other than the rest mass energy of approximately 140 MeV is available for star production, the number of prongs associated with these events was never greater than 4, and most of the stars had an even smaller number of prongs, as indicated by the histogram of figure 23.

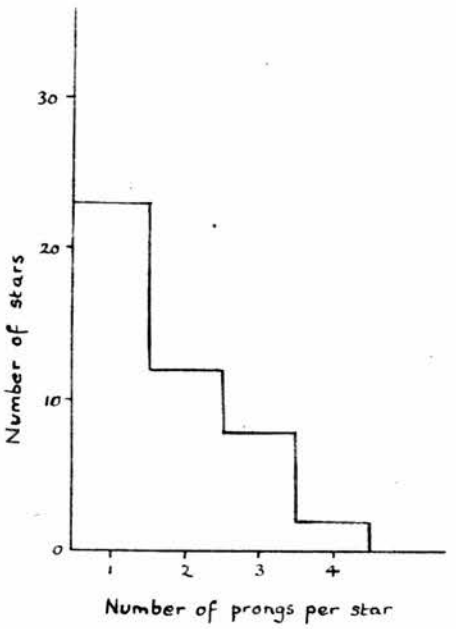

FIGURE 23 Distribution of prong numbers for stars produced by slow mesons

An attempt was made to determine approximately the mean energy of the neutral star producing radiation present in the atmosphere at sea level and on the mountain top, from the total energy released in the stars formed at these levels. However, since the energy released in a star depends not only on the number of the secondary particles, but also upon their mode of production, the contributions to the total energy of evaporation particles, prompt particles and mesons must be considered.

1. Black tracks: evaporation particles.

The energy carried by the black tracks of a star was determined from the theoretical relationship derived by LeCouteur (1950) between the expected number of evaporation prongs and the total excitation energy of the nucleus, taking into account the energy carried off by neutrons.

2. Grey tracks: prompt particles and some mesons.

The total energy in the black and grey tracks of a star with more than seven prongs may be obtained from an empirical formula given by Brown et al. (1949) namely:

$$E\ (\text{MeV}) = 37N + 4N^2 \qquad (32)$$

where N = total number of tracks with ionisation greater than 1.5 times minimum, and E includes the energy carried off by α-particles and neutrons. Using this equation it is possible to estimate the mean energy of a grey

track for a given star size, provided the number of evaporation tracks is known. It has been found that, in general, the ratio of the number of black tracks to the number of grey tracks is 3:1, so for any star size the number of black tracks may be calculated, and the energy which these represent can be determined as above. By subtracting this energy from the total calculated by means of equation (32), the energy of the grey tracks and the corresponding neutrons may be obtained. Calculations of this kind have shown that for the stars present in the cosmic ray plates used for this work the mean energy carried by a grey track is approximately 150 MeV, a value which includes the contribution of the prompt neutrons.

3. Thin tracks: shower particles (predominantly mesons).

Most of the stars with which shower particles were associated had between 3 and 8 prongs in all, including only 1 thin track. From the results of Camerini et al. quoted by Rochester and Rosser (1951), it appears that the mean energy of a shower particle under these conditions is approximately 750 MeV. No account was taken of the possible contribution of neutral mesons to the total star energy. It has been suggested by several authors (for example, Kaplon et al., 1954) that only one in every three mesons created in a disintegration is

a neutral particle, and since the number of thin tracks in any star was seldom greater than one, it is unlikely that this omission caused any serious error.

While these calculations are correctly applied only to stars formed in the heavy nuclei of the emulsion, namely silver and bromine, in this case they have been assumed to hold for stars of all kinds. However, it will be shown later that nearly 80% of all stars arise from disintegrations in the heavy nuclei, and since this method of determining total energy yields only an approximate value, the errors introduced by including the light element stars will be comparatively small.

The energy associated with each of the neutron-induced stars observed in the first expedition plates, which were exposed at sea level and on top of the ice cap, was assessed in the manner described above, and the mean energy of the neutron component of the star-producing radiation at these levels was found to be:

	Altitude (metres)	Mean energy (MeV)
Sea level	0	220 ± 20
Mountain top	1710	246 ± 20.

Although the errors involved in these calculations are large, the results are not inconsistent with the small expected increase in the average energy of the star-producing radiation, with altitude.

VII.1.2. Size distributions of stars.

The integral size distributions of all the stars, plotted on a semi-logarithmic scale as the number of stars N ($> n$) with more than n prongs, are shown in figure 24 (a, b and c), where all the star secondaries - evaporation particles, prompt nucleons and mesons created in the disintegrations - have been included. With the exception of the points n = 0, where the results are affected by the deficiency of one prong stars, each of the distribution curves may be represented by two straight lines which intersect at approximately n = 6, and which have equations of the form

$$N(> n) = A \exp(- kn) \qquad (33).$$

In Table XXXIII, the values of the constants k and A are given for each of the size distribution curves; the suffixes 1 and 2 refer to the points for which $n \leq 6$ and $n > 6$ respectively.

Table XXXIII.

Position	$n \leq 6$		$n > 6$	
	k_1	A_1	k_2	A_2
Sea level	0.55	332	0.30	77
Mountain top	0.56	1126	0.23	98
Under ice	0.57	815	0.20	79

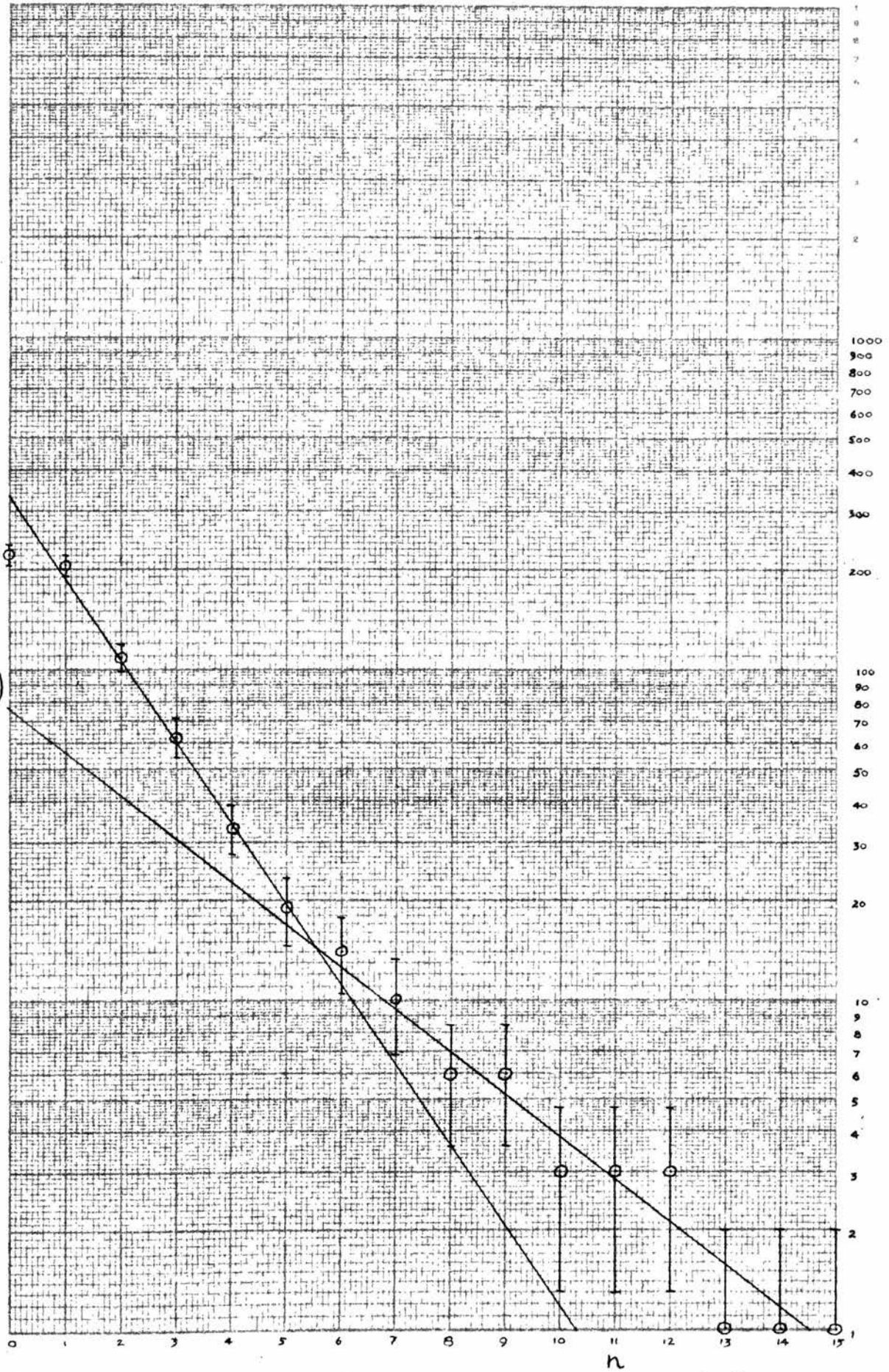

FIGURE 24a. Total number of stars with more than n prongs, N(>n), v. n in plates exposed at sea level.

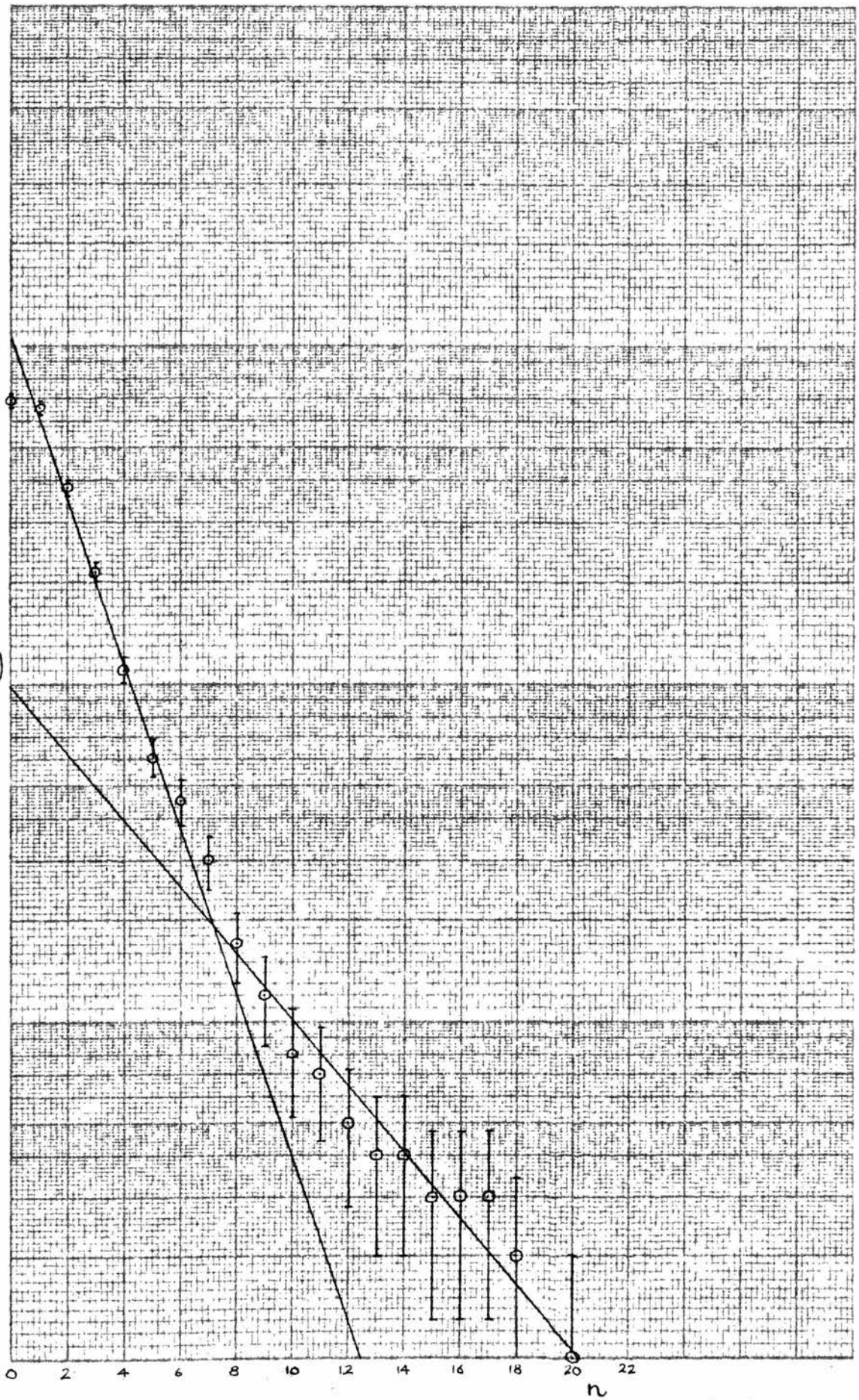

FIGURE 24b. Total number of stars with more than n prongs, N(>n), v. n in plates exposed at the mountain top.

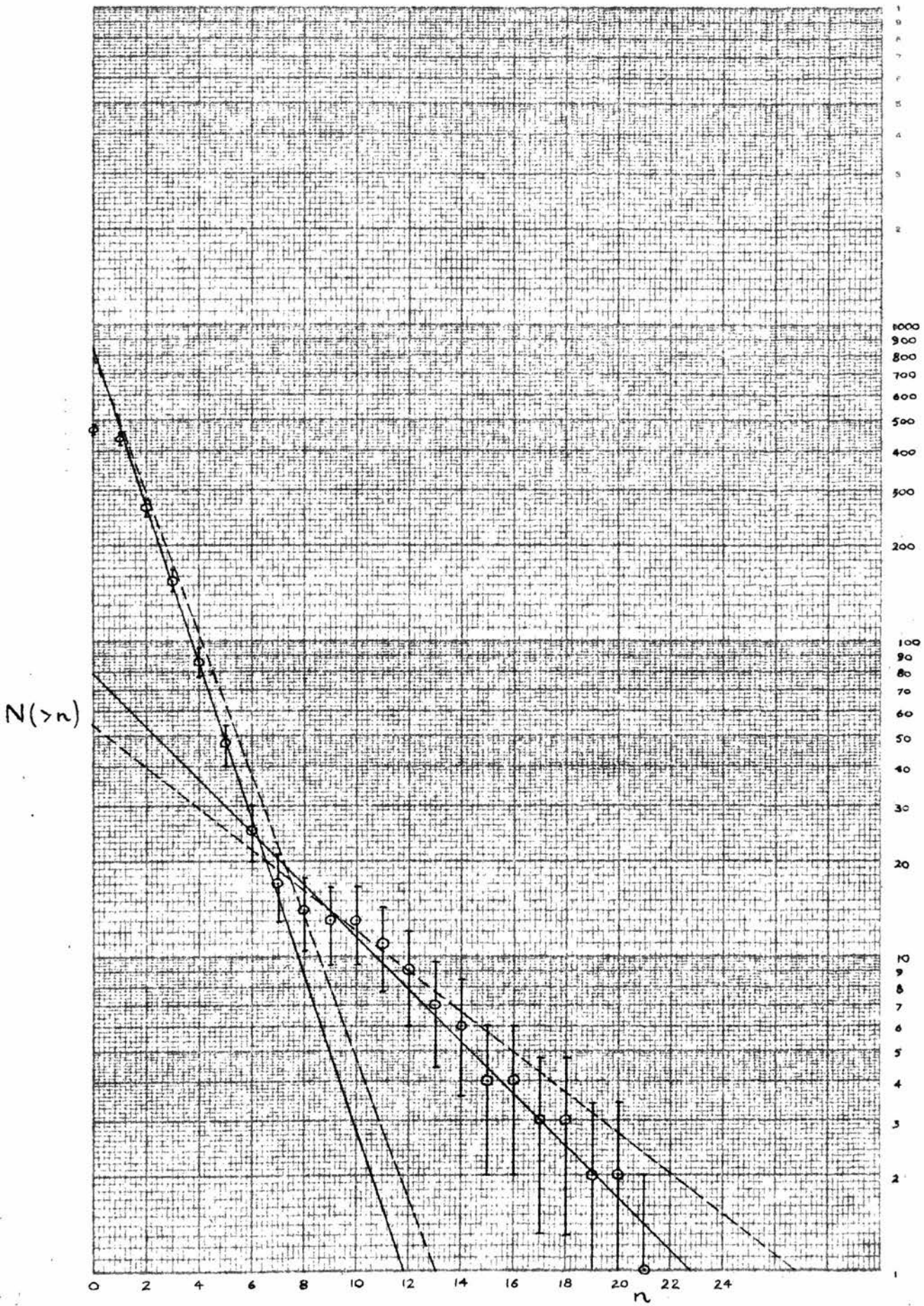

FIGURE 24c. Total number of stars with more than n prongs, N(>n), v. n in plates exposed under the ice cap.

These values were determined by the method of least squares, but their uncertainties are not given since they cannot be estimated from the integral data presented in figure 24, which, contrary to the requirements of the least squares theory, are not independent.

An examination of the values of k_1 and k_2 shows that while k_1 is approximately the same at sea level and on the mountain top there is a change in the value of k_2. However, since the number of stars with $n > 6$ was small, in fact never more than 5% of the total number observed, the statistical error in k_2 will be relatively large, and the discrepancy between the different values probably not significant. Were this variation significant, it would reflect the change in the energy spectrum of the star-producing radiation with altitude.

The effect on the value of k_2 of the inclusion of a single large star of 43 prongs is shown by the dotted line in the graph of figure 24c. This star, which was observed in one of the plates exposed under ice, has nearly twice as many prongs as any other star, and is thought to represent the annihilation of a negative proton in a silver nucleus. Since this event is the only one of its kind, with a primary which is not typical of the star-producing radiation present in the lower atmosphere, it has been omitted from the calculations.

Page (1950) carried out a similar analysis of the

data from stars produced in Ilford C2 emulsions, exposed on the Jungfraujoch at an altitude of 3450 m. and geomagnetic latitude of 48° N, with the following results:

$$N(>n) = A \exp(-0.52\ln) \quad \text{for } n \leqslant 6$$

$$N(>n) = 0.38A \exp(-0.33\ln) \quad \text{for } n > 6.$$

When allowance is made for the difference of approximately 1700 m. in altitude between this exposure and that in Arctic Norway, the values of k_1 appear to be consistent with each other, and show the expected increase with increasing atmospheric depth. There is, however, a discrepancy in the values of k_2 which suggests that the number of large stars produced at 1710 m. is greater than that at a higher altitude. This may perhaps be partly explained by the difference in sensitivity of G5 and C2 emulsions, for while the former are capable of recording the passage of even the fastest particles in the less sensitive C2 emulsions many of the fast charged disintegration products, particularly the shower particles, will escape unobserved, and consequently the high energy stars will be apparently smaller in size.

The change in the slope of the integral size distribution curve at a prong number of 6 or 7 has been observed in many nuclear emulsion experiments carried out over a wide range of altitudes from sea level to the stratosphere. Page (1950) suggested that this break in the distribution could be attributed to the composition

of the emulsion, which consists of two types of target nuclei: the light nuclei of carbon, nitrogen and oxygen which will not be capable of producing many stars with more than 6 or 7 prongs, and the heavy nuclei of silver and bromine, in which all the large stars will originate. Barton, George and Jason (1951) on the other hand preferred to interpret the size distribution in terms of the energy spectrum of the stars, which is determined initially by the energy spectrum of the primary radiation, and they regarded the shape of the distribution curve as fortuitous. However, Birnbaum et al. (1952), who collected and analysed the data from a number of nuclear emulsion studies at different altitudes, concluded, in accordance with the former hypothesis, that the effect was due mainly to the composition of the emulsion, and that there was a progressive change in the slopes of the lines, which reflected the variation with altitude, of the energy spectrum of the star-producing radiation. Assuming that the two straight lines of the integral size distribution curve defines the contributions of the light and heavy nuclei respectively, they calculated the ratio of the number of stars with three or more prongs produced in the two kinds of nuclei, and showed that the results were in agreement with that determined by Harding (1949), whose observations on the stars produced by cosmic radiation in ordinary C2

emulsion and in gelatin led to the conclusion that $36 \pm 4.5\%$ of all stars are formed in the light nuclei.

If this hypothesis regarding the shape of the curve is in fact correct, it should be possible to use this method to determine the proportion of stars formed in the light nuclei by any star-producing radiation, no matter what its energy. From the data obtained in several emulsion experiments in which plates were exposed to beams of monoenergetic protons and neutrons, the integral size distribution curves shown in figure 25 were drawn, where for comparison all the results have been normalised to $N(>n) = 400$ for $n = 1$. In none of these cases is it possible to determine the proportion of stars formed in the light nuclei, because the curves do not conform to the general shape of the cosmic ray curves, and do not show the characteristic change of slope at $n = 6$. One important feature of the curves is that they do illustrate the variation of the slope with the energy of the star-producing particles.

The conclusions from these experiments, together with the fact that neither Page's results, nor those obtained from the present work, yield a value of the relative numbers of light and heavy nuclei stars which is comparable with any of those quoted by Birnbaum et al., suggest that the assumptions made by these authors are not wholly correct. A more detailed examination

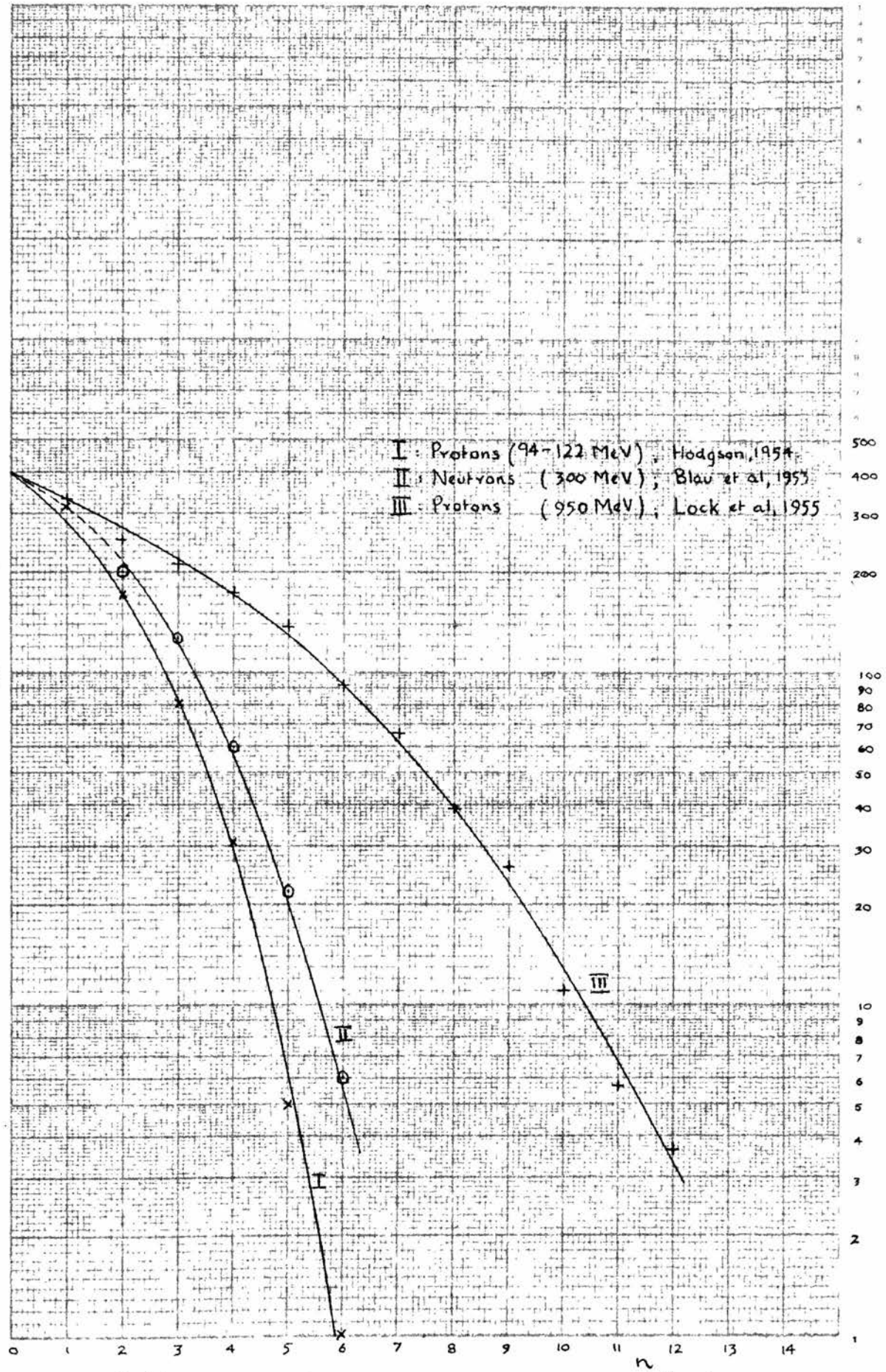

FIGURE 25. Total number of stars with more than n prongs, N(>n), v. n for stars produced by particles of known energy.

of the validity of these assumptions may be made by an analysis of the stars produced in the light and heavy nuclei, and the variation in their characteristics with the energy of the star-producing radiation.

It is possible to determine the relative numbers of stars formed in the light and heavy nuclei from an examination of the stars themselves, without reference to the size distribution curves. The method of separation is based on the fact that while the particles emitted in the disintegrations of the light nuclei have, in principle, no lower limit to their energy, α-particles of 9 MeV or less will have great difficulty in penetrating the Coulomb potential barrier of a heavy nucleus, even when allowance is made for the lowering of the barrier due to the excitation of the nucleus. Protons of the same range (50μ) will have kinetic energies of less than 2.4 MeV, and will have an even smaller chance of escaping from the nucleus. Thus, any star with a total of eight charged secondary particles (allowing for the complete disintegration of O_8^{16}) or less, and containing a track whose range was between 5μ and 50μ, was assumed to represent the disintegration of a light nucleus. The lower limit of 5μ was set to exclude the nuclear recoils, except where there was more than one of these very short tracks in a star (see page 18).

Experimental support for the validity of this

separation criterion has been obtained from experiments by Harding (1949) and Perkins (1949) with gelatin sandwich emulsions, and by Lees et al. (1953) who used diluted emulsions to examine the energy distribution of α-particles from proton induced stars. More recent work by Demeur et al. (1956) has suggested that the lower limit to the energy of the α-particles emitted from heavy nuclei stars should be reduced to approximately 6.5 MeV, corresponding to a residual range of 30μ. However, in order that the present results may be compared with those of other experiments, the stars have been separated according to the 9 MeV α-particle criterion.

There are inevitably certain limitations to the method; for example, occasionally a light nucleus will disintegrate without emitting a particle with a range between 5μ and 50μ, while on the other hand a low energy α-particle or proton will sometimes succeed in penetrating the Coulomb barrier of a heavy nucleus. Although the method of separation is not infallible, it is sufficient to show the main features of the disintegration of the light and heavy nuclei.

The numbers of stars with two or more prongs formed in the light nuclei, and the percentage of the total number of stars ($n \geqslant 2$) which these represent, is shown in Table XXXIV for plates exposed at sea level, on the

mountain top, and under the ice cap, respectively.

Table XXXIV.

Position	Number of stars formed in light nuclei	Total number of stars	%
Sea level	26	112	23 ± 5
Mountain top	79	337	23 ± 3
Under ice	114	435	26 ± 3

Allowing for the errors involved, these percentages are approximately the same at all the levels considered, and the mean percentage is 24 ± 2.

Studies of the nuclear disintegrations produced in emulsions by high energy protons and neutrons have shown that the proportion of stars formed in the light nuclei is a function of the energy of the star-producing radiation. To illustrate this, results from several of these experiments have been summarised in Table XXXV and in the graph of figure 26; only stars with two or more prongs have been included.

Thus, when the contribution of the light nuclei to the total number of stars is known, it should be possible to determine from the graph of figure 26 the mean energy of the star-producing radiation entering an emulsion.

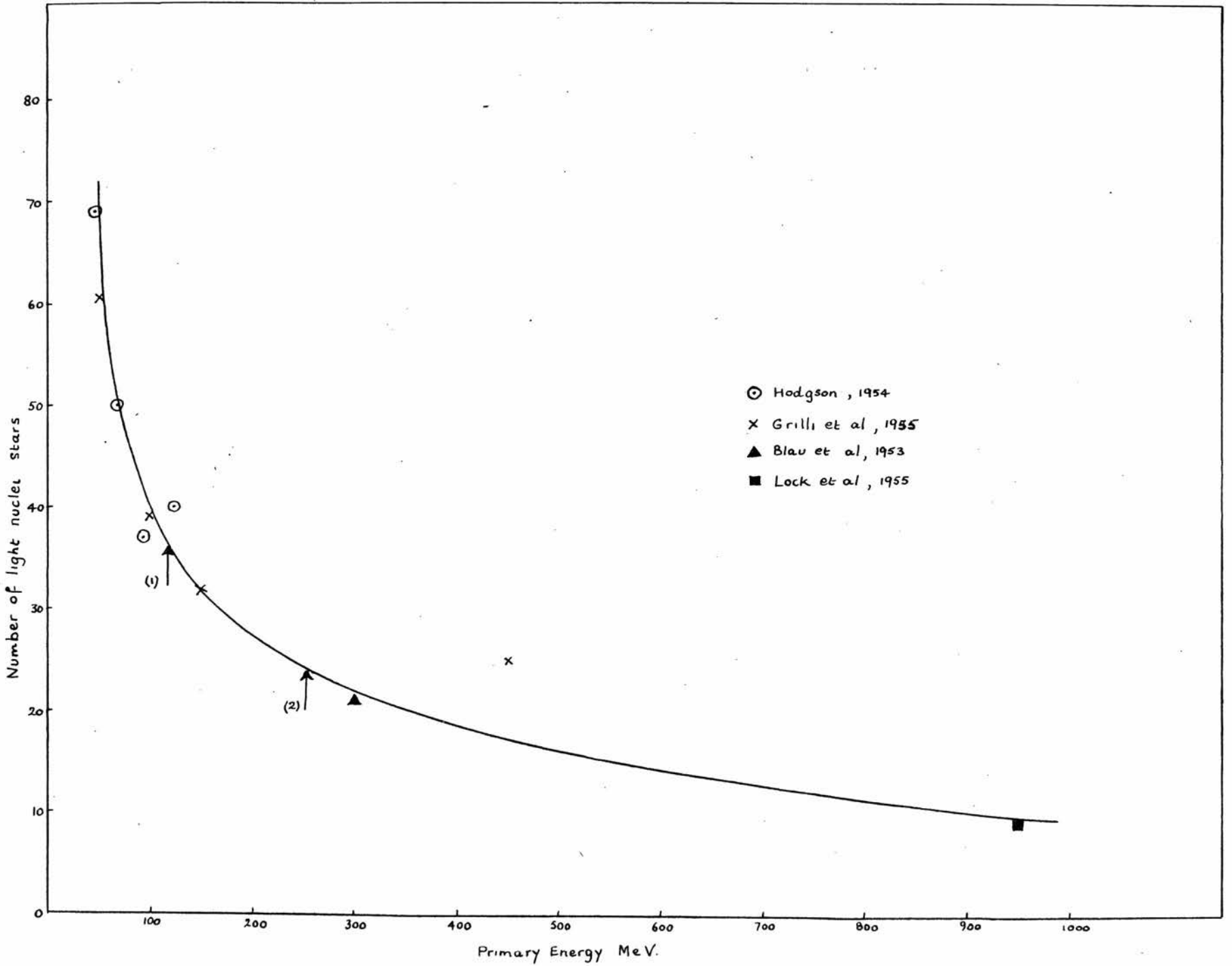

FIGURE 26 Number of stars formed in the light nuclei (expressed as a percentage of the total) as a function of the primary energy (in Mev)

Table XXXV.

Star-producing radiation	E MeV	% light nuclei stars	Reference
Protons	45	69	Hodgson (1954)
"	68	50	
"	94	37	
"	122	40	
Protons	50	60.5	Grilli et al. (1955)
"	100	39	
"	150	32	
"	450	25	
Neutrons	300	21	Blau et al. (1953)
Protons	950	9	Lock et al. (1955)

Applying this procedure to Harding's results from gelatin sandwich emulsions exposed on the Jungfraujoch at an altitude of 3650 m., and to those from the plates exposed in Arctic Norway, it is found that the mean energy of the star-producing radiation in Norway is greater than that on the Jungfraujoch, as shown in Table XXXVI.

Table XXXVI.

Geomagnetic Latitude	Altitude in metres	% light nuclei stars	E MeV
48° N	3650	36	120
66° N	1710	24	250

This value of 250 MeV confirms the result obtained earlier from the estimation of the energy released in each star.

The differential size distributions of the stars formed in the light nuclei at sea level, on the mountain top, and under the ice cap, were found to be sharper than Poissonian and to have a sharp peak at n = 3.5. Only a small number of these stars had fewer than three prongs, and none had more than eight as a result of the separation criterion for light and heavy nuclei stars. These results, which are comparable with those obtained by Hodgson for primary energies between 45 and 122 MeV, reflect the ease with which carbon and oxygen nuclei can break up into α-particles, even at comparatively low excitation energies. At considerably higher energies, the mean prong number is greater, as the primaries are capable of producing sufficient excitation to allow the break-up of the α-particles themselves. Thereafter, the mean prong number decreases, because particles of very high energy travel through a light nucleus in a time which may be too short to allow the transfer of enough energy to produce a disintegration.

In contrast to the peaked distribution of the light nuclei stars, the frequency of the stars which were formed in the heavy elements of the emulsion decreased exponentially with increasing prong number at all levels.

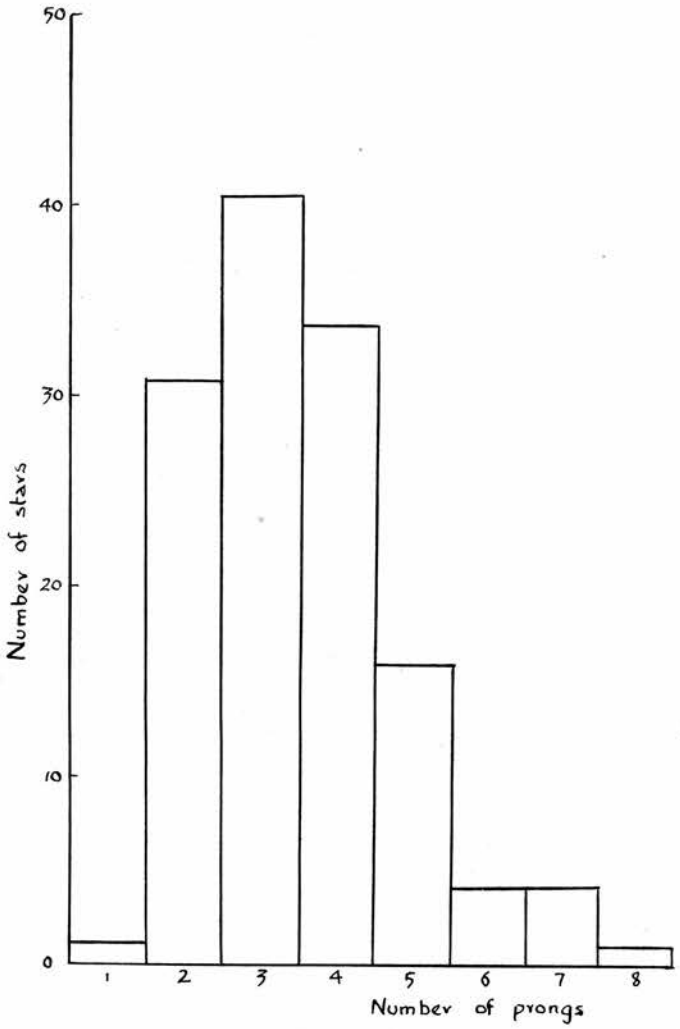

Distribution of prong numbers for stars produced in the light nuclei of G5 emulsions, exposed on mountain top.

Mean of distribution = 3·5

Standard deviation of distribution = 1·3.

Expressing these distributions in the form:

$$N(n_s) = Be^{-cn}$$

where $N(n_s)$ is the number of stars with n_s ionising secondaries, the values of c at the three points of exposure were found to be:

Position	c
Sea level	0.96
Mountain top	0.69
Under ice	0.69

The number of evaporation tracks in a heavy nucleus star is a function of the primary energy only up to a certain maximum value. At very high energies, the time of passage of the primary through a nucleus may not be long enough to produce excitation of the nucleus, and consequently the mean prong number decreases with increasing primary energy. At these very high energies, nearly all the stars are produced in the heavy elements because the distance which a primary has to travel through one of these nuclei is considerably greater than the distance across a smaller light nucleus, with the result that the time spent in it is correspondingly greater.

If the two lines of the integral size distribution curve represent the contributions of the light and heavy elements, it should be possible to use their equations to determine the shape of the differential size distribution curves. These equations are

$$N_1(>n) = A_1 e^{-k_1 n} \qquad \text{for } n \leq 6$$

$$N_2(>n) = A_2 e^{-k_2 n} \qquad \text{for } n > 6$$

and the second of these is assumed to contain the results from the heavy element stars alone. From this equation, it may be shown that the differential distribution for the heavy nuclei has an equation of the form

$$N_2(n_s) = A_2 e^{-k_2 n}(e^{k_2} - 1)$$

i.e.

$$N_2(n_s) = B_2 e^{-k_2 n} \qquad (34).$$

By subtracting the contribution of the heavy elements from the first equation, it may also be shown that the corresponding distribution for the light element stars is given by the equation

$$N_1(n_s) = A_1 e^{-k_1 n}(e^{k_1} - 1) - A_2 e^{-k_2 n}(e^{k_2} - 1)$$

i.e.

$$N_1(n_s) = B_1 e^{-k_1 n} - B_2 e^{-k_2 n} \qquad (35).$$

It is therefore possible to test the assumptions made by Birnbaum et al. in their calculations of the relative numbers of stars formed in the light and heavy nuclei, by considering these equations in the light of the present results.

(1) Heavy elements. From equation (34) it is evident that the exponential terms of the integral and differential size distribution equations are expected to be equal, but in fact they differ considerably as shown overleaf:

Position	Integral equation k_2	Differential equation c
Sea level	0.30	0.96
Mountain top	0.23	0.69
Under ice	0.20	0.69

(2) Light elements. According to equation (35), the differential distribution curves should be exponential in shape, but it has already been shown that at all levels these distributions are peaked, and this cannot be fitted to the equations derived from the integral curves.

It must therefore be concluded that the hypothesis which explains the shape of the integral size distribution curves in terms of the composition of the emulsions is incorrect for the following reasons:

(a) the shapes of the curves for stars produced by monoenergetic primaries do not conform to the general shape predicted by this theory,

(b) the theory does not account for the shapes of the differential curves,

(c) only under certain circumstances does it give a value of the relative numbers of light and heavy element stars which is comparable with those determined by other methods.

An alternative explanation of the shape of the curves in terms of the wide energy spectrum of the

incident cosmic radiation must now be considered. It is reasonable to assume that the star-producing particles of a given energy will give rise to a distribution curve similar to those shown in figure 25. Thus, the curves of figure 24a, b, c will be the result of adding together the contributions of primaries of different energies, taking account of the number of star-producing particles in a given energy range. The large stars with ten or more prongs will be induced only by high energy primaries, but the smaller stars will be produced at all energies.

It has already been noted that there were apparently more large stars in the plates exposed in Arctic Norway than in those exposed by Page at a higher altitude on the Jungfraujoch, and in fact the proportion of large stars in Norway is comparable with that obtained in stratosphere exposures at lower latitudes. This suggests that there is a greater proportion of high energy particles present in the star-producing radiation at high latitudes, and consequently that the energy distribution of the star primaries is a function of not only altitude, but also of geomagnetic latitude. As these star-producing particles have their origins in the disintegrations produced by the charged primary component of the cosmic radiation, their energy spectrum at different latitudes may be explained by considering the

behaviour of this component in the magnetic field of the earth.

At high latitudes, the primary protons entering the earth's atmosphere tend to maintain their direction near the vertical, with the result that the highest energy secondaries, produced in interactions with the atoms of the air, also tend to be vertically collimated. At lower latitudes, however, the primary protons are deflected by the magnetic field of the earth, and many of the higher energy secondaries, whose direction of travel is similar to the primaries, will probably not reach the earth. Also, the primary and secondary particles which are not moving vertically downwards will travel farther through the atmosphere before reaching the earth, and consequently they will be subject to greater energy losses. Thus, near the geomagnetic equator there will be a preponderance of low energy particles in the star-producing radiation.

Since the proportion of stars formed in the light nuclei varies inversely with the energy of the star-producing radiation, the interpretation of the integral distribution curves in terms of the primary energy spectrum, and its variation with geomagnetic latitude, provides an explanation of the difference in the numbers of light nuclei stars formed by cosmic radiation in Harding's plates and in those exposed in Norway. The

calculations of Birnbaum et al. suggested that the proportion of stars formed in the light nuclei does not vary with primary energy. These calculations were based on the data obtained from a number of experiments carried out at similar latitudes, over a wide range of altitude which would involve a considerable variation in the mean energy of the star-producing radiation. While this variation accounts for the change in the slopes of the two lines of the integral distribution curves, the fact that it is not reflected in the calculated numbers of light and heavy element stars sheds further doubt on the validity of the method of calculation.

It seems, therefore, that the shape of the integral size distribution curves must be explained on the basis of the energy spectrum of the star-producing particles. Although it was possible in some cases to obtain apparently consistent values of the relative numbers of light and heavy nuclei stars from the equations of the lines, these results must be regarded as fortuitous. However, while the absolute values of the slopes of the two lines yield no information concerning the target nuclei, they do reflect some features of the energy spectra of the star-producing and primary radiations.

VII.2. Neutral star-producing radiation.

In the lower atmosphere, the neutral component of cosmic radiation contains both neutrons and γ -rays, and also a number of neutral mesons. Of the neutral mesons, only the K^{o} will produce stars, as the π^{o} mesons have a short life time of approximately 10^{-14} sec., and decay readily into two γ -rays. However, as the intensity of the K^{o} mesons in the atmosphere is less than the intensity of the neutrons, and their cross-section comparatively small, these particles will account for only a few of the stars observed in the plates. Although the photons which are created during the very high energy processes taking place in the upper atmosphere, and in the decay of other particles, are capable of producing stars by photodisintegration, their cross-section for star production is considerably smaller than that of neutrons, and consequently their contribution to the neutral star-producing radiation will not be considered. While a number of events attributed to neutrons may in fact be the result of γ -ray interactions, only one such event was identified in the present work. Thus, in the calculations which follow, the "neutral star-producing radiation" will be assumed to consist only of neutrons, and all stars which have no visible charged primary will be assumed to be neutron induced.

Included in the total numbers of neutron induced stars are those which were produced by neutral particles ejected from other stars in the plates. However, it was not possible to make allowance for these stars because there was no means of distinguishing their primaries from the neutrons entering the plates from outside, nor could their intensity be computed from the number of stars whose primaries were observed to come from other disintegrations. Of the 217 charged star primaries, 8 were the secondaries of other stars in the same plate, but since some of the stars would have primaries which had their origin in events in other plates, this number is an under-estimate of the total number of these so-called "double stars".

VII.2.1. Absorption of the radiation in air and in ice.

Since the total star population in an emulsion is a measure of the intensity of the star-producing radiation incident on the plate, a study of the change in star population with depth in an absorbing medium provides a convenient method of determining the mean absorption length of the radiation in the medium. From the neutron induced stars observed in the first expedition plates exposed at sea level and on the mountain top, and at different depths below the surface of the ice, the mean absorption length of the neutral star-producing

radiation in the atmosphere and in ice have been calculated.

During the systematic searching of the plates, only a few one prong stars were recorded because, as has been explained earlier, those with which nuclear recoils were not associated could not be identified. It was therefore necessary to find the correct number of these stars so that the total star population in each plate could be calculated. For this purpose, use was made of the integral size distribution curves of stars with neutral primaries. The equation of the line drawn through the points for which $n \leqslant 6$ was determined for each box of plates, and the total number of stars was calculated from the intercept of this line on the $N(> n)$ axis. From these results, the number of neutron induced stars formed per cubic centimetre of emulsion during the total exposure time from the date of manufacture to the date of development was obtained.

In order to find the intensity of the stars produced during the 50-day mountain exposure, a correction was applied to these values to allow for stars which had been formed during the outward and homeward journeys. This correction term, which will be called "background", was calculated from the number of stars formed per day in each cubic centimetre of emulsion in the sea level plates during the entire 100 days' exposure. The

relevant information is given in Table XXXVII below.

Table XXXVII.

Sea level plates.	
Exposure time	100 days
Volume searched	706 cu.mm.
Total number of stars	256 ± 16
Total number of stars/c.c.	363 ± 22
Number of stars/c.c./day	3.63 ± 0.22
Mountain plates	
Mountain exposure time	50 days
Background exposure time	50 days
Background correction	182 ± 11 stars/c.c.

After correcting for the background stars, it was possible to determine the number of stars formed per day in each cubic centimetre of emulsion by the neutral star-producing radiation incident on the plates during the 50-day exposure on the mountain top and under the ice. These results are shown in Table XXXVIII where the uncertainties have been calculated from the probable error in the finite numbers of stars recorded, that is from the square roots of the total numbers of stars. The depths of the boxes exposed under the ice cap are given in units of gm./cm.^{2}, assuming that the mean density of the ice or firn was 0.7 gm./c.c.

Table XXXVIII.

Position	Depth		Volume searched cu. mm.	100-day exposure		50-day mountain exposure	
	metres	gm./cm.^{2}		Total number of stars	Number of stars per c.c.	Number of stars per c.c.	Number of stars/c.c./day
Mountain top	0	0	706	742 ± 27	1051 ± 38	869 ± 40	17.4 ± 0.8
Under ice	0.8	56	286	237 ± 15	828 ± 54	646 ± 55	12.9 ± 1.1
	2.12	148	291.5	172 ± 13	593 ± 45	411 ± 46	8.2 ± 0.9
	3.48	244	300.5	113 ± 11	376 ± 35	194 ± 37	3.9 ± 0.7

The star intensity I, at a depth h gm./cm.^{2} below the top of an absorbing medium, may be represented by

$$I = I_o \exp(-\frac{h}{\ell})$$

where I_o is the star intensity at the top of the medium, and ℓ the mean absorption length, or interaction mean free path, of the star-producing radiation in the medium. Using the results of Table XXXVIII, the value of ℓ for ice was determined from the least squares slope of the graph of figure 27 in which the number of stars formed per day in each cubic centimetre of emulsion has been plotted on a logarithmic scale as a function of the depth below the ice in gm./cm.^{2} It was found that

$$\ell_{ice} = 166 \pm 9 \text{ gm./cm.}^2.$$

This result is somewhat smaller than the value $\ell_{ice} = 200$ gm./cm.^{2} obtained by Harding et al. (1949) from Ilford C2 emulsions exposed horizontally under ice, at an altitude of 3650 m. ($\lambda = 48°$N)

Assuming that the variation in the intensity of the star-producing radiation in the atmosphere is also exponential, the value of ℓ_{air} was determined by substituting in the equation

$$\frac{I_1}{I_2} = \exp\left(\frac{h_2 - h_1}{\ell}\right)$$

the values of the star intensity at the mountain top (I_1) and at sea level (I_2) and the depth difference ($h_2 - h_1$). The magnitude of $h_2 - h_1$ was calculated from the

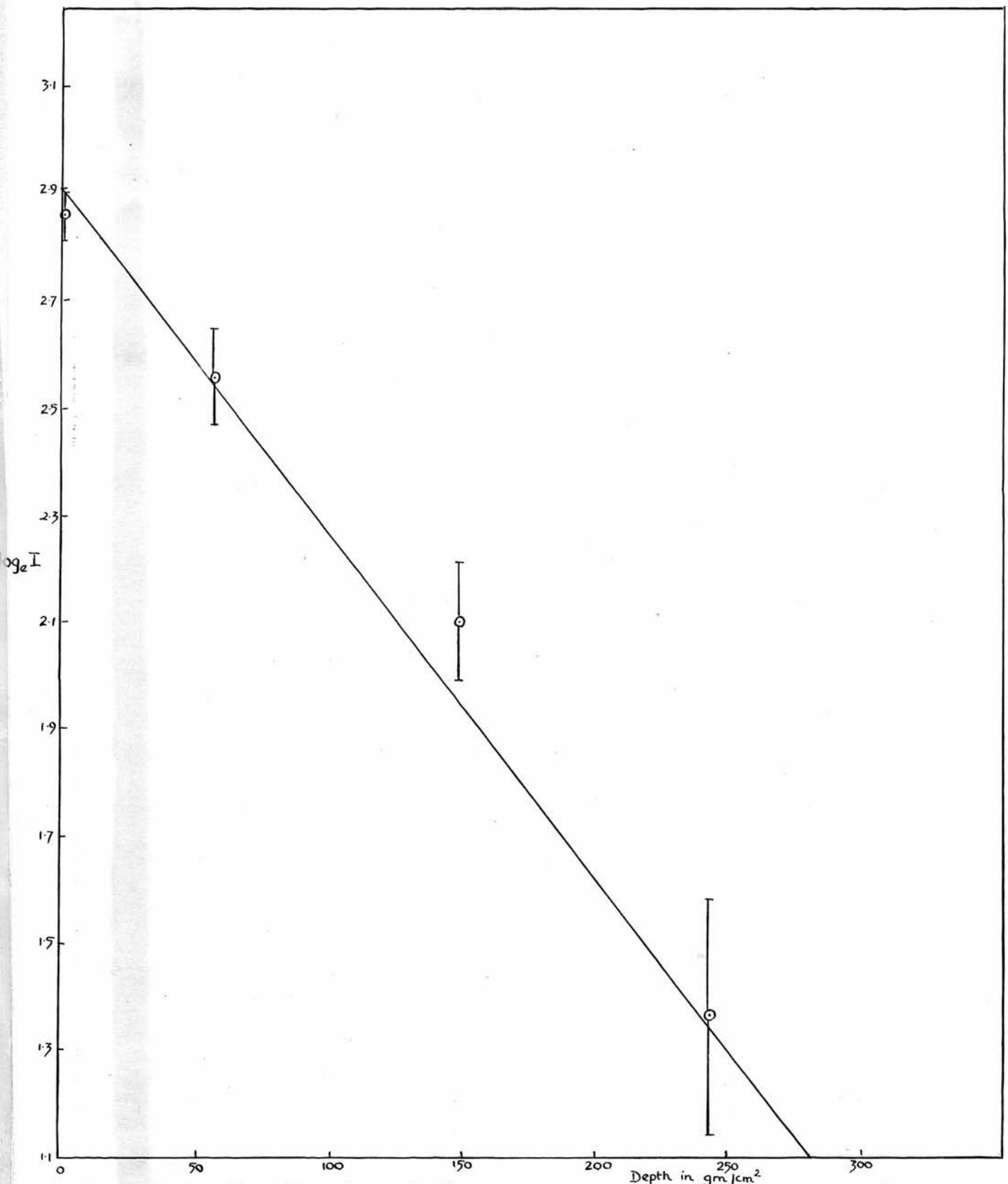

FIGURE 27. $\text{Log}_e I$ v. Depth (in gm/cm²) where I is the number of stars formed per cm³ per day in Ilford G5 emulsions exposed at different depths under ice-cap. (Density of firn = 0·7 gm/cm³).

difference in the atmospheric pressure at sea level (1013.2 millibars) and at 1710 m. (824 millibars), and was found to be 196 gm./cm.^{2}, from which it follows that:

$$\ell_{air} = 124 \pm 6 \text{ gm./cm.}^2.$$

These values of the mean absorption length of the neutral star-producing radiation in air and in ice may be compared with the results obtained from other emulsion studies, and with those obtained from neutron counter experiments.

VII.2.2. Variation of the mean absorption length with geomagnetic latitude.

Similar emulsion experiments by Bernardini et al. (1949), whose Ilford C2 emulsions were exposed in Italy at an altitude of 3500 m. and geomagnetic latitude of 47° N, led to the conclusion that the mean absorption length of the star-producing radiation in air is 135 ± 4 gm./cm.^{2}, and from Page's results (1949) obtained from plates exposed on the Jungfraujoch (altitude 3450 m., $\lambda = 48°$ N), it may be shown that ℓ_{air} is approximately 137 gm./cm.^{2}. George and Jason, on the other hand, who compared the star intensity in plates exposed on the Jungfraujoch with that in similar emulsions kept at sea level in London ($\lambda = 54°$ N), obtained a considerably higher value for the mean absorption length in air, namely 150 ± 4 gm./cm.^{2}. However, this last result

takes no account of a possible change in the star intensity at sea level in the range of latitude, 48° N to 54° N, concerned, and when the star intensity of 1.44 stars per cm.^{3} per day obtained by these authors is replaced by the value of 1.2 stars per cm.^{3} per day computed from Page's results, the mean absorption length becomes comparable with the other two values quoted.

While the present results include only the neutron-induced stars, the inclusion of stars produced by ionising primaries does not affect the value of ℓ_{air}, and these results may therefore be compared with those above. The smaller value of ℓ_{air} obtained at $\lambda = 66°$ N indicates that the mean absorption length of the neutral star-producing radiation is a function of geomagnetic latitude, and decreases as the latitude increases. This conclusion is similar to that obtained from measurements of the mean absorption length of fast and slow neutrons in air. Experiments carried out at high altitudes using neutron counters sent aloft in free balloons, by Simpson (1951), Staker et al. (1950 and 1951), Yuan (1951), and more recently by Soberman (1956) have shown that the mean absorption length varies from 212 gm./cm.^{2} at the geomagnetic equator to approximately 160 gm./cm.^{2} for latitudes greater than 50° N. It will be noted that these values are higher than the corresponding absorption lengths for the neutral star-producing radiation, and this has been confirmed by Mather (1954) who found that at $\lambda = 21°$ N

the mean absorption lengths were 148 gm./cm.^{2} and 139 gm./cm.^{2} for slow neutrons and fast star-producing neutrons respectively.

This difference in the values of the absorption length may be accounted for by considering the effect of local neutron production in the oxygen and nitrogen nuclei of the atmosphere on the numbers of slow and star-producing neutrons. In any layer of the atmosphere, the slow neutrons which are recorded by the counters, and by the boron-loaded emulsions used by Mather, include all those which have been produced in disintegrations occurring at higher altitudes, and which have reached this layer without absorption. Among these neutrons will be some whose kinetic energy is small, but which are, nevertheless, recorded by the counter. The star-producing neutrons, on the other hand, consist of a number of fast primary particles, and some of the neutrons produced in disintegrations, but the number of these will be confined to those which have enough energy to initiate a star. Thus, there will be a cut-off in the energy spectrum of the star-producing neutrons at approximately 100 MeV, and in the lower atmosphere, where there are few primary neutrons and a large number of slow secondary neutrons, the intensity of the star-producing neutrons will decrease more rapidly with altitude than the intensity of slow neutrons.

The values quoted above for the mean absorption length of the neutral star-producing radiation at different latitudes may be applied to the results obtained from emulsion studies of the intensity of cosmic ray stars in plates exposed at different altitudes and latitudes, so that the variations of the star intensity may be determined.

In the experiments carried out in Italy and on the Jungfraujoch, it was found that the intensity of stars with three or more prongs produced by the neutral and charged components of the radiation was in every case approximately 14 stars/cm.^{3}/day. If exponential absorption of the star-producing radiation is assumed, with a mean absorption length of 135 gm./cm.^{2}, it follows that the star intensities at 1710 m. and at sea level are respectively 4 stars/cm.^{3}/day and approximately 1 star/cm.^{3}/day. In the plates which were exposed at $\lambda = 66^\circ$N, however, the intensity of stars with three or more prongs produced by the incoming radiation - including charged particles - is 6.5 $\pm$ 0.5 stars/cm.^{3}/day at an altitude of 1710 metres, and 1.20 $\pm$ 0.14 stars/cm.^{3}/day at sea level. When these results are compared with the corresponding intensities at the lower latitudes, and with the value of 1.44 stars/cm.^{3}/day obtained by George and Jason (1949) from plates exposed at sea level ($\lambda = 54^\circ$ N), it is seen that at the higher altitude there is an increase

in the intensity of the total star-producing radiation (taking into account both charged and uncharged components), with geomagnetic latitude, although at sea level the values are all approximately the same.

VII.2.3. Absorption cross-section of the neutral star-producing radiation in air and in ice.

Using the experimentally determined mean absorption lengths of 124 ± 6 gm./cm.^{2} for air, and 166 ± 9 gm./cm.^{2} for ice, it may be shown that the ratio

$$\lambda_{air} : \lambda_{ice} = 1:1.34 \pm 0.10.$$

If, however, it is assumed that the cross-section for absorption of the star-producing radiation is proportional to the geometrical cross-section, the ratio of the mean absorption length in air to that in ice may be calculated from theoretical considerations. For the purposes of this calculation, only the main components of the atmosphere, namely nitrogen and oxygen, were included, and since the hydrogen atoms in ice do not in general produce recognisable stars, the cross-section for ice was determined from the number of oxygen atoms present.

In a medium of atomic weight A_r and density ρ_r, containing N_r atoms/cm.^{3}, with a geometrical cross-section σ_r and absorption cross-section σ'_r where

$$\sigma'_r = k\sigma_r$$

the average number of collisions which result in

absorption is $N_r \sigma'_r$ per cm., and thus the mean absorption length of the radiation is:

$$l_r = \frac{1}{N_r \sigma'_r} \text{ cm.} \qquad (36)$$

For a heterogeneous medium, the contribution of each different element must be taken into account, and the equation (36) replaced by

$$l_H = \frac{1}{\sum_r N_r \sigma'_r} \text{ cm.}$$

Since $\sigma_r = \pi R_r^2 = \pi r_0^2 A_r^{2/3} \text{ cm.}^2$ (R_r = nuclear radius $= r_0 A_r^{1/3}$ cm.) and $N_r = \frac{N_0 \rho_r}{A_r}$ where N_0 is Avogadro's number, it may be shown that

$$l_H = \frac{1}{k N_0 \pi r_0^2 \sum_r \rho_r / A_r^{1/3}} \text{ cm.}$$

This value, when multiplied by the density of the medium, gives the mean absorption length in units of gm./cm.^{2}. In TableXXXIX, the values of the constants used in the calculation of the mean absorption lengths in air and ice are given

Table XXXIX.

	Air		Ice
	Nitrogen	Oxygen	Oxygen
A_r	14	16	16
ρ_r (gm./cm.^{3})	8.634×10^{-4}	2.654×10^{-4}	0.62
ρ_{medium} (gm./cm.^{3})	1.144×10^{-3}		0.7

As the density of air varies with altitude, the magnitude of ρ_{air} was calculated from the pressure difference between sea level where the atmospheric pressure is 1013.2 mb. and 1710 m. where the pressure is 824 mb. From this it follows that the total mass of air traversed is 195.5 gm./cm.^{2}, and the corresponding density is therefore 1.144×10^{-3} gm./cm.^{3}. Taking $r_o = 1.4 \times 10^{-13}$ cm., and $N_o = 6.025 \times 10^{23}$ gm./mole, the values of the mean absorption lengths in air and ice, in terms of k, the unknown constant of proportionality, were found to be

$$\ell_{air} = \frac{66.5}{k} \text{ gm./cm.}^2$$

and $$\ell_{ice} = \frac{76.7}{k} \text{ gm./cm.}^2.$$

When this theoretical value of ℓ_{air} is compared with the experimentally determined ℓ_{air} of 124 gm./cm.^{2}, it is seen that the constant k is approximately equal to one half, and thus the cross-section for absorption of the star-producing radiation in air is approximately half the geometrical cross-section. For ice, the constant has a slightly smaller value, and this would indicate either that the absorption cross-section is less than half the geometrical cross-section, or that there is a change in the flux of the star-producing radiation in ice. A variation of this kind would cause a change in the mean absorption length and consequently in the calculated absorption cross-section.

The ratio of the mean absorption length in ice to that in air calculated from these theoretical values is

$$\lambda_{air} : \lambda_{ice} = 1:1.16$$

which is significantly different from the experimental value of

$$\lambda_{air} : \lambda_{ice} = 1:(1.34 \pm 0.10).$$

This discrepancy, together with the apparently small value of k for ice, must be explained by a change either in the cross-section or in the flux of the incoming radiation.

Determinations of the cross-section for absorption of the star-producing radiation in air, lead and aluminium by Bernardini et al. (1949) showed that for each of these media this cross-section is equal to half the geometrical cross-section of the absorbing medium. It seems unlikely therefore that the cross-section in ice will be significantly different from half the geometrical cross-section, and an alternative explanation in terms of a change in the flux of the star-producing radiation must be sought.

So far no account has been taken of the behaviour of the incoming neutrons in the presence of the hydrogen nuclei of the ice. While these nuclei do not contribute to the number of stars produced, they are capable of undergoing elastic collisions with the incident neutrons. In such a collision, the recoiling proton will, on the

average, carry away half of the available kinetic energy, with the result that the energy of the neutron will be reduced to one half of its original value. Very fast neutrons, which would in general pass through a nucleus without causing a disintegration, will thus be slowed down by the hydrogen nuclei, and there will be a greater probability of their producing a disintegration in one of the nuclei of an emulsion buried in ice.

The cross-section for an elastic collision between a neutron and a hydrogen nucleus varies according to the energy of the neutron, and consequently the mean free path of the neutrons is also a function of their energy, as shown in Table XL. Values of the cross-sections are taken from Adair's graphs (1950).

Table XL.

Neutron energy (MeV)	Cross-section (barns)	Mean free path (cm.)
100	0.07	300
300	0.035	600

Although these mean free paths are relatively long, they are comparable with the distance travelled in ice by the incoming neutrons other than those which are vertically incident, and thus allow quite a large probability for a

collision of this kind. As a result of elastic scattering by the hydrogen nuclei in the ice, the direction of the incoming radiation will be altered, and there will be a change in its energy spectrum because some of the neutron energy will be lost to the recoiling protons.

Above the ice, the radiation incident on an emulsion will consist of neutrons which may be divided into three groups:

(1) low energy neutrons which are not capable of producing stars in the emulsion.

(2) neutrons in the medium energy range ($\sim$ 100 or 200 MeV) which are responsible for a large number of the stars.

(3) very high energy particles which have a finite chance of passing through a nucleus undeflected, and because of this transparency of the nuclei, these particles will rarely produce stars.

During the passage of this radiation through ice, the overall intensity will be reduced as a result of absorption by the oxygen nuclei. However, elastic collisions with the hydrogen nuclei may cause an increase in the number of particles in group (2) at the expense of those in group (3), with the result that the intensities of stars in plates exposed under ice will be greater than those predicted by cross-section calculations. These increased values of the intensity will also have the

effect of reducing the slope of the graph of figure 27. Consequently the value of the mean absorption length of the star-producing radiation in ice calculated from the slope of the graph will be too great, and the cross-section for absorption of the radiation determined from λ_{ice} will be smaller than the true absorption cross-section. It will be assumed that the difference between these two values of the cross-section is due only to the change in the intensity of the star-producing radiation, and that the cross-section for absorption is equal to half the geometrical cross-section of the absorbing nuclei.

In air, where hydrogen is present only in very small quantities, the incoming radiation will not be subject to collisions of the kind experienced in ice. The change in intensity with increasing atmospheric depth is due to absorption alone, and the cross-section for absorption is equal to half the geometrical cross-section of the nuclei present in the atmosphere.

VII.2.4. <u>The flux of neutral star-producing particles in the lower atmosphere</u>.

When the rate of production of stars in nuclear emulsion plates exposed at a given altitude and latitude is known, it is possible to calculate the flux of star-producing particles provided that the cross-section for star-production in the emulsion is also known.

It has already been shown that the cross-section for absorption of the neutral star-producing radiation is approximately equal to one half of the geometrical cross-section. This implies that each star-producing neutron will, on the average, pass through two nuclei before being absorbed. There are then two possibilities for star-production, which are shown schematically in figure 28:

(1) the incident neutron (denoted by the solid line) passes through the first nucleus without causing a disintegration, but is absorbed by a catastrophic collision with the second nucleus.

(2) the incident neutron collides with the first nucleus and produces a star; then either

(a) the same neutron emerges from this disintegration and produces another star in the second nucleus in which it is absorbed, or

(b) an energetic secondary neutron ejected from the first star produces the second star.

In this case, it would not be possible to distinguish between events of the type (a) and those of the type (b). These two possibilities suggest that the cross-section for star production, σ_S , is either equal to the absorption cross-section, σ_A , as in (1), or that it is equal to the geometrical cross-section, σ_G , as in (2).

Experiments by Perry (1952), who determined the

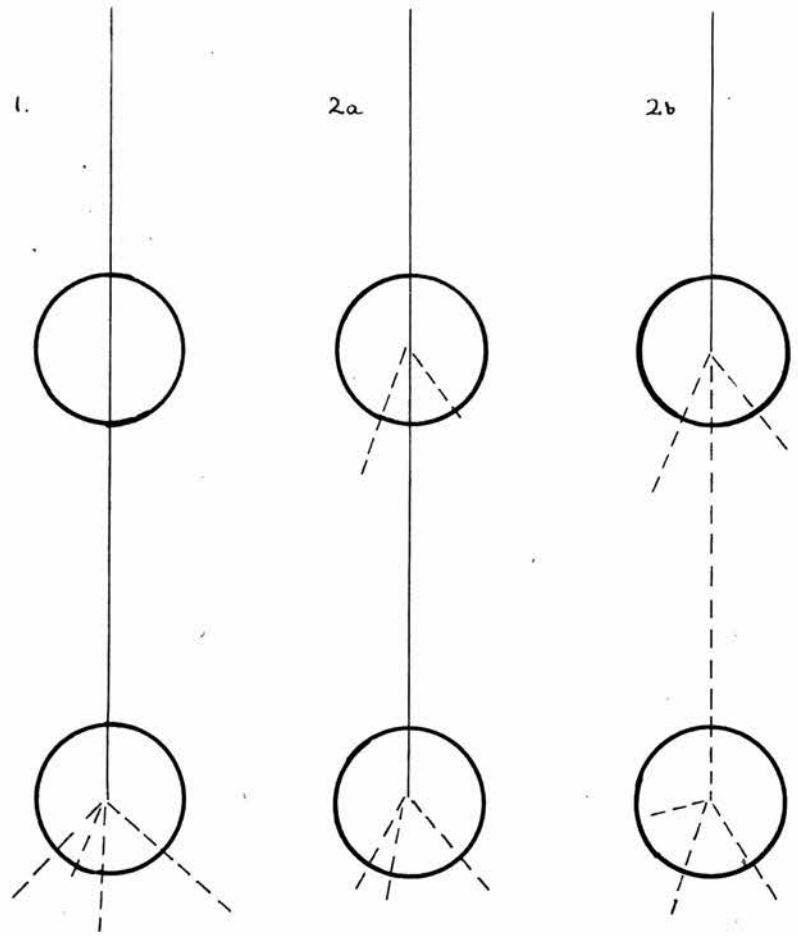

FIGURE 28 Schematic diagram showing absorption of a neutron (solid line) in atomic nuclei. Dashed lines represent secondary disintegration products.

mean free path for inelastic collisions of 240 MeV protons in emulsions, showed that, while the inelastic cross-section was less than the geometrical cross-section, it was certainly greater than $0.5\,\sigma_G$. These conclusions have been confirmed by other authors whose results also indicate that the cross-section decreases as the energy of the incident particle increases (Lock et al., 1955). This variation in the star-production cross-section with energy is to be expected, because, when the wavelength of the particle is comparable with the distance between the nucleons, the probability of an energy transfer is appreciable. As the energy of the particle increases, however, the wavelength decreases, until at several hundred MeV, it is much smaller than the distance of separation of the nucleons, and the probability of a disintegration is small. Thus, the cross-section for star production varies inversely with energy, except for very high energies where the process of meson production will probably cause an increase in the cross-section.

However, the neutral star-producing radiation which is incident upon nuclear emulsions exposed to cosmic radiation has a wide energy spectrum, and consequently the cross-section for star production is not the same for all the neutrons. For low energy particles, the cross-section is approximately equal to the geometrical

cross-section, and for high energy particles it may be as small as half this value, but for the purposes of calculating the neutron flux at $\lambda = 66^{\circ}$ N, it will be assumed that the mean cross-section is the same as that of protons, and is equal to σ_G, since the average energy of the incident neutrons is not great.

In order to determine the total cross-section for the emulsion, it is necessary to consider the contribution of all the elements, with the exception of hydrogen, which does not in general give rise to recognisable stars. In the rth component of the emulsion, which has density ρ_r, and atomic weight A_r, of which there are N_r atoms per cm.^{3}, the number of stars ds_r formed per day in 1 cm.^{2} of emulsion dx cm. thick is

$$\frac{ds_r}{I} = N_r \sigma_r dx$$

where I is the total flux of star-producing particles per cm.^{2} per day, and σ_r the geometrical cross-section. Replacing N_r by $\frac{N_o \rho_r}{A_r}$ (N_o, Avogadro's number), and σ_r by $\pi r_o^2 A_r^{2/3}$ as before, and summing over all the components of the emulsion, we have

$$\frac{S}{I} = N_o \pi r_o^2 \sum_r \frac{\rho_r}{A_r^{1/3}} \, dx \qquad (37)$$

where S is the total number of stars formed per day in 1 cm.^{2} of emulsion, dx cm. thick.

From the values of ρ_r and A_r shown in Table XLI for all the elements of the emulsion, and using

$N_o = 6.025 \times 10^{23}$ and $r_o = 1.4 \times 10^{-13}$ cm. as before, the ratio of S, the number of stars per cm.^{2} per day in 1 cm. of emulsion, to I, the number of incoming particles per cm.^{2} per day, was found to be

$$\frac{S}{I} = 0.038.$$

Table XLI.

Element	ρ_r (gm./cm.^{3})	A_r
C	0.30	12
N	0.073	14
O	0.20	16
S	0.011	32
Br	1.496	80
Ag	2.025	107
I	0.026	127

The total flux of the neutral star-producing radiation at sea level and at an altitude of 1710 m. for geomagnetic latitude $\lambda = 66^\circ$ N was then calculated; these results are shown in Table XLII.

Table XLII.

Altitude	S (stars/cm.^{3}/day)	I (particles/cm.^{2}/day)
Sea level	3.63 ± 0.22	95 ± 5
1710 m.	17.4 ± 0.8	458 ± 21

These values of I include all the neutrons which have an energy greater than a certain minimum value. The cut-off is determined by the amount of energy which must be transferred to a nucleus in an inelastic collision in order that at least one charged secondary will be emitted in the disintegration, and is of the order of 100 MeV.

It has already been shown that 14% of the total number of stars were produced by charged particles. If it is assumed that the cross-section for star production is the same for these particles as for the neutrons, it may be shown from the results above that the total flux of star-producing particles is approximately 110/cm.^{2}/day at sea level, and 550/cm.^{2}/day at 1710 m. for geomagnetic latitude of 66° N.

In all these calculations it has been assumed that the cross-section for star production is equal to the geometrical cross-section of the emulsion, and while this may be true for the lower energy primaries, it will certainly be an over-estimate of the cross-section for high energy particles. Although the very high energy particles which penetrate the atmosphere to these low altitudes are comparatively few in number, the error involved in assuming too large a value for the cross-section may be considerable. The present results therefore give lower limits for the flux.

A further error arises because so far no account has been taken of the possibility that some of the neutrons entering the plates may have their origin in the ground, or in the material surrounding the plates. Although many of these particles will have energies less than 100 MeV, some may be capable of producing disintegrations in the plates. These neutrons will cause an increase in the number of small stars, which will result in an over-estimate of the neutron flux.

It was also shown, in section VII.2.1 above, that the rates of production of stars with three or more prongs, in the plates exposed in Norway, were comparable with those determined at different latitudes. At 1710 m. the star intensity varies from approximately 4 stars/cm.^{3}/day at $\lambda = 48^\circ$ N to 6.5 stars/cm.^{3}/day at $\lambda = 66^\circ$N, giving an increase of more than 50% in this range of latitude. These results indicate that the flux of star-producing particles at 66° N is approximately 1½ times that at 48° N.

This method of estimating the change in the intensity of the star-producing radiation with latitude is preferable to a comparison of the absolute values of the intensity determined by different workers, because of possible variations in the values chosen for the cross-section in equation (37). It does assume, however, that the composition of the radiation, its mean energy

and the cross-section for star production are the same at different latitudes: these factors will now be considered in turn.

(1) The composition of the radiation. It was shown in VII.1.1 that 14 ± 1% of the stars observed in the plates exposed at $\lambda = 66^{\circ}$ N had ionising primaries, and that the corresponding value for plates exposed by Page at $\lambda = 48^{\circ}$ N was 17 ± 3%. As these results are not significantly different, it may be assumed that there is an equal proportion of ionising particles present in the radiation at these latitudes, and that there is an overall increase in intensity with latitude, rather than an increase in the intensity of any one component.

(2) The mean energy of the radiation. The integral size distributions of the stars produced in plates exposed at $\lambda = 66^{\circ}$ N and at $\lambda = 48^{\circ}$ N (Page), showed that there was a greater number of large stars formed at the higher latitude, and therefore that the proportion of high energy particles present in the radiation increased with latitude. This conclusion was supported by the fact that the mean energy of the star-producing radiation, calculated from the proportion of light element stars, was greater at $\lambda = 66^{\circ}$ N than on the Jungfraujoch (see page 143), although this method of determining the mean energy is only approximate.

However, from the values of the mean absorption

length of the star-producing radiation at latitudes 66° N and 48° N (124 ± 6 gm./cm.^{2} and 135 ± 4 gm./cm.^{2}, respectively), it appears that the mean energy is greater at the lower latitude, where the absorption length is longer, and the absorption cross-section consequently smaller. If the difference between the values is significant, it may be due to a difference in the shape of the energy spectrum of the radiation at the two latitudes, which was in fact not taken into account in the earlier considerations of the absorption lengths of slow and star-producing neutrons, since it does not affect the slow neutron measurements.

Since the exposures at $\lambda = 66°$ N were made at much lower altitudes than those at $\lambda = 48°$ N, the number of stars in these plates will include a larger proportion of low energy events because of the increased path length of the radiation through the atmosphere. On the other hand, it was shown above that the number of high energy star-producing particles is also greater at the higher latitude, and these two effects together will lead to an increase in the width of the energy spectrum.

The experimental results may then be explained if it is assumed that the presence of these high energy particles causes an increase in the mean energy of the radiation, without altering the mean absorption length. This assumption is not unreasonable because, while the

calculated value of the mean energy can be altered considerably by the inclusion of a small number of high energy events, the value of the mean absorption length is governed by the total numbers of stars, and is therefore most influenced by the small stars which are present in much greater numbers than the large stars. The shape of the energy spectrum of the star-producing radiation and the value of the mean energy may therefore be assumed to vary with latitude.

(3) The cross-section for star production. It was stated earlier that the cross-section for star production varies inversely with the energy of the incident particle, except at very high energies. In the calculation of the total flux at $\lambda = 66^{\circ}$ N, it was assumed that the cross-section was equal to the geometrical cross-section for all the particles. An exact determination of the flux would, however, require that changes in the cross-section be taken into account, and consequently the total flux at a given latitude could only be computed if the numbers of particles in each range of energy E to E + dE over the entire spectrum were known.

From these considerations it is clear that, while the composition of the star-producing radiation is approximately the same at different latitudes, the shape of the energy spectrum and the mean energy vary considerably with latitude and with altitude. Thus, any

comparison of the intensities of the radiation at different places, which does not make allowances for changes in energy and cross-section, can give no more than an indication of the true results. More accurate determinations of the absolute intensity of the star-producing component of cosmic radiation in the lower atmosphere cannot be made until the effect of these changes is known, and an exact value of the cross-section for star production at different energies is available.

VII.3. Conclusions.

From the observations on the cosmic ray stars formed in emulsions exposed in Norway at sea level, and at an altitude of 1710 m., it has been possible to determine some of the properties of the stars, and of the radiation responsible for their production.

The results show that in the lower atmosphere, at a geomagnetic latitude of 66° N, 86 out of every 100 stars have no visible primary, and must therefore be produced by neutral particles, which are almost exclusively neutrons. Of the remaining stars, 3% were the result of disintegrations produced by slow negative π-mesons, and the others were produced by protons, fast mesons, and a few α-particles. Thus, neutrons form the main component of the star-producing radiation in the lower atmosphere.

At these altitudes, evaporation stars, whose tracks were produced chiefly by charged particles of a few MeV kinetic energy, were more frequently observed than high energy events in which a number of fast particles was emitted, and it was found that the average excitation energy of all the stars was approximately 250 MeV. Unfortunately, the difference in altitude of the two points of exposure was too small to show conclusive evidence of a decrease in mean energy with increasing atmospheric depth.

This value of the mean energy was also obtained from a consideration of the numbers of stars formed in the light elements (H, C, N, O) of the emulsion. From the results of a number of emulsion experiments by other authors, it was shown that the proportion of light element stars is a function of the primary energy, but the values of the energy obtained by this method are only approximate.

A study of the integral star size distribution curves drawn for each set of plates revealed that the shape of the curves could only be interpreted in terms of the energy spectrum of the star-producing radiation. Contrary to other hypotheses, it was found that the curves do not yield information concerning the relative numbers of stars produced in the light and heavy elements.

Finally, the behaviour of the neutron component of the star-producing radiation was measured under different conditions, and it was found that the mean absorption length of the radiation in air was comparable with the values obtained by other authors. The cross-section for absorption in air is equal to half the geometrical cross-section, and a similar value is thought to hold for ice, since allowance must be made for a change in the energy spectrum of the radiation in ice, due to elastic collisions with the hydrogen nuclei.

Assuming that the cross-section for star production in the emulsion is equal to the geometrical cross-section, the neutron flux at sea level and at 1710 m. for $\lambda = 66^{\circ}$ N, was determined from the intensity of neutron-induced stars in the plates, and was found to vary from 95/cm.^{2}/day at sea level, to 458/cm.^{2}/day at the mountain top. These results, and the corresponding values of 110/cm.^{2}/day and 550/cm.^{2}/day for the total flux of star-producing radiation, must however be treated as approximate values for the lower limit of the flux. Accurate determinations can only be made when the shape of the energy spectrum and the variation of the star-production cross-section with energy are known.

Chapter VIII.

CONCLUSIONS.

From the time of its first application to the study of nuclear disintegrations produced by cosmic radiation, the photographic emulsion technique has provided a valuable source of information in the investigation of the properties of the particles present in cosmic radiation, and their interactions with atomic nuclei. In the course of the present study, observations were made on the stars produced by cosmic rays incident upon emulsions which were exposed in Arctic Norway, and from the results it has been possible to determine some of the characteristics of the behaviour of cosmic ray particles under different conditions. Details of the exposure and processing of the emulsions were given in Chapter II, and in Chapter III the examination of the plates was described.

One of the main problems in a nuclear emulsion study of cosmic ray phenomena is that of identifying the particles which produce the disintegrations, and the secondary charged particles ejected as a result of these nuclear interactions. In Chapter IV, the general relationships used in track analysis were described, and the applications of residual range, multiple Coulomb scattering, and delta-ray density measurements, to the identification of particles in nuclear emulsions, were

discussed.

However, the most convenient method of determining the nature and energy of a particle, was found to be that in which observations were made of the change in grain density with range, and in order to simplify the technique of calculating grain density the gap count method, considered in detail in Chapter V, was developed. It was found that a reliable estimation of the grain density of a track, and its variation with range, could be obtained from measurements of the numbers of gaps greater than a given minimum size. This method has the advantage over direct grain and blob counting that it is applicable to thin and heavy tracks alike, and that the grain density can be determined from a comparatively small number of observations. Also, it is not subject to personal errors, and the results obtained by one observer are comparable with those obtained by a second observer, or by the same observer at different times. Some of the applications of the gap count method to the determination of the mass of slow particles, to the identification of tracks formed in wet emulsion and to the "joining" of tracks were described.

In order to simplify further the identification of the primary and secondary particles of stars, the variation of grain density with the velocity, kinetic energy and residual range of a number of singly charged

particles was established from experimental observations on the tracks of protons, as shown in Chapter VI. The nature and energy of a particle could then be ascertained by comparing the observations on this track with those of the standard particles. During the course of the work described in this chapter, it was found that the experimental relation between the rate of loss of energy of a particle and the grain density of its track could be fitted by the Demers expression for the probability of development of a silver bromide grain.

Each of the stars observed during the systematic searching of the plates was examined and classified as described in Chapter III, and where it was necessary gap count measurements were made on the tracks in order to establish the identity of the particles concerned. Estimations of the energy of single charged particles were also made in this way. From these results it was found that 14% of the stars had charged primaries, and of these only 20% were slow π -mesons. The mean energy of the neutral star-producing radiation was found to be approximately 250 MeV, and observations on the number of stars formed in the light nuclei of these emulsions and others exposed at a lower latitude indicate that the mean energy decreases with decreasing latitude. A possible explanation of this variation has been suggested.

It was also shown that the shape of the integral

star size distribution curves could not be interpreted in terms of the contributions of the light and heavy nuclei of the emulsion, although it could be explained on the basis of the energy spectrum of the star-producing particles.

Finally, the intensity of the star-producing radiation in the lower atmosphere, and its absorption in air and in ice, were considered. The experimental results are consistent with an absorption cross-section equal to half the geometrical cross-section. Values for the intensities of the neutral and total star-producing radiations have been determined, but since these calculations were based on the assumption that the cross-section for star production is equal to the geometrical cross-section, which is not the case for fast particles, these results are minimum values.

An alternative determination of the neutron flux could be made if the numbers of proton recoil tracks in the plates were known. Not all the single proton tracks occurring in the plates are recoils, as some are produced in low energy inelastic collisions, but provided the appropriate correction for inelastic events can be applied, the number of elastic collisions can be determined. One possible method of calculating the number of one prong, neutral induced stars is by using the integral size distribution curves described in Chapter VII.

An estimation of the neutron flux from the number of proton recoil tracks would yield valuable information concerning the shape of the energy spectrum of the neutrons, the cross-section for star production and its variation with the energy of the star-producing particles.

One interesting feature of the stars in the present plates, which has yet to be studied, is the apparently high frequency of events in which two tracks emerge close together, with only a very small angle between them. Preliminary measurements have shown that, while in a few of these events the two particles emerge as a single particle which subsequently decays at a short distance from the star, this is not the case in many of the events, and further observations will be required before the mechanism of disintegration can be understood.

Much work remains to be done before a complete picture of the variation of the intensity of the neutral component of cosmic radiation over the earth's surface can be obtained. At present, observations are being made on a number of nuclear emulsion plates which were exposed and processed in the Antarctic by the Royal Society's expeditions to Halley Bay in 1956-57, and on other plates exposed at high altitudes on Kiliminjaro by the Geological Expedition from the University of Sheffield in 1957. When the results from these plates have been analysed, it is hoped that they will furnish

further information concerning the behaviour of cosmic radiation in the lower atmosphere, and the effects upon it of the magnetic field of the earth.

ACKNOWLEDGMENTS.

I should like to express my thanks to Professor N. Feather, F.R.S., for kindly extending to me the facilities of his laboratories.

My warmest thanks are due to Dr. M.A.S. Ross, who suggested the topic for this thesis, for her advice and constant encouragement throughout the course of this work. I am deeply indebted to Mrs. M.D. Smith, who scanned a large number of the plates, and carried out many of the gap and grain measurements, and I should also like to thank Mrs. Henderson, Mrs. Kellard and Mrs. Miller for their invaluable assistance in scanning.

My thanks are due to the Department of Scientific and Industrial Research for the award of a Maintenance Grant for one year of the research.

REFERENCES.

1. Adair, R.K., Rev. Mod. Phys. 22, 249, 1950.

2. Alvial, G., Bonetti, A., Dilworth, C., Ladu, M., Morgan, J. and Occhialini, G., Nuov. Cim. Suppl. 4, 244, 1956.

3. Barton, J.C., George, E.P. and Jason, A.C., Proc. Phys. Soc., Lond., A 64, 175, 1951.

4. Bernardini, G., Cortini, G. and Manfredini, A., Phys. Rev. 76, 1792, 1949.

5. Birnbaum, M., Shapiro, M., Stiller, B. and O'Dell, F.W., Phys. Rev. 86, 86, 1952.

6. Blau, M., Phys. Rev. 75, 279, 1949.

7. Blau, M., Oliver, A.R. and Smith, J.E., Phys. Rev. 91, 949, 1953.

8. Bohr, N., Phil. Mag. 25, 10, 1913.

9. Bose, D.M. and Chouduri, B., Nature (London) 147, 240, 1941.

10. Bradner, H., Smith, F.M., Barkas, W.H. and Bishop, A.S., Phys. Rev. 77, 462, 1950.

11. Brown, R.H., Camerini, U., Fowler, P.H., Heitler, H., King, D.T. and Powell, C.F., Phil. Mag. 40, 862, 1949.

12. Brown, W.W., Phys. Rev. 93, 528, 1954.

13. Caldwell, D.O., Phys. Rev. 100, 291, 1955.

14. Catala, J. and Gibson, W.M., Nature (London) 167, 551, 1950.

15. Cuer, P., C.R. (Paris) 223, 1121, 1956.

16. Demers, P., Canad. J. Res. A 25, 223, 1947.

17. Demers, P. and Lechno-Wasiutynska, Z., Canad. J. Phys. 31, 480, 1953.

18. Demeur, M., Huleux, A. and Vanderhaeghe, G., Nuov. Cim. 4, 509, 1956.

19. Dilworth, C.C., Occhialini, G.P.S. and Payne, R.M., Nature (London) 162, 102, 1948.

20. Dilworth, C.C., Occhialini, G.P.S. and Samuel, E., Bulletin du Centre de Physique Nucleaire de l'Université Libre de Bruxelles No. 2, August 1948.

21. Dilworth, C., Goldsack, S.J. and Hirschberg, L., Nuov. Cim. 11, 113, 1954.

22. Fay, H., Gottstein, K. and Hain, K., Nuov. Cim. Suppl. 11, 143, 1954.

23. Fowler, P.H., Phil. Mag. 41, 169, 1950.

24. Rotblat, J., Progress in Nuclear Physics, Vol. I p. 43.

25. George, E.P. and Jason, A.C., "Cosmic Radiation", Colston Papers, p. 31.

26. Goldschmidt-Clermont, Y., King, D.T., Muirhead, H. and Ritson, D.M., Proc. Phys. Soc., Lond., 61, 183, 1948.

27. Gottstein, K., Menon, M.G.K., Mulvey, J.H., O'Ceallaigh, C. and Rochat, O., Phil. Mag. 42, 708, 1951.

28. Grilli, M., Vitale, B., Hodgson, P.E. and Ladu, M., Nuov. Cim. 1, 314, 1955.

29. Harding, J.B., Nature (London) 163, 440, 1949.

30. Harding, J.B., Lattimore, S., Li, T.T. and Perkins, D.H., Nature (London) 163, 319, 1949.

31. Hodgson, P.E., Brit. J. Appl. Phys. 3, 11, 1952.

32. Hodgson, P.E., Phil. Mag. 45, 190, 1954.

33. Kaplon, M.F., Walker, W.D. and Koshiba, M., Phys. Rev. 93, 1424, 1954.

34. Lattes, C.M.G., Occhialini, G.P.S. and Powell, C.F., Proc. Phys. Soc., Lond., 61, 173, 1948.

35. LeCouteur, K.J., Proc. Phys. Soc., Lond., A 63, 259, 1950.

36. Lees, C.F., Morrison, G.C., Muirhead, H. and Rosser, W.G.V., Phil. Mag. 44, 304, 1953.

37. Livingston, M.S. and Bethe, H.A., Rev. Mod. Phys., 9, 245, 1937.

38. Lock, W.O., March, P.V., Muirhead, H. and Rosser, W.G.V., Proc. Roy. Soc. A 230, 215, 1955.

39. Mather, K.B., Austral. J. Phys. 7, 601, 1954.

40. Molière, G., Zeits. Naturforsch. 2a, 133, 1947;
Ibid 3a, 78, 1948.

41. Page, N., Proc. Phys. Soc., Lond., A 63, 250, 1950.

42. Perkins, D.H., Phil. Mag. 40, 601, 1949.

43. Perry, A.M., Phys. Rev. 85, 497, 1952.

65. Hodgson, P.E., Phil. Mag. 41, 725, 1950.

66. O'Ceallaigh, C., Rep. Cosmic Ray Congress, Bagnères de Bigorre, 1953, p73.

44. Powell, C.F., Occhialini, G.P.S., Livesey, D.L. and Chilton, L.V., J. Sci. Instrum. 23, 102, 1946.

45. Rochester, G.D. and Rosser, W.G.V., Rep. Progr. Phys. 14, 227, 1951.

46. Rotblat, J., Nature (London) 167, 550, 1951.

47. Shapiro, A.M., Rev. Mod. Phys. 28, 164, 1956.

48. Simpson, J.A., Phys. Rev. 83, 1175, 1951.

49. Soberman, R.K., Phys. Rev. 102, 1399, 1956.

50. Staker, W.P., Phys. Rev. 80, 52, 1950.

51. Staker, W.P., Pavalow, M. and Korff, S.A., Phys. Rev. 81, 889, 1951.

52. Sternheimer, R.M., Phys. Rev. 103, 511, 1956.

53. Vigneron, L., J. Phys. Radium 14, 145, 1953.

54. Idanov, A., J. Phys. Radium 6, 233, 1935

55. Williams, E.J., Proc. Roy. Soc. A 169, 531, 1939.

56. Williams, E.J., Phys. Rev. 58, 292, 1940.

57. Williams, Elwyn J., Ph.D. Thesis, University of Wales, 1955.

58. Yuan, L.C.L., Phys. Rev. 81, 175, 1951.

59. Zajac, B., Ph.D. Thesis, University of Edinburgh, 1949.

60. Menon, M.G.K., O'Ceallaigh, C., and Rochat, O., Phil. Mag. 42, 932, 1951.

61. O'Ceallaigh, C., and Rochat, O., Phil. Mag. 42, 1050, 1951.

62. Gottstein, K., and Mulvey, J.H., Phil. Mag. 42, 1089, 1951.

63. Menon, M.G.K., and Rochat, O., Phil. Mag. 42, 1232, 1951.

64. Voyvodic, L., Progress in Cosmic Ray Physics, Vol. II, p243, 1954.